

Geotechnical Issues in the Conservation of Sites

Robert E. Englekirk

THE FORCES OF NATURE have been reshaping our planet for millions of years. Humankind has been reasonably successful, at least locally, in attempts to control the impact of this process where a concerted effort can result in a decided benefit. The cost and effectiveness of constraining natural geotechnical processes are important considerations in the development of new structures, since permanent solutions may not be possible regardless of cost. Time and cost are also of concern in efforts to preserve ancient grottoes; an added factor here, however, is the impact of the control methodology on aesthetics. Accordingly, the objective becomes the appropriate balance between effectiveness, cost, and aesthetics.

What constitutes a “balanced” program will not be decided by the geotechnical consultant. Accordingly, those involved in the decision-making process must understand the geotechnical issues at hand and the mitigation alternatives available, which together are the focus of this chapter.

Geotechnical Issues

Site soils and geology are fundamental to every grotto preservation effort. Two problems are exclusively geotechnical in nature: deterioration of the grotto structure and water intrusion. The grottoes at Dunhuang and Yungang in China are cases in point.

Geological instability of grotto structure

Excavated caves such as those at Dunhuang and Yungang were created in relatively soft sandstone deposits, which allowed easy excavation but whose surface is easily eroded by water or wind. Sandstones form when sand is consolidated under uniform triaxial pressure, typically in a marine environment. Pressure, or the removal of pressure, is a major consideration in the deterioration of grotto structures, as the face of a sandstone cliff is subjected to pressure on all sides except for the exposed cliff face. This lack of surficial pressure causes the compacted sandstone to expand laterally in the direction of the cliff face, thereby promoting surficial

delamination and/or the creation of weakened planes parallel to, but behind, the cliff face. Once a weakened plane has been created, it is soon further weakened by the intrusion of water until a block is formed. Surficial erosion and cliff recession are caused by these two related events, generally identified as surface deterioration and block failure. The rate of cliff recession, though not uniform, given the episodic occurrence of block failure, is fairly predictable. At the Mogao grottoes near Dunhuang, a reasonable estimate of this rate is about 1 cm per year based on an observed rate over the last twelve hundred years. Anomalies, either extant or introduced, can significantly accelerate the process. This will depend to a large extent on the nature and amount of the erosion, whether by wind and sand abrasion or by water. Consequently, any cliff recession abatement program must strive to (a) restore lateral pressure and thereby maintain the internal integrity of the sandstone formation, and (b) reduce the impact of abrasives on the surface of the cliff.

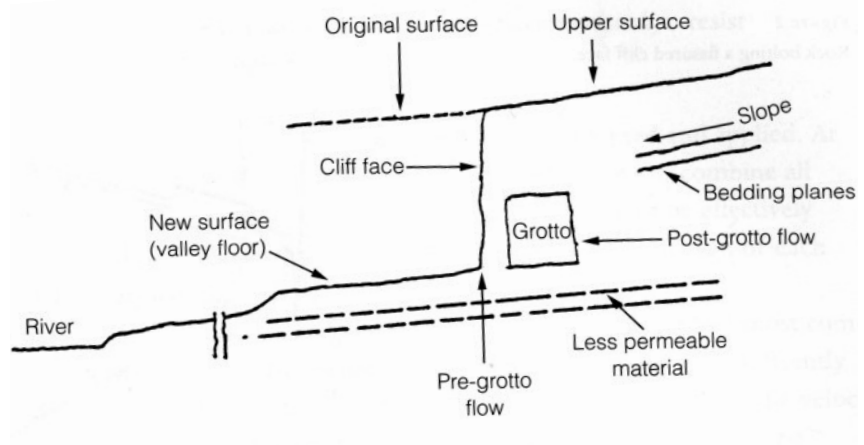
At the Mogao grottoes, the surficial deterioration is largely the result of wind and sand abrasion and clearly illustrates how a historically predictable rate of cliff recession can accelerate when uncontrolled. Understanding the deteriorative process at Dunhuang also suggests how it may be most effectively controlled. Sand deposits (dunes) above and behind the cliff face are continually being moved by the wind down the back slope above and over the cliff face itself. This action is, at least in part, responsible for the cliff's uniform recession. Accelerated erosion has occurred near the main site. Here, an anomaly has caused the sand flow to concentrate over a grotto, collapsing the grotto roof and creating an over-recessed condition. Well-intended attempts to control or eliminate surficial delamination have been undertaken in the past. The placement of a Ming-period pagoda and construction of a rock facing in the 1950s have succeeded in eliminating the recession of the cliff face at those locations. These remedies, however, have not stopped the recession of the back slope; and this recession has tended to channel the sand flow, causing accelerated erosion to areas where the cliff face mediation has not been undertaken. Attempts have also been made to control the rate of deterioration of the back slope by covering it with a cementitious material. These interventions have been entirely ineffective, however, because the hardened surface has broken down, allowing slabs of cemented sand to slide down the back slope.

The cliff face at Yungang has also receded. Here the recession is wind- and water-related, and block failures appear to have been common. Ming-epoch interventions to control cliff recession have been, and should continue to be, more effective than at Dunhuang, because the amount and effect of abrasive agents flowing over the adjoining cliff face at Yungang appear to be less than at Dunhuang.

Water intrusion

Grottoes located in regions where rainfall is considerable and groundwater tables are likely to fluctuate will experience variations in the moisture con-

Figure 1
Schematic cross section through the cliff face
at Yungang.



tent of the rock that constitute the grotto structure. At Yungang, water reportedly flows from the base of grotto walls during the rainy season. The natural geotechnical process that originally formed the cliff site selected for grotto excavation is both the main source of the problem and a resource for possible solutions.

A sandstone cliff face, as shown in cross section in Figure 1, is usually created by the formation of a river valley. Water will flow through the ground in the direction of the valley floor, especially if the bedding planes slope in that direction. The toe of the cliff will usually coincide with a change in the character of the sedimentary material near the valley floor, which is often less permeable than that of the cliff face. Water will descend to this less permeable stratum and then flow toward the river valley. Before the grotto was excavated, water would, because of the change in overburden pressure, tend to flow out at the intersection of the valley floor and the cliff face, contributing significantly to its recession. With the excavation of the grotto and the associated change in overburden soil pressure inside the grotto, the water intrusion point moved back to the intersection of the grotto floor and wall.

Understanding this water-flow pattern suggests two mitigation strategies: (1) remove or reduce the source of underground water, and/or (2) install an intercept that provides an alternative escape path for the subsurface water.

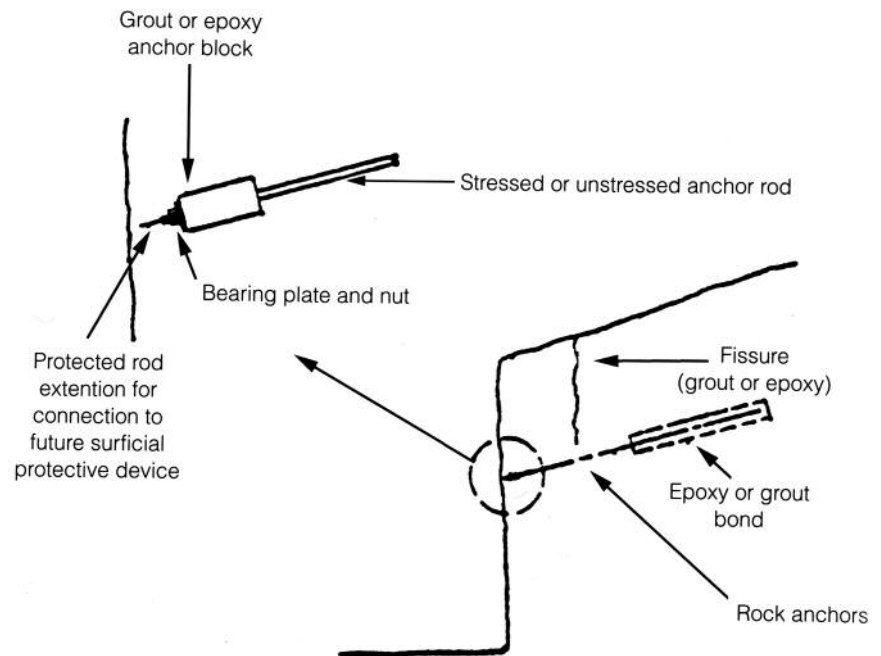
Alternatives for Cliff Recession Abatement

Cliff recession at Dunhuang

Cliff recession at Dunhuang is caused almost entirely by the abrasive flow of sand over the surface of the cliff face and back slope. The effectiveness of any abatement effort will depend on the quantity of abrasives it must resist. Accordingly, wind-tunnel studies and field experimentation directed toward reducing the flow of the sand should be pursued.

Surficial cliff protection alternatives should be installed when the experienced "average" recession rate cannot be tolerated for long or when accelerated recession is occurring or might reasonably be anticipated.

Figure 2
Rock bolting a fissured cliff face.



Where cliff recession rates can be tolerated but block failures seem likely, mitigation measures may be undertaken. Rock bolting, in conjunction with crack or fissure repair, may proceed in anticipation of the future addition of a surficial cliff-protection device. One means of accomplishing this staged abatement process is described in Figure 2.

Any slope or cliff face will recede if entirely unprotected. When a slope, such as the back slope at Dunhuang, is uniform, the rate of recession may be tolerable if the flow of abrasive agents over the surface is minimized. Cohesionless material will tend to erode unevenly, even on a regular slope, and this tendency will increase as surface irregularities develop.

Erosion control of otherwise stable slopes is a problem commonly encountered in highway construction, especially in areas where rainfall is heavy. Durability, cost-effectiveness, and maintainability are the principle variables with which abatement alternatives are measured. In many cases, the surfaces of stable slopes are irregular, as they are at Mogao, and this irregularity impacts the cost and effectiveness of erosion-control devices. Surficial back-slope treatments should be attempted at Dunhuang. Back-slope stabilization will not be easily accomplished here because the back slope contains topographic irregularities that will make the development of a uniform mitigation methodology difficult.

Slope erosion control devices may be broadly categorized according to the following objectives:

1. limiting the impact of erosive agents;
2. protecting or isolating the surface material with a covering device; and



Figure 3
Erosion control by controlled-velocity vertical channels and gradual swales at the Getty Center, Los Angeles.

3. improving the ability of the surface material to resist erosive agents.

Usually only one of these approaches is adopted and applied. At Dunhuang, the most effective solution will probably be to combine all three. Before describing how these methodologies might be effectively combined, the following summarizes the usual implementation of each method and its effectiveness.

Limiting the impact of the erosive agent is the method most commonly used to control erosion by water, since water will not significantly erode a surface if both the quantity flowing over the surface and the velocity of flow are controlled. This is accomplished by reducing the slope length and steepness and increasing its roughness. Time-tested methods include terracing and roughening the surface by plowing it across the slope. Channeling the flow of the erosive material is also a commonly adopted methodology. The construction of channels controls the velocity, direction, and location of flow. The introduction of gradual swales and controlled-velocity vertical channels is shown in Figure 3. Clearly, the aesthetic impact is significant. Swales and channels must be continuously maintained, as the concentrated flow, if allowed to deviate from protected paths, will cause local failures that may be of significant proportion. Treatment between swales, usually vegetation, must also be maintained in a manner consistent with the mitigation program.

Protecting or isolating the surface material from the erosive agent by installing a layer of concrete is a method commonly used to protect highways in Japan. The basic features of this technique include rock bolts that extend through loose surficial deposits and are anchored into firmer substrata; a mat of ferrous reinforcement placed over the surface material; and, finally, concrete applied over the existing surface. An appropriately designed and installed application, if maintained, should virtually eliminate longevity concerns. Unfortunately, concrete is not easily applied to difficult surfaces and volume changes in the material itself will cause cracks to form, especially where the surface is irregular and material thickness is not uniform. Cracks will allow water to penetrate, causing the reinforcement to rust and creating flow channels or piping in foundation material below the concrete. Thus, the protective device may itself become a significant problem. For example, the installation of a reinforced concrete surficial device at the Yulin grottoes near Anxi was in progress in 1991, and some of the difficulties described above are apparent in Figure 4. Given the extremely irregular nature of the exposed cliff face at Yulin, this type of surface protection is probably the appropriate solution, but its maintenance will undoubtedly be a problem.



Figure 4
Steel reinforcing laid on the surface in preparation for application of surficial concrete as an erosion-control measure, Yulin grottoes.

Improving the ability of the surface material to resist erosion is another alternative. *Bare-earth* erosion control is most frequently used on oversteepened construction slopes. The process involves spraying the exposed surface with a chemical, such as potassium silicate, that will bind the particles. The procedure is most effective in cohesionless materials such as sand, which is easily penetrated and readily absorbs a fluid. The

aesthetic advantages over the previously described alternatives are obvious, as is the impact on cost. Longevity then becomes the issue, which may be significantly improved in the design of a program that minimizes the impact of secondary actions, and through the introduction of nonmetallic fiber reinforcement. Periodic retreatment of the surface must take place, or the resulting problem may be worse than the original one.

The erosion of the back slope at Dunhuang is probably best controlled by integrating a bare-earth treatment with localized enhancements, provided topographic irregularities and anomalies—such as excavated grottoes—are considered and carefully incorporated into the program. The development of a bare-earth treatment program must consider how maintenance is accomplished and recognize that any surface hardening is likely to create a weakened plane below the zone of hardened material, which may result in a slide. These two considerations can be included in a general solution that maintains the aesthetics of the slope. The tendency of the hardened material to slide can be controlled by the introduction of either horizontal or vertical channels that are rock bolted into the firm underlying sandstone strata. These reinforced areas can then be tied to the surface strata by introducing nonferrous fiber reinforcement into the upper sands before the bare-earth treatment is applied. Reinforced areas should also provide access for construction and maintenance.

The treatment of anomalies will undoubtedly require a combination of solution methodologies. One example is the condition that now exists at caves 272 and 460. A cross section through this portion of the cliff (Fig. 5) graphically illustrates the problems. Major issues that must be addressed by any solution include the cracking and differential settlement in the roof of Cave 272, the expanding hole in the roof of Cave 460, and the accelerated erosion caused by the “river of sand” flowing over Cave 460.

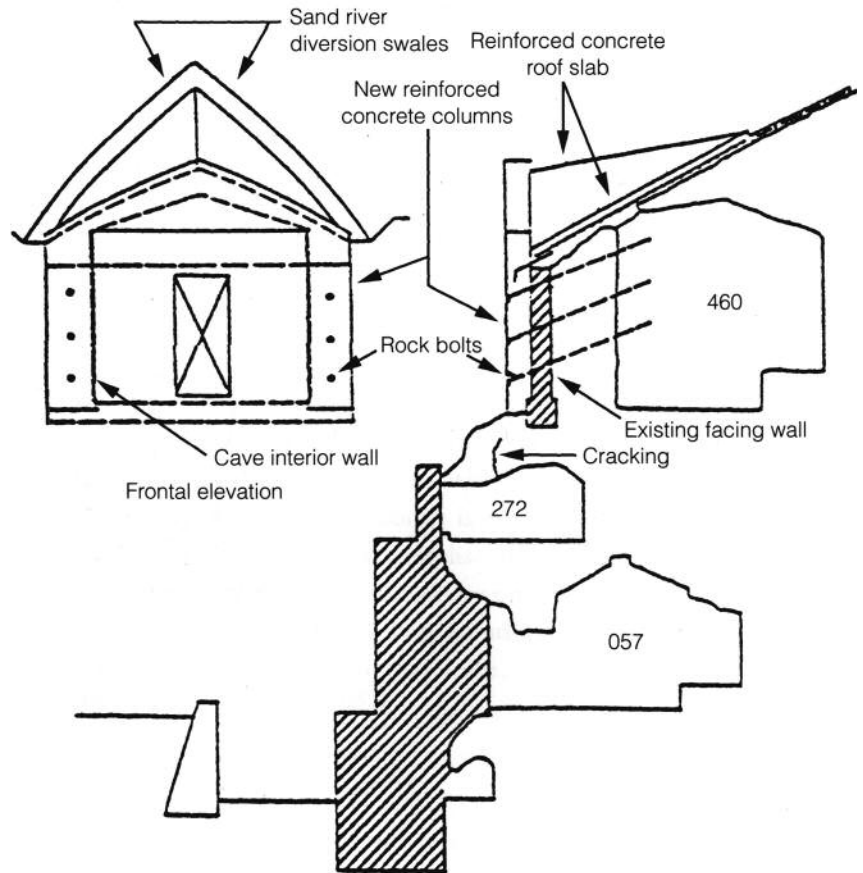
The elements of the solution illustrated in Figure 5 include

- the reinforcement of the cliff face by the installation of reinforced concrete buttresses;
- the installation of upward-sloping rock anchors, which secure the buttresses to the grotto facade and relieve the vertical load imposed on the roof of Cave 272;
- the integration of a new concrete roof structure supported by the grotto walls and new buttresses supporting the existing grotto roof structure; and
- the integration of reinforced concrete sand-diversion channels into the surficial treatment above the grottoes in the back slope; an alternative here would be a gunitite-reinforced surface applied locally.

Cliff recession at Yungang

The cliff recession at the Yungang grottoes appears to be almost exclusively attributable to block failure. The average rate of recession appears to be

Figure 5
Cross section of Caves 272 and 460 at Mogao.



about the same as at Dunhuang, although the rate is not regular. Block failures may be prevented by anchoring the separating block to the base material with rock anchors, as shown in Figure 2. At Yungang, fissure propagation is more rapid than at Dunhuang because rainfall is greater and the surface of the grotto roof tends to drain toward the cliff face. The effectiveness of any rock-anchoring procedure will require a thorough fissure-repair program and may be enhanced by a diversion of the surficial water flow above the grottoes.

Cave 19 at Yungang poses a special problem of cliff face delamination, as the roof over the grotto does not appear to be thick enough to safely accept rock anchors. Figure 6 shows a section of what remains of Cave 19, once the inner chamber of the original shrine. The antechamber no longer exists, as it was the victim of successive surficial block failures. Figure 7 shows an elevation of the extant exterior wall of Cave 19. The left side window once contained two smaller windows similar to those that still exist on the right side. Clearly, the structural deterioration of the facade is in immediate need of abatement. A physical enclosure of the grotto has been proposed, the primary intent being to control pollutant intrusion via fabric filters. The strengthening described in Figures 6 and 7 may be integrated into the facade development. The two major elements of the strengthening program are the provision of a vertical support for the grotto roof over the left window and the construction of a horizontal truss within the roof enclosure. The latter will provide lateral support for

Figure 6
Vertical section of Cave 19 at Yungang grottoes.

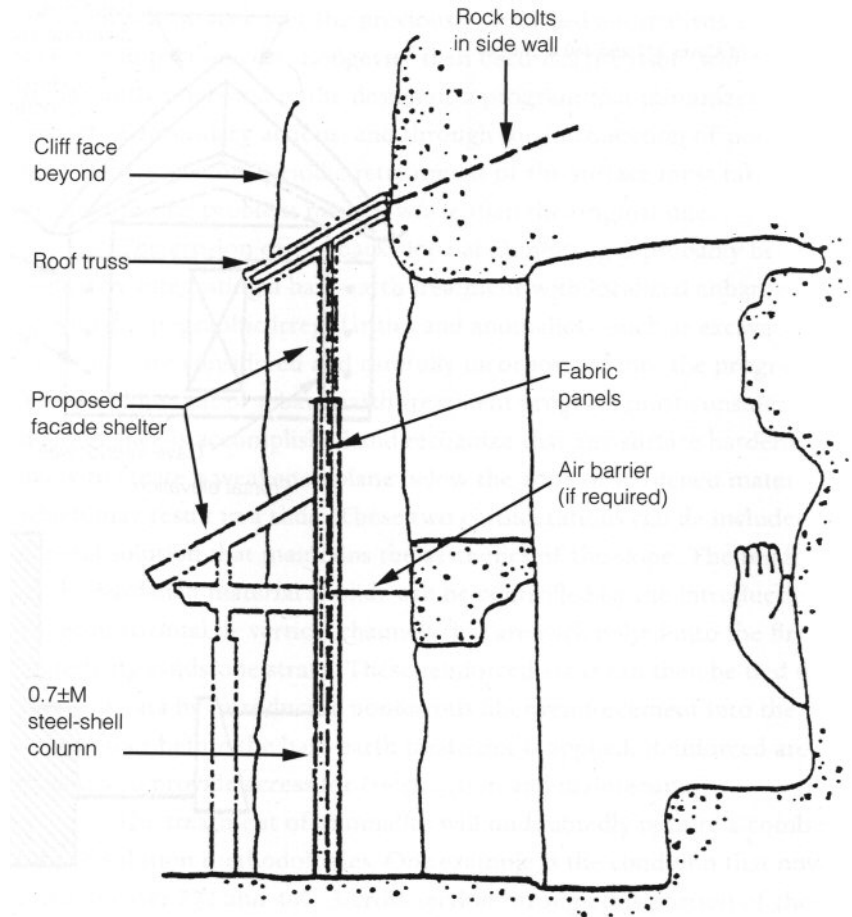
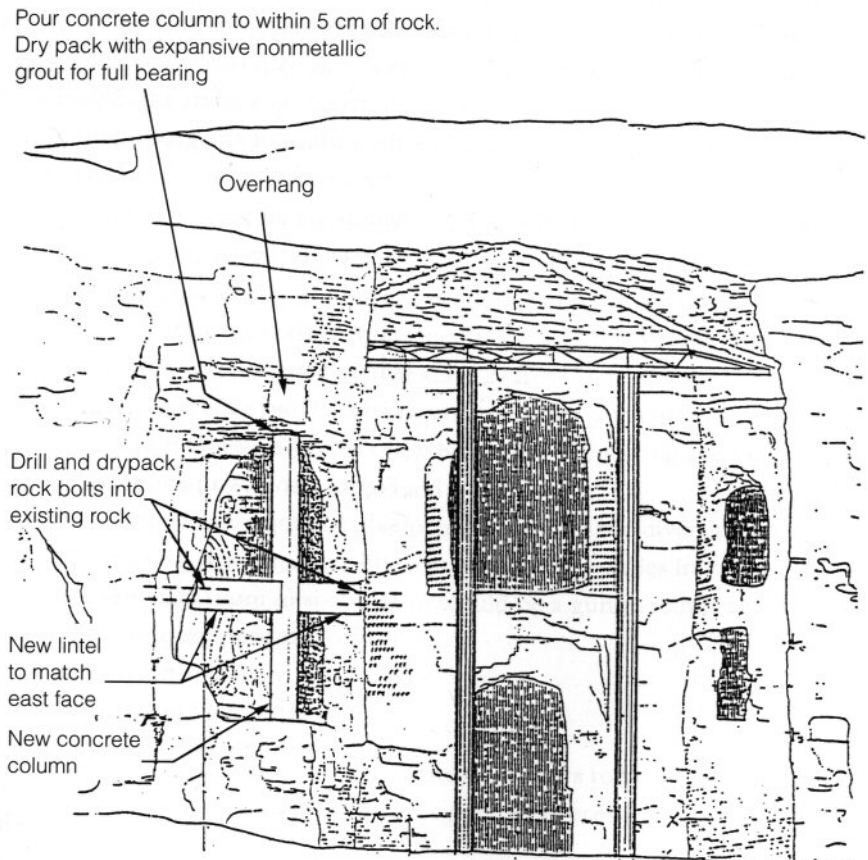


Figure 7
Frontal elevation of the extant exterior wall of Cave 19, Yungang.



the sandstone fascia over the door, allowing it to be anchored into the side walls of the grotto instead of the fragile roof of the grotto itself. The only constraints to the aesthetic objectives of this strengthening strategy will be the need to provide vertical support for the overhanging ledge at the left window and the provision of lateral support to the blocks of sandstone over the grotto entrance at the roof line. The latter support must be high enough to reach competent material that can be penetrated with confidence on either side of the grotto.

Planning for Erosion Abatement

Effective erosion-control programs at Mogao and Yungang and other grotto sites will require a significant effort in terms of engineering as well as cost. A variety of solutions do exist, however. Alternatives should be planned to the extent that feasibility is ensured and aesthetic impact and cost may be assessed. This accomplished, the most reasonable program will usually become clear. Creativity on the part of the conservator, engineer, and builder is essential. Easy solutions and “quick fixes” will often create more problems than they solve.

Water-Intrusion Abatement

Water mitigation at Yungang

Two mitigation measures have previously been identified: source reduction and flow interception. The amount of water that reaches an aquifer or water-bearing strata is a function of the permeability of the material overlying the aquifer and the extent to which water is allowed to accumulate on the surface. Source-reduction objectives must then typically focus on improving the surficial flow of water that would otherwise reach the aquifer and, where necessary, introducing an impermeable barrier.

Surficial flow can be improved by grading and the installation of drainage swales. This objective is contrary to that associated with erosion control, since the velocity of the surficial water must be maintained to minimize the rate of absorption. The appropriate slope will be a function of the soil characteristics and ground cover. Where the slope is not sufficient, concrete or a less permeable channel must be created to rapidly convey most of the water to the valley floor, thereby reducing the amount of water that will flow through the aquifer.

The permeable characteristics of the surficial soils can be altered chemically or through the introduction of geotechnical products such as geodrain or geomat. These are generic names for a particular type of sub-surface drain and an impervious polymer sheet, respectively, which create a barrier and reduce the velocity of flow that might otherwise be required to effectively remove the water at the surface. Geodrain is a fabric that captures and channels water to an included pipe, while geomat is essentially an impermeable barrier. The various approaches to improving surficial flow can be combined as shown in Figures 8 and 9. Before localized drainage solutions such as these are attempted, site geology and hydrology characteristics must be studied to ensure that the source of water reaching the aquifer has been identified.

Figure 8
Plan of proposed surface drainage-control system, Yungang.

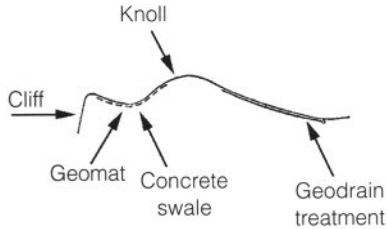
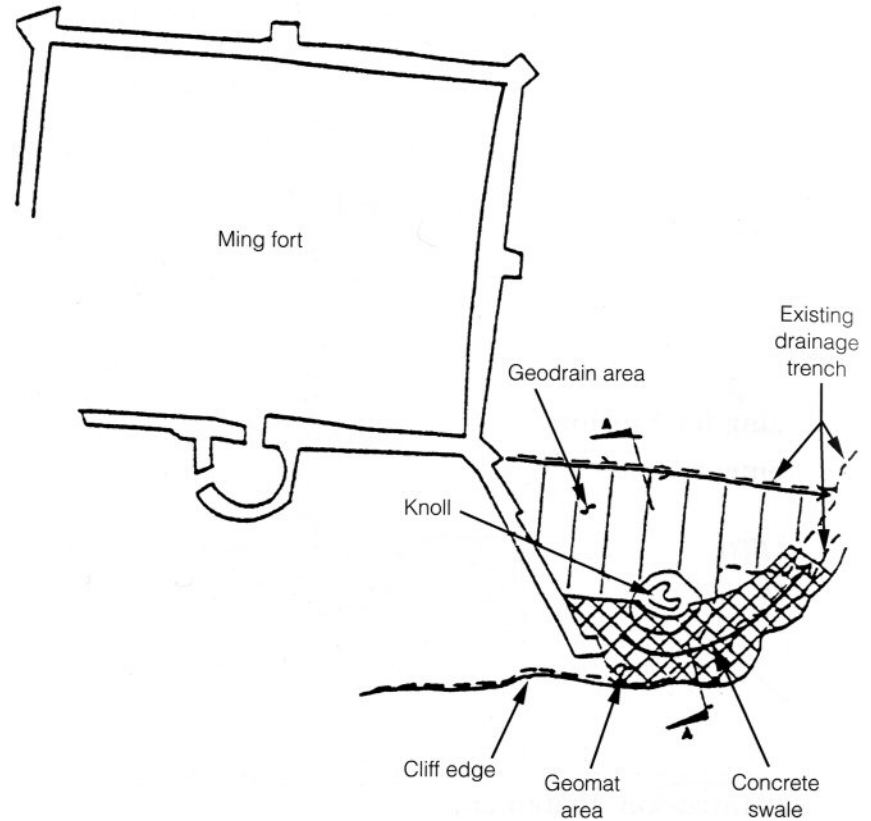


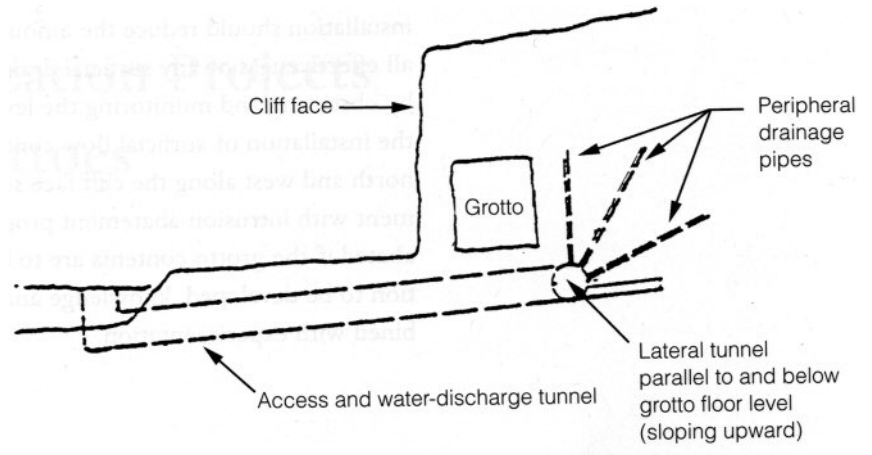
Figure 9
Schematic section of a proposed drainage-control system, Yungang.

Water interception can be an effective means of diverting the flow of underground water. This procedure involves the construction of a major access tunnel or tunnels from which a peripheral drainage system may be constructed. The major access tunnel usually serves as the drainage channel, collecting water from the peripheral tubes and discharging the flow beyond the area of concern. Advantages associated with a water-interception program include the ability to more accurately locate the aquifer and alter the intercept field until the objectionable flow has been eliminated. The conceptual development of a water-interception program is described in Figure 10, with a typical detail connection of a collector tunnel shown in Figure 11.

Planning for water mitigation

In general, source reduction will, if effectively accomplished, reduce the level of moisture experienced in the grotto walls as well as eliminate the water flow into the grotto. The major drawback is the difficulty associated with identifying the source of the water supply to the aquifer. If site geology and hydrology are complex, it is unlikely that the source of water to the aquifer will be sufficiently reduced by surficial treatments. Water interception, on the other hand, allows for an accurate location of the aquifer and its effective control. An effective, peripheral drainage system will rely on pressure relief much the same way as the subterranean flow was initially attracted to the grotto (Fig. 1). Accordingly, it may be impossible to

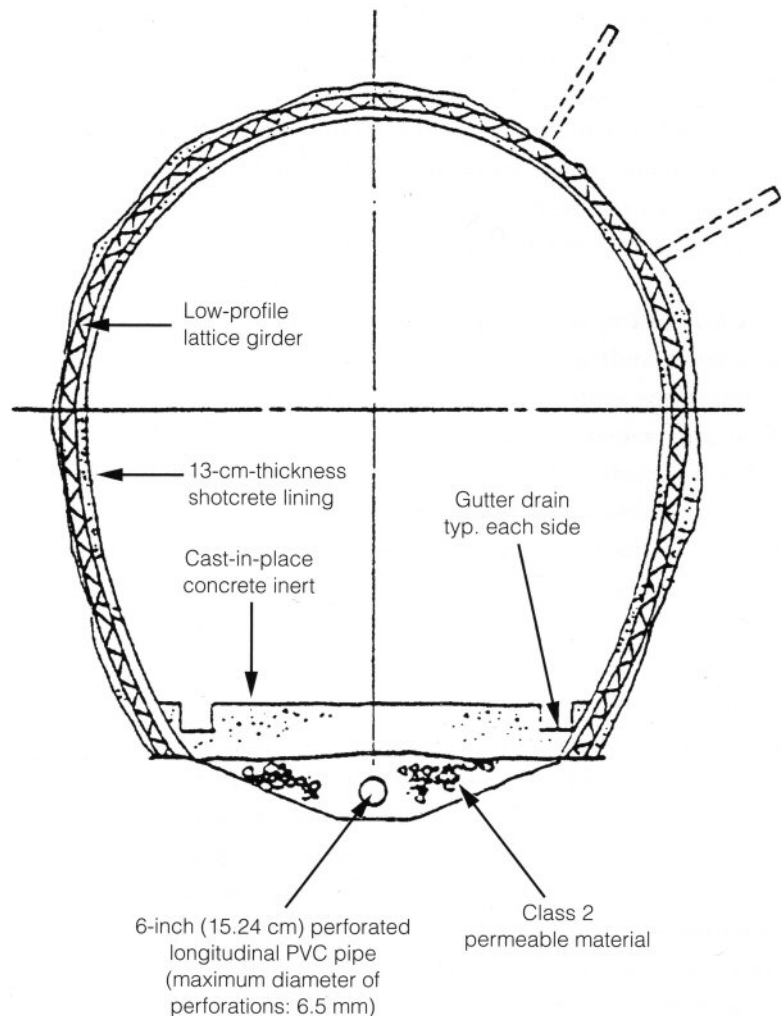
Figure 10
Schematic section of a conceptual water-inception system for Yungang.



control moisture occurring at the wall of the grotto since the grotto will, in effect, remain a pressure relief tube.

Each mitigation system has proved effective, depending on site characteristics. Site geology and hydrology are typically complex, especially in sedimentary formations. The drainage, or source-control, system illustrated in Figures 8 and 9 appears to have a reasonable chance of success. Its

Figure 11
Typical water-interception system used in tunnels.



installation should reduce the amount of water from the source. The overall effectiveness of any surficial drainage program will be determined only by observing and monitoring the level of subsurface water before and after the installation of surficial flow control devices. Similarly, the grottoes north and west along the cliff face seem to afford an opportunity to experiment with intrusion-abatement programs. Clearly, water intrusion must be abated if the grotto contents are to be preserved. For an appropriate solution to be developed, knowledge and experience must be effectively combined with experimentation.

Review of Stabilization Projects at the Mogao Grottoes

Sun Rujian

THE DECISION TO UNDERTAKE STABILIZATION of the Mogao grottoes was made by the Ministry of Culture in the autumn of 1962. On 20 November of that year, the Ministry sent a document to the Cultural Bureau of Gansu Province, noting that “with regard to the project for stabilization of the rock of the cliff, the Ministry of Culture has already reported to the Premier and applied for funds and materials. Design and construction are to be the responsibility of units designated by the Ministry of Railways.” Geological study, survey, and mapping began in November–December 1962.¹ Discussions of the stabilization plan and construction design took place in the spring and summer of 1963, and the construction team arrived at the Mogao grottoes site in June to begin the stabilization project.² In July 1966, after three years of construction work, the project was essentially completed. A length of 576.12 m of cliff face and 358 caves were stabilized or reinforced.

The first and second phases of the three-phase project had as primary objective the stabilization of the grottoes. The third phase was mainly devoted to building walkways outside the grottoes, integrating the first two phases of the project. Through a series of activities—beginning with experimental stabilization of the northern and southern sides of Cave 254 in the 1950s and ending with the completion of a fourth phase of the project in the 1980s—the danger of geological deterioration of the grottoes and related issues of visitor safety have been largely eliminated.

Basic Causes of Deterioration

The Mogao grottoes were excavated in the steep cliffs on the western side of Daquan River. The site is 1,680 m long and 20–25 m high and was excavated out of the Jiuquan stratum of the Quaternary period—a stratum composed of conglomerate, gravel, and sand, poorly consolidated with a little calcareous cementation. The Dunhuang region is characterized by lack of humidity and rain, great diurnal temperature differences, and the tendency of the rock formations to weather easily. On the national classification of seismic intensity zones, Dunhuang is a degree 6 seismic region. According to seismic records, seven earthquakes occurred between

1927 and 1960. Although they were not high on the Richter scale, they were of high frequency and were damaging to grottoes that had been excavated in close proximity to one another and in which there were rock fractures.

Deterioration of the Mogao grottoes is caused by a combination of environmental, geological, and human factors, as discussed in the following sections.

Cracks parallel to the cliff face

Cracks parallel to the cliff face and generally perpendicular to the ground pose a significant threat to the grottoes. The cliff was formed by action of the river cutting downward through the soft sediments. As the cliff formed, its outer face became a stress-release region, and cracks gradually developed parallel to the face. Excavation of the grottoes further weakened the rock, reducing stability and resulting in widening of the cracks. Under the combined action of the cliff's own weight and external forces, partial and strip collapses have occurred many times over the course of time. In an initial survey, twenty-three cracks and crevices were found in 157 caves on various levels in a 160 m section, from Caves 21 to 59. Cracks were mainly located on the third and fourth levels, and cut through 90 caves. Crack 13, between Caves 442 and 434, was 45 m long. On the basis of long-term observations, there were signs that this crack had grown larger before stabilization.³ Caves 289 and 290 on the second level; Caves 435, 436, and 438–442 on the third level; and the antechambers and main chambers of Caves 446 and 448 on the fourth level—all within the range of this crack—collapsed about a thousand years ago (Figs. 1, 2). Clearly, the existence and growth of crack 13 has constituted a serious danger to the safety of the grottoes within this section (Fig. 3). There are many other places in the caves where conditions are similar. Therefore, this is a form of deterioration in the grottoes to which special attention must be given in all stabilization projects.

Cracks perpendicular to the cliff face

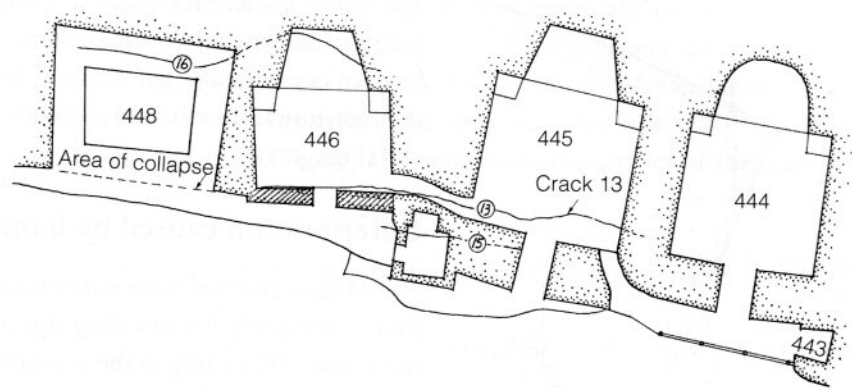
Structural crevices are generally perpendicular to both the ground and the cliff face and may have developed from bedrock joints. They occur at 5–20 m intervals. The orientation of the cracks has a relatively consistent pattern of direction, from the first- and second-level caves to the top of the bedrock and extending 2–9 m into the caves. Although they do not have as severe an effect on grotto safety as do edge crevices, they crosscut the bedrock and can cause large-scale grotto collapse if they happen to be present in the same area as the parallel cracks.

Other cracks

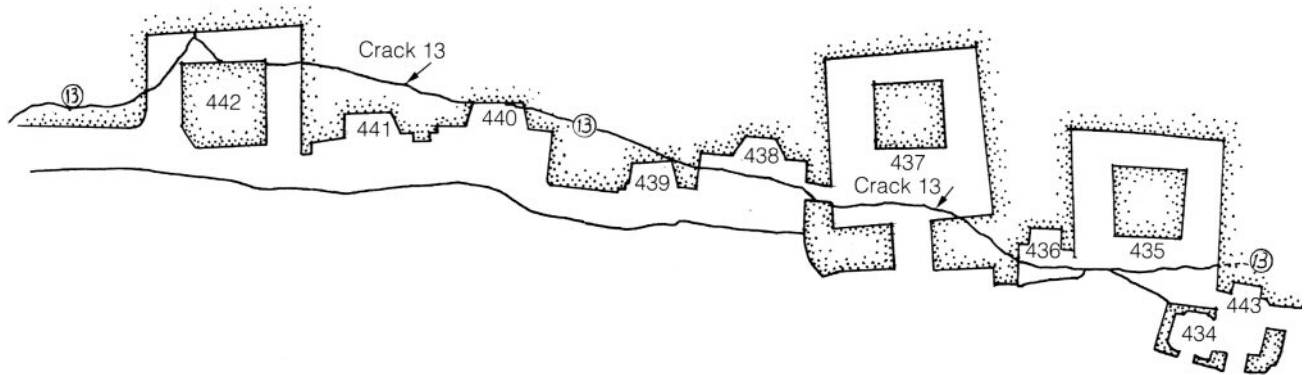
In addition to the two types of cracks already described, other vertical and horizontal cracks are found on the cliff faces. Vertical cracks are, for the

Figure 1

The front part of Caves 446 and 448, fourth level, section 3, collapsed along crack 13. The front adobe wall of Cave 446 was built in the Song dynasty. About 20 m on that level are affected by this crevice.

*Figure 2*

The front part of five caves (third level, section 3), with wall paintings dating from the Five Dynasties period, has collapsed. About 40 m on this level are affected by crack 13.



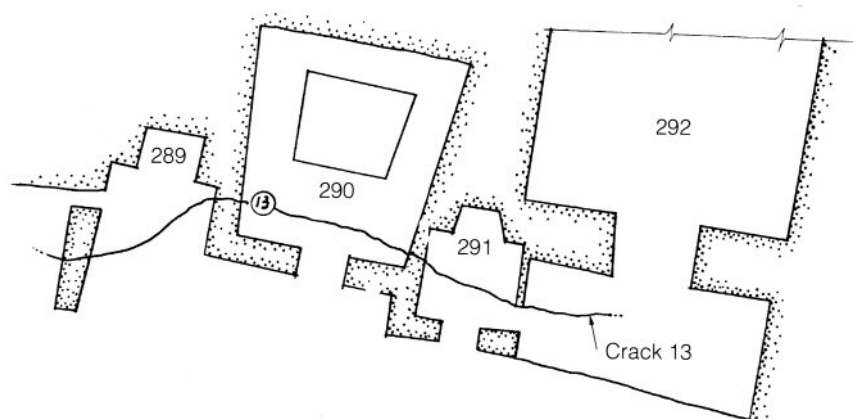
most part, seen at the tops of antechambers and corridors and are not particularly obvious. They were formed as a result of stress generated at the tops of the caves after excavation. Small-scale rock flaking readily occurs along the cracks. Horizontal cracks are produced by weathering and erosion of the thin layers of fine sand interspersed between the gravel layers.

Overhanging cliffs and unstable rocks

Resulting from the development of the types of cracks described here and the bedrock collapses, many unstable rock masses have been left overhanging the cliff faces. For example, there is a 55–65° negative slope of overhanging and fragmented upper bedrock above Caves 401, 402, 202–205,

Figure 3

Second-level caves in section 3. About 15 m are affected by crack 13.



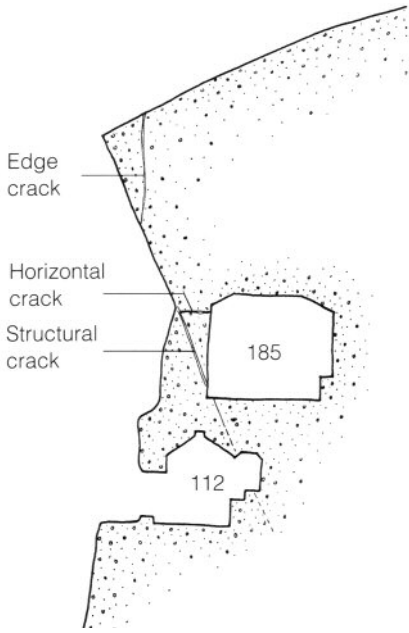
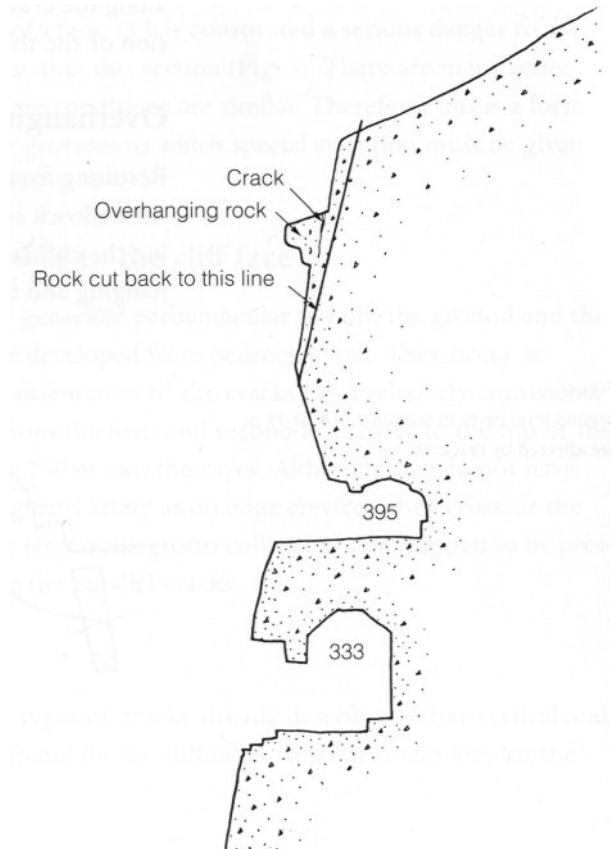
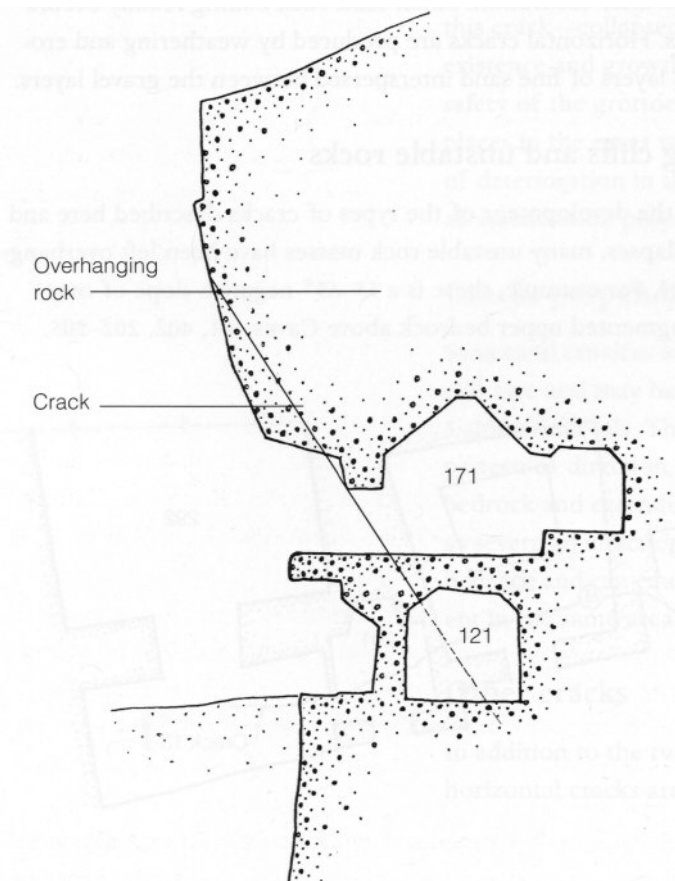


Figure 4, above
Section showing cracks of many types in the same vicinity.

Figure 5, below
Sections showing suspended rock masses and cracks, and reduction of dangerous overhangs by cutting back the rock face.



and 170–172. The rock edges of Caves 328–365 have been eroded over a long period by wind-driven sand and occasional rain. This has left many isolated overhanging rock masses; these subsequently disintegrate due to the moisture from rain and snow, and shed material that falls down the cliff (Figs. 4, 5).

Deterioration caused by human factors

The Mogao grottoes were constructed from around 400 c.e. to the latter part of the ninth century. Over this period of time, the cliff face, which is more than 900 m long in the southern part of the site, comprised a virtual honeycomb of caves. According to records of the time, all available space for excavation of grottoes had already been used up by the late Tang dynasty.⁴ In the region of early grotto construction, in the middle section of the southern area, three to four levels of caves are distributed across a sectional cliff 15–25 m high and 160 m long, from Caves 21 to 59. Of the early grottoes, these are in the best condition. There are 157 caves concentrated in this 2,500 m² cliff face, with one cave every 16 m², on average.

Altogether, there are 78 caves that represent the essence of the Tang grottoes. They are concentrated on a 2,100 m² area of cliff face, 140 m long, each cave averaging 27 m². Under such dense conditions, the middle and lower parts of the bedrock have been hollowed out, depriving the upper rock of firm support and creating conditions of instability. Moreover, the small grottoes excavated between the large ones have further weakened the stability of the outer face of the bedrock.

Prior to the Sui dynasty, grottoes were usually excavated in the upper part of the bedrock, specifically on the second and third levels. In the Sui dynasty, small caves were formed between the antechambers of the grottoes that already existed, for there was very little space remaining on the cliff face itself (Figs. 1, 2). Several typical examples of these small caves include

- Cave 425 (Sui dynasty), excavated between Caves 423 and 424 (Sui dynasty);
- Cave 426 (Sui dynasty), inserted between the antechambers of Caves 424 and 427 (Sui dynasty); and
- Cave 430 (Northern Zhou dynasty), cut between the antechambers of Caves 428 and 431 (Northern Wei dynasty).

The formation of caves such as these often caused damage to surrounding structures. For example, two small Sui dynasty grottoes, Caves 433 and 434, were excavated between the antechambers of Caves 432 (Western Wei dynasty) and 435 (Northern Wei dynasty) (Fig. 3). After the small caves had been excavated, the wall thickness was only 10–30 cm, severely weakening the rocks between the caves. Similar damage was caused between grottoes produced on different levels, as in the case of Cave 292 (Sui dynasty), situated below Cave 435 (Northern Wei dynasty). Since the rock that serves as both the roof of Cave 292 and the floor of Cave 435 is rather thin, the floor in front of the central pillar in Cave 435 (on the northern side of Cave 436) collapsed under the pillar's weight. Similarly, Cave 44 (Tang dynasty)—the antechamber of which runs 6 m into the cliff face—was excavated beneath Cave 290 (Northern Zhou dynasty) and Cave 289 (Sui dynasty) to the south of it. The weight of the wall separating Caves 290 and 289 (60 cm thick) is concentrated on the middle portion of the roof plate of the antechamber of Cave 44, and the force produced by the load caused the collapse of the front parts of Caves 290 and 289 (Fig. 6a, b). There have been many similar cases. Some of the unstable factors resulting from grotto excavation have been located and resolved. However, some may not have been discovered yet, posing a hidden threat to the long-term survival of the grottoes.

Stabilization Measures

As early as 28 June 1954, the existence of various forms of damage and deterioration of the grottoes was pointed out by the Ministry of Culture in a letter to the Dunhuang Cultural Relics Institution:

The most serious problem at the moment is that the grottoes themselves are in danger of collapsing due to geological causes and that the wall paintings and statues are being constantly eroded by wind, sand, snow, and water. Therefore, it is necessary to keep up our good efforts in the preservation and repair work.

The government departments responsible for cultural relics were required to reinforce the grottoes, to eliminate the threats to the grottoes

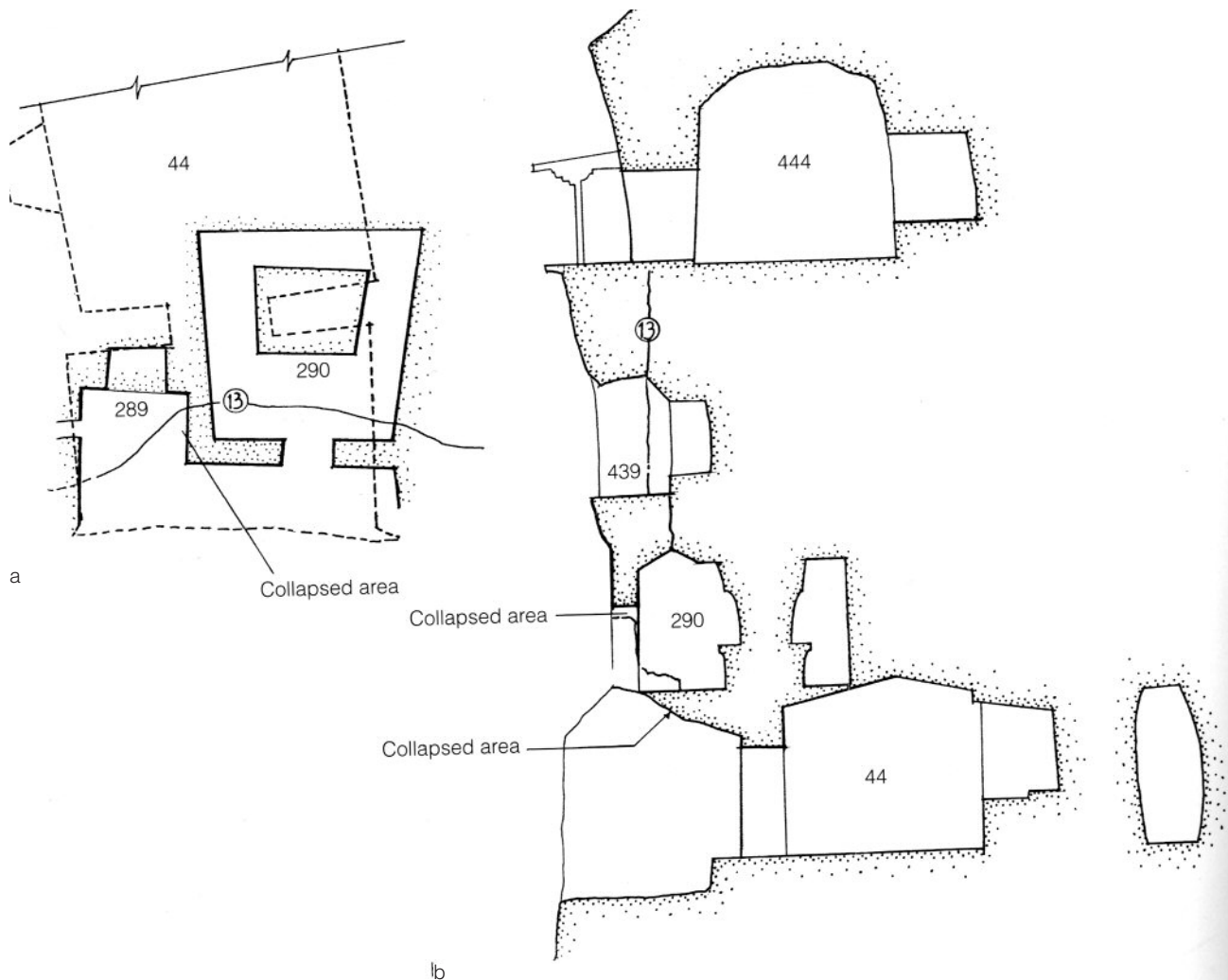


Figure 6a, b

Plan (a) and cross section (b) showing the relationship between deterioration of Cave 44 and Caves 289 and 290. The wall separating Caves 289 and 290 fell onto the roof of the anteroom of Cave 44, collapsing the left side of Cave 289 and the front part of the right side of Cave 290. Cave 44 was created during the Tang dynasty, with a span of nearly 8 m and a depth of 5 m. The excavation of this cave caused the front part of Caves 289 and 290 to collapse.

caused by deterioration, and to preserve the original style and features of the grottoes as far as possible. Many discussions were carried out in the spring and summer of 1963, and programs were proposed based on existing construction technology and on the patterns of occurrence and development of deterioration in the grottoes. Several of these technological measures are as follows:

Roof support

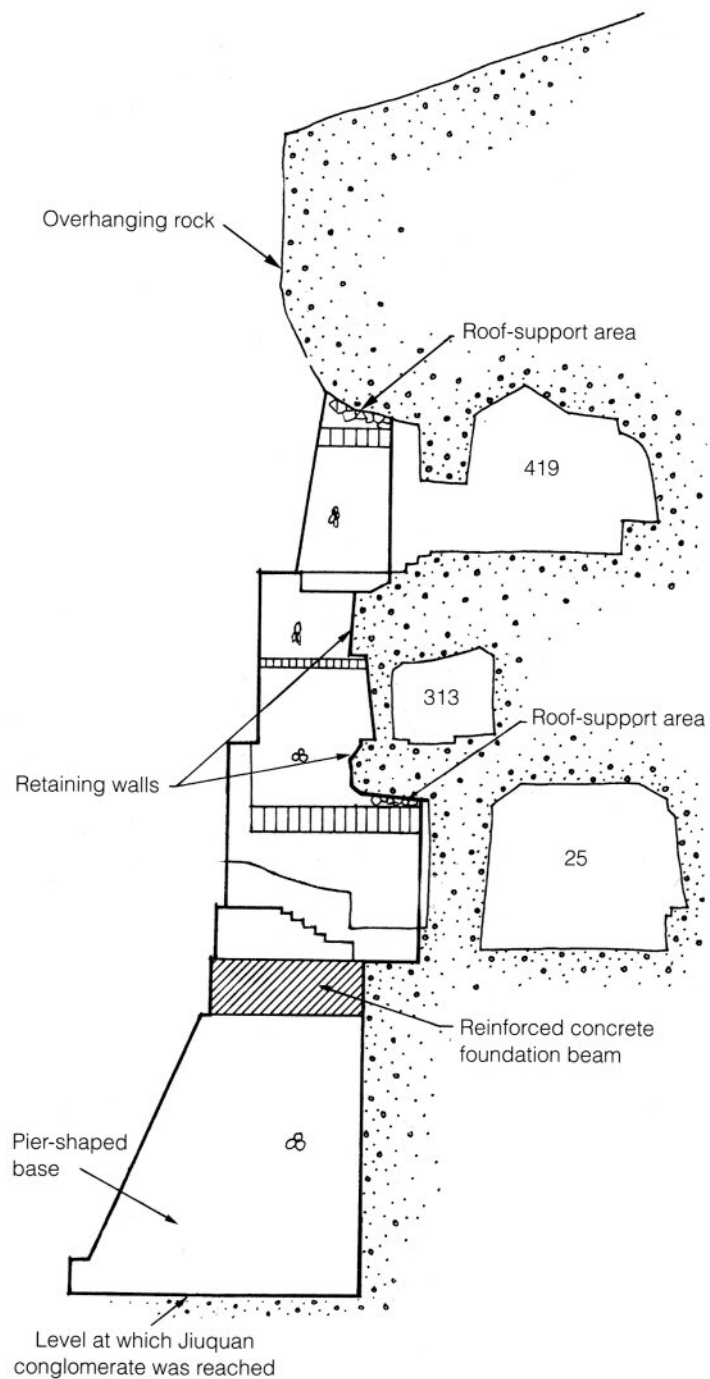
Since most Mogao grotto antechambers are open on one side, each antechamber roof is supported on only three sides by bedrock, and the front roof section is in a state of virtual suspension. If the antechamber has a wide span and runs deep into the cliff, horizontal cracks often develop in the roof, resulting in eventual collapse and the formation of an arch where the plane of collapse intersects the antechamber. Sometimes cave-ins in the antechambers of the lower caves directly affect the stability of the upper ones. Under these circumstances, stone slabs or reinforced concrete pillars have been used to provide support for suspended masses. In several stabilization projects, roof support measures were taken to pre-

vent further deterioration in the antechambers of Caves 351, 342, 334, 202–205, 218, 217, 61, 171, and 172, among others (Fig. 7).

Retaining walls

Retaining walls or buttress walls built with large stones or reinforced concrete have been constructed in front of the sloping faces of the grottoes to resist the lateral pressure of earthquakes and prevent bedrock from buckling outward along cracks parallel to the cliff. In the Mogao grotto stabilization projects, this retaining technique has been extensively

Figure 7
Section through a portion of a retaining wall.

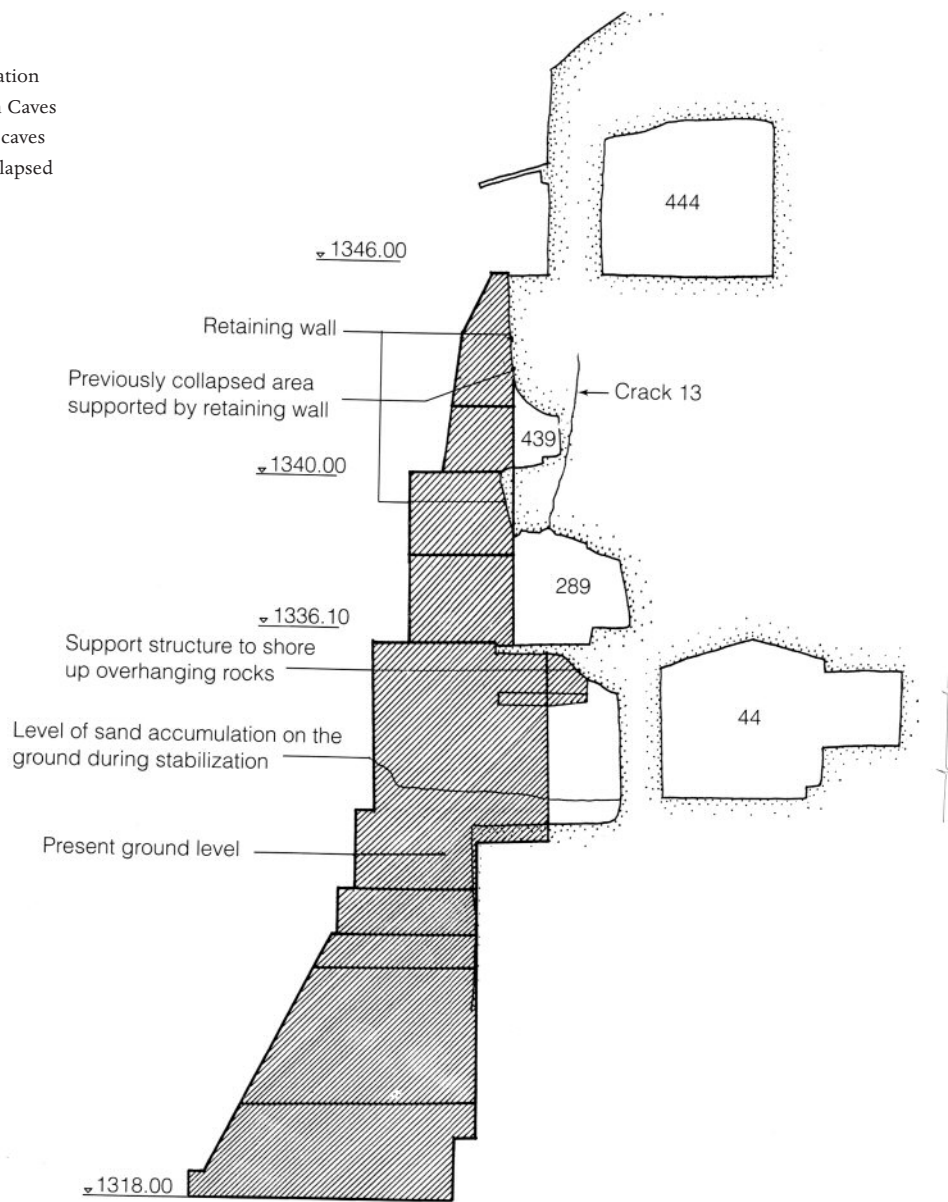


employed and has been an important means of preventing bedrock from collapsing (Fig. 8). When a retaining wall is designed, architectural style must be determined while mechanical and structural requirements are simultaneously met. Practical installations, such as scaffolding with wooden walkways, were constructed to facilitate the work.

Reduction of overhangs

Unstable and dangerous external overhanging rock masses were reduced or rebated by chiseling. This was done not only to remove precarious rocks from the cliff edge but also to reduce the load on the bedrock (Fig. 5).

Figure 8
 Section showing retaining-wall stabilization and support on the four levels between Caves 289 and 439. The front part of the five caves to the north and south of Cave 439 collapsed long ago.



Combined techniques

The following techniques were designed to combine roof-support and retaining-wall measures. Depending on the condition of the cliff face, support systems fall into three general categories: post-and-lintel, pillar, and retaining-wall structures. Post-and-lintel structures act only as apex supports. The base is built directly on the rock floor, and the lintel stone slabs are placed in close contact with the overhanging bedrock. When pillars are used, they are placed away from the antechamber walls to protect wall paintings. The retaining wall is used when stabilization of a fairly large area of the grotto cliff face is necessary. To satisfy various mechanical requirements, the retaining-wall structure should have sufficient mass and strength, and yet leave room for grotto entrances. It should be broader at the base and gradually decrease in cross-sectional area from base to top, forming what is essentially a pyramid-shaped stairway on which walkways can be built on different levels (Fig. 8).

Treatment of Foundations and Construction of Settlement Joints

In the process of stabilization, an effort was made to build all the supporting structures on bedrock. In some individual sections with overhanging rocks, however, the area requiring support was inevitably rather wide, and the support structure needed to be enlarged accordingly. If all such foundations had been built entirely on bedrock, it would have been necessary, in some cases, to construct foundations tens of meters thick. To solve this problem, an enlarged base area would be laid down first and observations made as to its degree of subsidence into the compressible, sandy soil below. Then the support structure would be constructed to a corresponding distance below the roof rock to be supported. After a period of gradual settling and establishment of relative stability, the space between support and roof would be filled. At that point, a tight support of the bedrock roof could be achieved. This mode of construction was used to support the roof of the antechamber of Cave 171.

When a support structure needed to be wide enough for part of it to stand on bedrock and the other part on compressible soil, two separate foundations were constructed with settlement joints between them (Fig. 9). Since the outer parts of a structure may also settle to a certain extent, those areas of the foundation should be established on the same soil to maintain a uniform degree of subsidence for the entire structure. If a fairly large area and variable foundations were required, a horizontal deformation joint should be constructed every 20–30 m to serve as both the expansion and settlement joints.

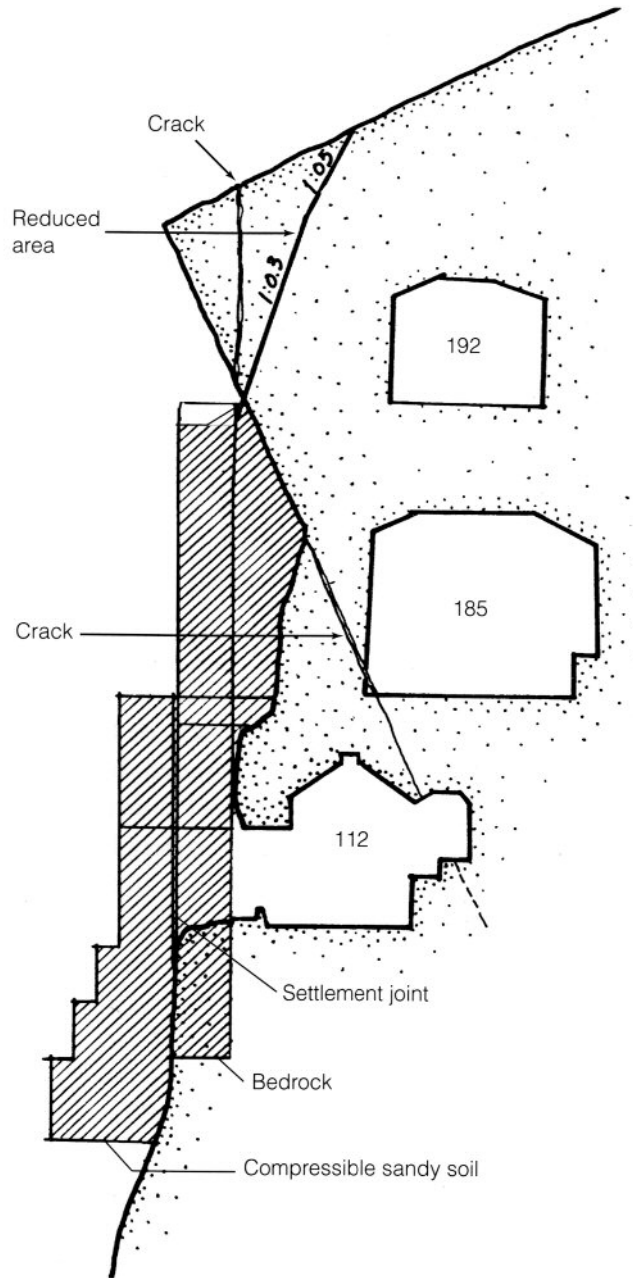
Conclusion

In reference to the Mogao grotto stabilization project, the cultural relics administration stated:

The principles of engineering design should give priority to ensuring the safety and stability of the grottoes and, at the same time, take into account

Figure 9

Section showing the foundation of a retaining or buttress wall. The foundation of the retaining wall outside the settlement joint is on compressible sandy soil. Reduction or rebating of the unstable, cracked section was carried out to remove dangerous rock and to reduce load.



the question of aesthetic style, so that major changes will not be made to the appearance of the Mogao grottoes. Therefore, it is essential to bring the structures of the stabilization project into line with the original style of the grottoes and make the utmost effort to preserve their original appearance.

On 9 August 1963, the late architect Liang Sicheng noted in his *Comments on the Dunhuang Conservation Project Program* (1963:239):

Our main focus today is to build walls and basically preserve the appearance of the grottoes, which is the best we can do. Therefore, I endorse this general principle. . . . As far as I can see, everything of major value is housed inside the grottoes. . . . Our objective is to protect what is inside the grottoes by stabilizing them from the outside, and this objective of ours should be thoroughly understood.

After implementation of this project, which grew out of continuous investigation, a uniform style and local variations were achieved. The retaining walls follow the contour of the cliff face and rise and fall according to stabilization requirements and locations of the grottoes. The external wall paintings on the cliff face were preserved to the greatest extent possible, and all the exterior Tang and Song dynasty eaves were suitably protected. Railings, built with reinforced concrete, were installed on the walkways built outside the caves on all levels, presenting a visual contrast to the solid and often massive retaining walls. The concrete of retaining walls was given a sand-and-gravel-textured surface, in imitation of the conglomerate surface of the cliff itself, to provide a more natural appearance and avoid a monotonous texture for the exterior of the site.

Upon completion of the stabilization projects, access between caves was improved. Along with the structural changes, the walkways between the caves were built to take advantage of the engineering features. These included the various levels of step-shaped retaining walls with supporting cantilever beams protruding from them. Generally, the three stabilization projects implemented from 1963 to 1966 aimed at ensuring the safety of the grottoes. The rational approach not only solved the problem of access between caves but also gave rise to a solid, stable, simple, and graceful architectural style that did not overemphasize architectural form or decorative aspects and harmonized with the original appearance of the grottoes.

Between 1984 and 1985, these principles were again followed in reinforcing the twenty-six caves in a 172 m section to the south of Cave 130. The conservation of this area—the most desolate and dilapidated of the Mogao grottoes—marked the initial completion of the stabilization projects and the macroconservation stage of the site. This created favorable conditions for overall scientific research on further aspects of protection of the Mogao grottoes, as well as for the conservation of Chinese cultural heritage.

Notes

- 1 From 1 November to 31 December 1962, the Dunhuang group of the second survey team under the First Design Institute of the Ministry of Railways carried out on-site engineering, hydrological investigations, and grotto surveys at the Mogao grottoes.
- 2 The Bridge and Tunnel Division of the First Design Institute carried out the design according to the directions of the Ministry of Railways and the Ministry of Culture. The construction team was organized by the First Construction Division of the Urumchi Railway Bureau, under the Ministry of Railways.
- 3 Two obvious cracks were measured in Caves 438 and 445. They widened from 0.5 mm in 1959 to 1.0 mm in 1962.
- 4 Recorded in the *Tablet of Zhang Huaishen* of the late Tang dynasty, kept in Cave 17 of the Mogao grottoes.

Reference

- Liang Sicheng
- 1963 *Comments on the Dunhuang Conservation Project Program*. Vol. 4 of his collected works. n.p.

Stabilization and Consolidation of the Kizil Grottoes

Jiang Huaying and Huang Kezhong

THE KIZIL GROTTOS, located 50 km east of Baicheng county, Xinjiang Uygur Autonomous Region, were excavated during the third to the ninth century C.E. and are considered a jewel of the ancient Silk Road. The murals, sculptures, and architecture of the grottoes illustrate how Chinese Buddhist art was adapted from foreign grotto art. The scope of this site is second only to that of the Mogao grottoes at Dunhuang. The Kizil grottoes provide important data for the study of art history and the history of cultural exchange between China and foreign countries and are of great significance among the grotto sites of China.

This artistic treasure has been subjected to more than a thousand years of damage caused by natural weathering, looting, and ravages that occurred during foreign invasions and religious wars. Wall paintings and clay sculpture in the caves have been destroyed by weathering, damaged by knife and ax blows, blackened by smoke, and burned by fire; only a few wall paintings in the caves remain relatively intact.

After the founding of the People's Republic of China, the Kizil grottoes became a matter of great governmental concern. Because the caves were excavated in a loosely cemented rock formation, the strata tend to collapse when affected by water. In addition, prolonged erosion by natural forces has resulted in the development of ravines above the grottoes and cracks inside the caves. Rainwater seeping into the caves has caused extensive salt efflorescence, flaking, and separation of the wall paintings from their support. Roof collapse and rockfalls are common. In a preliminary survey of the caves, most of the front chambers were found to have collapsed, and the temporary suspended walkways were very shaky.

In 1986, a conservation team was invited to undertake the task of planning the restoration and reinforcement of the Kizil grottoes (Kizil Design Group 1987). Work was formally begun in 1988, after two years of surveying damage, conducting on-site experiments, and evaluating plans. In 1989, the work of reinforcing Caves 2–30 and 31–48 (the first and second repair and stabilization phases, respectively) was completed. After an initial inspection, the reinforcement was found to be effective and the quality of the construction complied with design requirements. Following is a summary of the principal working methods used.

Geology

The Kizil grottoes are located in the contact zone between the Kuche Baicheng depression and the Qiulitake uplift of the east-west Tianshan complex tectonic zone on the north side of the Weigan River. Two active faults are located at the south bank of the river but are not considered significant, as the tectonic stresses at the grotto site itself are relatively stable.

On the basis of records published in 1985 on seismic activity in Xinjiang, an earthquake greater than magnitude 6 on the Richter scale has not occurred over the past 270 years in this region. Because of the frequent low-magnitude earthquakes in the Baicheng and Hojing seismic zones, it is considered unlikely that an earthquake of magnitude 7 or greater will occur in this area over the next 100 years. The danger of an earthquake with a magnitude around 6 does exist, however; and the area is currently designated as a magnitude 8 earthquake zone.

The strata of the grottoes are Pliocene epoch (N_2^4), grayish brown and grayish yellow sandstone interbedded with mudstone and occasionally with conglomerate showing significant variation in the lateral facies. The strata consist of 70% sandstone and 30% mudstone. Sandstone contains approximately 36.5% calcium carbonate along with soluble salts, such as calcium bicarbonate, $Ca(HCO_3)_2$; magnesium chloride; sodium chloride; and gypsum. The rock is weak, with a poor degree of cementation by calcareous materials; it crumbles into sand when wet. The mudstone is mostly silty with a relatively low degree of cementation. The cement is carbonate (26.41%) and organic materials. X-ray diffraction analysis of the clay suggests that it consists mainly of calcium and magnesium montmorillonite (5.72%), illite, and trace amounts of kaolinite. This argillaceous rock expands on contact with water and weathers easily.

The mechanical strength of all the rock is extremely low. Point-load tests show that the tensile strength of the weathered sandstone is 0.66 kg cm^{-2} and the compressive strength is 13.93 kg cm^{-2} . The tensile strength of the semiweathered sandstone is 0.86 kg cm^{-2} , and its compressive strength is 18.23 kg cm^{-2} . The tensile strength of the semiweathered mudstone is 23.58 kg cm^{-2} and its compressive strength is 497.8 kg cm^{-2} . The large area of collapse at the Kizil grottoes was caused by weathering of the poor rock quality.

State of Deterioration

The Kizil grottoes consist of 236 caves distributed over a distance of 2 km. Muquan canyon divides the site into four natural areas: west, east, the interior, and the area to the rear of the mountains. The caves have suffered severe deterioration and damage. About 60% of the caves have exposed main chambers caused by the collapse of the front chambers. Even some of the relatively intact caves are in danger of collapse. Preliminary assessment showed that only ninety-two caves with murals and statues, four with inscriptions, and forty-five relatively complete monks' chambers remain intact. Many types of damage are apparent around the grottoes, the primary causes of deterioration being crisscross cracks in the rock and water erosion.

The Kizil grottoes were cut into a steep cliff face. The weight of the rock itself, its geological structure, and the force of the lithification process have produced natural stresses inside the rock; in other words, irrespective of the caves, the rock is constantly being subjected to natural stresses, and the state of these stresses changes over time. If there are no large-scale disturbances, these stresses will gradually stabilize throughout the rock. The introduction of the caves disturbed the stress field of the rock body, redistributed the stresses, and introduced new avenues of energy release that formed many sets of cracks.

In the grotto area, there are two sets of cracks. One set of cracks, caused by tectonic movement, consists primarily of shear fractures with a northwest strike of 330–340°. The other set consists of tensile cracks, generated after excavation of the grottoes, parallel to the cliff face to the west and east of the canyon, with a northwest strike of 290–330°. These two sets of cracks crisscross each other and cut the cliff rock into many fragments of different sizes. Inspection of the main 111 caves revealed that 59 caves have cracks, and some have three or more. Many caves are cut all the way through by cracks. The action of external forces and weathering on the fragmented caves have caused many of them to collapse progressively from the outside walls toward the inside. Precarious overhanging rocks can be found almost everywhere within the grotto area. In the area west of the canyon, there were eleven locations with unstable overhanging rocks of about 314 m³ in total volume.

Water erosion has damaged the caves in two ways. First, heavy rain and floodwaters created numerous gullies on top of the grottoes and in the cliff rock. The preliminary assessment revealed about seventeen large gullies and thirty-two small ones within an area of 1 km². These gullies cut into the cliff rock, making collapse inevitable. Some of the gullies penetrate the roofs of caves and allow water infiltration that erodes the surface of the rock and causes spalling of the wall paintings.

A horizontal hole was drilled in a weathered zone in the western region of the Kizil valley, and a weathering depth of about 2 m was found. During heavy rain, the rainwater—combined with large amounts of mud—flows straight downward, and sand carried by the water produces scratches, grooves, and mud stains on the murals. Analysis of the archaeological data showed that about 2–6 m of the cliff face had already collapsed. A large quantity of collapsed rock—along with the mud and sand that had washed off the top of the grottoes—buried many caves and blocked entrances, posing problems for protecting the grottoes, as well as severely limiting access for visitation.

Reinforcement

Reinforcing the Kizil grottoes was a large-scale repair project. The geological and geographic environment of the grottoes is complicated, and the project was difficult and dangerous. The design and implementation of the entire project were based on the results of rigorous scientific experiments. Detailed surveys of the grottoes, repeated tests, and consultation with

experts were used to develop a comprehensive plan that involved a combination of roof support, anchoring, and chemical consolidation.

Anchoring of unstable rocks

Anchoring involved the insertion of metal bolts of different lengths into the rock body. These bolts penetrate cracks to anchor precarious rocks against firm bedrock. In the course of repairing and reinforcing the caves, the degree of stability of the caves was found to be related to that of the mountain as a whole. The caves are surrounded by mountain, and it was necessary to stabilize the mountain to ensure the safety of the grottoes. The anchoring method must make full utilization of the strength of the rock strata, release stress concentrations, and inhibit further development of tensile cracks. To ascertain whether the anchor bolts could provide sufficient anchoring force, and whether the depth of the anchoring was suitable in the particular rock of the Kizil grottoes, the Gansu Construction Research Institute and the Gansu Fifth Construction Engineering Company were asked to perform extraction tests of the anchor bolts. The tests were carried out on sandstone in the vicinity of Cave 30 and on mudstone in the vicinity of Cave 80, west of Muquan canyon. Sixteen-gauge, cold-drawn, manganese spiral-steel rods with a design strength of $4,500 \text{ kg cm}^{-2}$ were used. Bolt no. 257 was anchored in sandstone and bolt no. 156 was anchored in mudstone. The results of the extraction tests are shown in Table 1.

When the anchor depth in the sandstone reached 50–60 cm, the extraction-resistance force was about 14 t, demonstrating a sufficient anchorage strength. In mudstone, however, the design-required anchorage strength could not be obtained until the depth was 110–160 cm. During the experiments, it was found that bolts could be easily inserted into 100–200 cm deep drill holes, which were filled with ordinary concrete and compression grouting. However, it was difficult to insert the bolts by hand into holes 300–400 cm deep because of the strong water-absorbing capacity of the Kizil sandstone; the concrete grout lost water quickly to the surrounding rock, causing the concrete to become less fluid. The problem was resolved by either wetting the holes before grouting or using another type of water-retaining concrete. Results demonstrated that reinforcing dangerous loose rock with bolts is effective and feasible.

Protection by consolidation

The collapse of some of the Kizil caves is directly related to the physical and chemical properties of the rock itself and to the erosive action of natural weather stresses of the external environment on rock. To slow deterioration, the rock surface was treated with a protective chemical consolidant to inhibit weathering and to increase its strength and water resistance.

Three types of materials—organic (methyltrimethoxy silane), inorganic (potassium silicate), and a mixed organic-inorganic (of the first two)—prepared in fifteen formulations were tested on the basis of the

Table 1 Test results on rock bolts grouted with standard concrete

Sample No.	Rock bolt			Pull out test						Bolt-yielding characteristics
	Diameter (cm)	Yield strength R_g (kg cm^{-2})	Anchoring depth (cm)	Hole diameter (cm)	Pulling force P (kg)	Stress on bolt σ_a (kg cm^{-2})	Cohesion between bolt and grout	Cohesion between hole and grout	σ_a/R_g	
A-1 ^a	1.8	4565	54	5.4	15000	5893	49.18	16.37	1.29	Bolt yielded and pulled out of grout.
A-2					15000	5893	49.18	16.37	1.29	
A-12					1400	5500	45.90	15.28	1.20	
A-3	1.8	4565	54	5.4	13600	5343	44.59	14.86	1.17	Bolt broke and pulled out of grout.
A-4					14000	5500	45.90	15.28	1.20	
A-5					14000	5500	45.90	15.28	1.20	
B-1 ^b	1.8	4565	54	4.5	6000	2357	19.67	7.86	0.51	Bolt and grout were pulled out together.
B-2					7000	2750	22.95	9.17	0.60	
B-3					6000	2357	19.67	7.86	0.51	
B-7	1.8	4565	108	4.5	13500	5304	22.13	8.84	1.16	Bolt and grout were pulled out together.
B-8					13000	5108	21.31	8.52	1.12	
B-9					12000	4715	19.67	7.86	0.03	
B-13	1.8	4565	162	4.5	>14000	>5510	15.30	6.11	>1.2	Bolt yielded but was not pulled out.
B-14					>14000	>5510	15.30	6.11	>1.2	
B-15					>14000	>5510	15.30	6.11	>1.2	

^a A series = bolts anchored in sandstone.

^b B series = bolts anchored in mudstone.

principal lithological characteristics and climate of the Xinjiang area. Four of these preparations were selected for field tests. Field studies were also conducted of spray application techniques and the composite organic-inorganic material was finally selected. Clear improvement of the properties of the rocks was obtained after they had been treated with this material.

Test results

The compressive strength and tensile strength obtained using a point-load test machine were 47.51 kg cm^{-2} and 2.26 kg cm^{-2} , respectively. These values were 3.4 times higher than those of the weathered rock and 2.6 times higher than those of the semiweathered rock.

The porosity of the rock as determined after treatment was $0.016647 \text{ cm}^3 \text{ g}^{-1}$, which is about 85% lower than the original porosity of $0.11267 \text{ cm}^3 \text{ g}^{-1}$.

The original sandstone disintegrated, and the sand was dispersed after ten minutes of soaking in water. The treated rock remained intact even after one year of soaking.

The untreated sandstone had a capillary rise of 5 cm in ten minutes, whereas the treated stone had a capillary rise of 2 cm in two hours (Table 1).

The penetration depth of this chemical material in the rock was 5 cm in the laboratory and 4–5 cm on-site.

Freeze-and-thaw, stability, and aging tests were also performed. All of the data demonstrated that this consolidant was clearly effective in decreasing further weathering of the rock. This finding was further corroborated by the experts at the Kizil survey and design approval meeting.

Tests of walkway cantilever beams

The walkway of the Kizil grottoes was designed on the basis of tests on cantilever beams conducted by the Gansu Fifth Construction Engineering Company and the Gansu Construction Research Institute. The test data are shown in Table 2.

Load tests were carried out by adding loads to the end of the cantilever beams. The beams, of reinforced concrete, were anchored at a depth of 4 m into the sandstone and mudstone. The moment of fracture resistance in sandstone was 2.88, which was 1.61 times the designed value. The moment of fracture resistance in mudstone was 2.26, which was 1.60 times the designed value. On-site experiments showed that when the load on the outer edge of the beam in mudstone reached 3.5 t, one visible crack formed, with complete extraction of the beam occurring at 6 t of load. The test data indicated that these cantilever beams, like ordinary cantilever beams, could satisfy the design requirements in both sandstone and mudstone. Only when the load was too high did the bending angle at the root of the beam exceed the required limit. This is because the Kizil rock is weak. When the steel bolts were stressed and pulled outward, the base of the beam was extruded and the rock was fractured. The method for solving this problem was to install a 200 × 600 mm reinforced-concrete foundation at the base of the walkway beam to increase the area bearing pressure, disperse pressure at the base, and eliminate the destructive effect caused by the bending angle.

Table 2 Designed and tested values for beams

Beam number	Anti-bending moment T-M		M_T' / M_T	Deflection under standard load				Breakage strength		Note
	M_T (calculated)	M_T' (measured)		f_T' (mm)	f_R' (mm)	f_T' / L_0	f_R' / L_0	$M_p / T-M$	K_p	
No. 215 (sandstone)	1.747	2.88	1.61	1.495	1.07	1/735	1/1028	6.78	4.43	Rebar yielded first, then bent and broke.
No. 150 (mudstone)	1.41	2.26	1.60	8.98	6.38	1/122	1/172	5.65	3.69	Base of the beam was 350 mm high. Beam yielded and broke at the base.

M_T' values taken at the first appearance of a visible crack in the beam.
 f_T' is the measured bending.
 f_R' is the bending resulting from rotational displacement of the beam.
 Designed bending moment is 1.53 T-M.

Major Measures for Stabilizing and Reinforcing the Kizil Grottoes

The caves of the Kizil grottoes are crowded together and extend continuously over a distance of several kilometers. They show different types of damage and different levels of deterioration. For this reason, it was necessary to repair the most valuable caves and to address the overall effect in regions that are clustered with caves. After an overall survey was conducted, the western part of the valley was divided into four working sections: Caves 2–30 composed section 1, Caves 31–48 made up section 2, Caves 57–70 composed section 3, and Caves 76–82 were designated as section 4. Work on these four sections were to be completed in two stages. At present, the first and second sections have been completed.

Emergency reinforcement of the cliff rock and caves

The major reinforcement work in the first and second sections involved implementing retaining walls and roof supports and anchoring large areas. The cliff is discontinuous with many structural entities. The interior has undergone weathering, fracture, cracking, and cutting, with independent and partially independent blocks being formed. However, these blocks have their own self-supporting force and this needs to be taken into consideration in the reinforcement.

In reinforcing the cliff rock in the first and second sections, different techniques were applied in accordance with the different conditions of each cave. Three levels of caves in the vertical direction were grouped in the first working section. The front chambers of these caves had collapsed, and some had very thin roof rock. Stress-relief cracks had occurred inside many of the caves, making it unsuitable to insert bolts into the rock. Retaining walls were the principal means of reinforcement used, supplemented with bolts. Archaeological data were used as references to restore parts of the front chambers to their original shapes. Concrete mortar was poured on-site for use in the restoration of the entrances and walls of the caves. For example, portions of the front walls of Caves 2–6 were anchored to the wall of the cave entrance and to the cliff rock in a single entity by bolts, thereby combining partial restoration and reinforcement.

The caves in section 2 are scattered. The front chambers of these caves had collapsed, whereas the rear chambers remained intact. Most of these caves are located at the base of the cliff. For this reason, the anchoring technique used for large areas was principally applied in this section. Bolts 16 mm in diameter were spaced 1.5–2 m apart and arranged in a plum-blossom shape with an anchor depth of 2–4 m. Where cracks were present, the anchor depth was about 0.5–1 m beyond the location of the last crack.

One case that deserves particular comment involved a large, precarious rock about 10 m high, 3 m wide, and 2 m thick that constituted the wall between Caves 33 and 34. A crack about 10–20 cm wide ran through the rock from top to bottom. In front of the rock were some remains from the front chamber that were used as an archaeological reference point. There was no alternative but to preserve this rock, as it could not be ignored for structural reasons. In the course of the work, two waist frames

were installed in the middle of the rock to attach it tightly to the cliff in back and prevent it from collapsing during drilling. Bolts were installed in a plum-blossom pattern. To prevent further erosion by rainwater, the crack in the rock was filled with concrete mortar and the surface sealed with cement. This not only eliminated the dangerous condition, but it also preserved the historical evidence of the original shape of the grotto.

Water control

Water damage to the Kizil grottoes is primarily manifested in erosion by rainwater and surface runoff from the rock. The climate of the Xinjiang area is characterized as arid with low precipitation. The annual precipitation of the Heizi area is only 94.9 mm, and most of the rainfall occurs in June, July, and August. Because there is no soil, surface runoff occurs immediately during heavy rainfall. This water exerts a strong eroding force on the cliff rock, with numerous gullies of different sizes forming rapidly, some reaching several tens of meters in depth. These gullies create the greatest danger of collapse to the grottoes.

From the top of the grottoes, the gullies present a crisscross pattern. In the western region of the valley alone there are nineteen gullies of different sizes, five of which were directly endangering the caves, either undermining the bases or eroding the tops of the cliffs. Moreover, new gullies are developing constantly.

Under present conditions, it is difficult to eliminate the danger of erosion completely. The current policy is to treat gullies that are directly threatening or directly eroding the caves. In the course of conducting a comprehensive survey of the gullies, a portion of an ancient sandstone brick wall was discovered in the fore portion of the top of the cliff in the western region of the valley. The direction of the wall was essentially parallel to the cliff face. It was presumed by the Guizi Grotto Research Institute that this wall may have been built in ancient times to divert sand and floodwaters. If a new water-diversion wall were to be constructed at the top of the cliff in imitation of this ancient method, its position would have to be moved to the rear. However, this still would not solve the drainage problem on the front slope. Therefore, interception, diversion, and conveyance of the surface runoff away from the caves in accordance with the different specific conditions of each situation were adopted insofar as possible to eliminate severe erosion caused by runoff.

In section 1, the caves are very close together. Several key caves on the upper level are subjected to continuous erosion by runoff. The tops of Caves 14–17 were already very thin. Because rainwater often seeps into these caves, it was important to have a good drainage system. The principal method taken here was to dig a drainage ditch running east-west about 7–8 m from the top of Cave 9. The western end ran through the large gully in the eastern side of Caves 2–7 and the eastern end reached the large gully on the eastern side of Cave 17. The southern wall of the drainage ditch was high, and its other wall was low. In this way, it has intercepted the flow from the roof of the cliff in the north and diverted the

flow into the gullies in the east and west. More than a year of study has shown that the results have been very good and that the drainage ditch successfully intercepted and diverted the flow.

It was difficult to build a retaining wall and drainage ditch on the front slope of the cliff top of section 2 caves. Instead, a reinforced concrete awning was built at a fixed height at the fore wall of the cliff. This served to prevent water from directly eroding the caves.

External awnings or shelter structures have been considered. The design should be simple and practical. Anchor bolts used to reinforce the cliff face could support the awning. However, aesthetically it would be best to integrate the awning style with the appearance of the caves and add arched or trapezoid-shaped figures.

Restoration of entrance walls and single-chambered caves

Almost all the Kizil caves are either rectangular or square in plan and have front and back chambers. The front chamber usually has a niche on the cliff side and a statue inside the niche. The inner chamber has a passageway to the side, and to the rear of the passage way is either an arched or a squared ceiling. Some of the rectangular caves have central pillars and arched ceilings. Most of the front chambers of the caves are collapsed, and only their inner chambers remain intact. Reconstruction of an entrance wall often involves either the front or the back wall of the front chamber. Accurate reconstruction of these areas is advantageous for the long-term protection of the caves, and also for future research on them. The stability and safety of the cave interiors also obviously depend on proper restoration of these areas.

The Kizil work section 1 divides naturally into three major groups: Caves 2–6, 7–17, and 27–29. Different techniques were used to repair the entrance walls in these three groups. Caves 2–6, which served as the monks' living chambers, had very thin roof strata. Most of the entrance walls had been temporarily restored using mud bricks that did not have any reinforcing effect and resulted in changes of configuration.

The front chambers and parts of the inner chambers of some caves no longer exist. For example, the inner chamber of Cave 3 was half collapsed and its entrance wall had been restored. In the course of the current reinforcement, the entrance wall was removed and cleaned, exposing the base of the walls in the inner chamber. The cave was then restored with reinforced concrete mortar to its original shape and style. A small area of original gypsum floor remaining in the front chamber was used as a basis for the restoration of the front chamber. However, there was no information about the depth of this chamber or the shape of the roof. For this reason, a structure was built outside the entrance wall to indicate that there had originally been an outer chamber. Other caves were restored in the same manner. To avoid a rigid and dull appearance, the inside of the entrance wall was made smooth and perpendicular to the ground surface,

and the outside surface of the entrance wall was made to resemble the natural cliff.

Caves 7–17 are, for the most part, decorated with exquisite murals and have arched ceilings and central supports. All the front chambers of this group had collapsed. However, the inner chambers are well preserved. The cave entrance walls support the roof and have an external frame structure that indicates the previous existence of a front chamber.

Caves 10–17 are distributed vertically in two levels. When the upper-level caves were reinforced, the entrance walls had to be supported on bedrock, and it was thus necessary for the walls to penetrate through the caves at the lower level. In the reconstruction, a reinforced concrete pillar-beam was used. The intermediate walls of the upper caves were built using hidden pillars, either seated on the bedrock at the lower level or directly positioned on the horizontal beams at the tops of the entrance walls of the lower-level caves. A walkway between the levels has preserved the layered pattern. Cave 7 is on the westernmost end of this group and is very close to the area threatened by the gullies. Its front chamber had collapsed in the past, and the extant eastern half of the inner chamber was on the verge of collapse due to a gully on its western side. In the process of repairing this cave, loose dirt was first removed and a hole was dug into the bedrock. The floor was then restored with reinforced concrete mortar to its original level. The style and the size of the cave were reconstructed based on estimates made from the remains of the cave. After this work, the inner chamber of Cave 7 was completely protected.

The wooden walkway

The Kizil grottoes were excavated on a high, steep cliff face. Some caves were made more than 50 m above the ground. Most of the original walkways or stairs built along the cliff face had deteriorated, and some of the recently built simple, crude ladders were also on the verge of collapse. Sand that had accumulated in front of the caves buried many caves and blocked the walkways, making many caves inaccessible. In response to the development of tourism, the major objectives of this project were the construction of a new walkway, the removal of accumulated sand, the filling of cracks, and the paving of new roads. The walkway was designed to connect the scattered caves, thus facilitating visitation, while also harmonizing with the natural environment. Therefore, the floor of the walkway was left unpainted, with the original color of the concrete being maintained, and the railings were painted yellow to match the yellow-sandstone color of the grottoes.

Archaeological survey work

Many caves of the Kizil grottoes are buried beneath rock debris from the collapse of other caves. Cave 1 is a relatively intact cave that was discovered in 1973. Before conducting repair and reinforcement, exploratory work was needed to locate any caves or relics that may have been buried

beneath it. The intent was to avoid affecting future archaeological excavations by installing permanent structures on top of buried caves.

The authors asked the Railway Building Institute to conduct a geophysical exploration using C-1 microdepth measuring equipment (Zhong 1983). The principal survey sites were the front slopes of the sections between Caves 6 and 27, 52 and 70, and 110 and 120. An overall area survey was performed first by the intermediate gradient method. In regions showing anomalies, three-electrode electrical depth measurements were conducted. Final confirmation was carried out by the five-electrode vertical depth-measurement method. Results indicated that there were caves buried beneath both the first and the second work sections. Excavation was carried out by the Xinjiang Archaeology Research Institute.

After Cave 1 was excavated, the relics beneath it were found to be damaged because protection work had not kept pace with the excavation. In light of this finding, the principles adopted for future excavation were (a) that sections and caves that do not have an effect on the course of the project will not be excavated; and (b) that systematic excavation of the caves that must be excavated will be conducted by specialized archaeologists who will prepare the excavation reports and do preparatory work for the scientific conservation of the relics found.

Conclusions

All the reinforcement and repair projects in the first and second sections of the Kizil grottoes and all other work have essentially been completed except for chemical consolidation, which was limited by engineering considerations. The extent of the work completed to date accounts for only a small portion of the tasks of repair and conservation of the Kizil grottoes. There is certainly much to be learned, and it is the authors' sincere hope that their colleagues in the field of grotto stabilization and consolidation will provide valuable suggestions to ensure the successful completion of the repair and reinforcement of the Kizil grottoes.

References

- Kizil Design Group, Chinese Cultural Relics Institute
1987 Research on the Characteristics of the Destruction of the Kizil Grottoes and Remedial Measures. Internal report. Collected Papers of the Kizil Grottoes Preliminary Survey, Design Specialists' Meeting, September.
- Zhong Shihang
1983 The Application of Cartridge-Type Grouting in the Support Protection of Tunnels in Loess. Internal report. Beijing: Chinese Academy of Railway Sciences, Railway Building Institute.

Application of Cartridge-Type Grouting in Grotto Conservation

Zhong Shihang

IN THE FIELD OF GROTTO CONSERVATION, it is common practice to use concrete-mortar grouting and steel bolts for the reinforcement of rock and slopes and in the construction of new walkways. Comparatively speaking, concrete grouting bolts are inexpensive, resistant to aging, and do not pollute the environment.

The general procedure is to begin by pumping the concrete mortar into the grout hole and then to insert the steel bolt. Pumping the concrete is a troublesome procedure. A pump is required, and sometimes a compressor, as well; and if the grout hole is inclined upward, complete filling of the grout hole with mortar cannot be guaranteed. However, the technique of applying a cartridge-type grouting is simple and makes it easier to fill a grout hole with mortar. The author frequently uses a fast-cure thioaluminate cement developed by the Chinese Academy of Railway Sciences (Table 1). This cement is noncorrosive and undergoes only very slight expansion. The cartridge-type grout made with this cement has been used extensively in railway tunnels, water tunnels, grotto consolidation projects (e.g., Longmen grottoes), and the construction of walkways on cliff faces, all with excellent results.

This grouting technique is simple to perform and ensures that the holes will be filled with mortar. The thioaluminate cement is mixed with sand at various compounding ratios. A TS-type additive¹ is added, and the mixture is then poured into a specially designed paper cartridge. The diameter of this cartridge, which is 20–25 cm in length, can be designed to fit the size of the grout hole. The cartridge paper is tough when dry and

Table 1 Physical properties of cartridge-type, fast-cure concrete mortar

Cement type	Compressive strength (MPa)		
	Curing time		Anti-freeze
	4 hours	3 days	
Fast cure	>10	>25	D 200
High strength	>15	>40	D 200



Figure 1
Soaking cartridges in water.

has an extremely high water-absorption capacity. The cartridge is soaked in water immediately before it is inserted into the bolt hole (Fig. 1); after it has been soaked in water, the paper can easily be torn. The water rapidly permeates the bag to form a concrete mortar with a water:solid ratio of 0.4:0.5 within one to three minutes. At this point, the cartridge is rigid and can be inserted easily into the bolt hole. A steel bolt can be placed into the bolt hole after it has been calculated that a sufficient number of cartridges are in place. At this time, the paper cartridges will break and release the mortar into the hole, with the mortar completely filling the hole and enclosing the bolt. Better results are achieved if the steel bolt is pushed in using a rotational motion. Setting of the mortar begins in less than eight minutes; complete setting can be adjusted by the user to between ten and forty minutes by varying the quantity of additive. Within two to four hours after the bolts have been inserted, resistance to extraction can reach 20–40 kN at room temperature and can increase to more than 80 kN after ten hours.

Extraction-resistance tests

The author tested the resistance to extraction of this grout at the Longmen grottoes (Table 2). Ten steel rods of 20 mm in diameter and 2.5 m in length were inserted into holes with diameters of 40–50 mm. Fast-cure cement was used, and resistance to extraction after twenty-eight days exceeded 140 kN.

Cantilever beam tests

The author further tested this grouting technique in the construction of cantilever beams at the Longmen grottoes. Two rows of grouted bolts were anchored 2 m into a rock body in a vertical arrangement with 1.5 m of the bolts exposed. The free ends served as the main reinforcing bars, and concrete slabs were formed between the two beams at a distance of 2 m. Loads of up to 20 kN were applied to the outer edges of the concrete slabs, with the bending of the beams remaining within the design limit.

Table 2 Extraction-resistance tests

Bolt no.	Resistance to extraction (kN)		
	Time		
	4 hours	6 hours	8 hours
2		47	56
3	27		>100
4	27	>100	
5	17	>100	
6		61	

Fast-cure concrete mortar. Hole diameter, 45 mm; rock bolts 2.5 m long and 20 mm in diameter.

There was no residual deformation after loading. The beams' rupture load reached 50 kN, which is far beyond design requirements.

Grout Filling Test

Complete filling of the bore holes with mortar and bolting to the full anchoring depth of the bolts are the essential criteria for the long-term durability of any anchoring project. Statistically, the percentage of anchorings failing to meet quality standards because of incomplete filling with mortar reaches 20–30%. For many years, a good test of the adequacy of mortar filling was not available.

At present, tests of resistance to extraction are used to evaluate the quality of concrete grout. However, despite the poor quality of the grout filling, many rock bolts exhibited very high resistance to extraction. Theoretically speaking, as long as the length of a filling is greater than forty times the diameter of the steel bolt, the bolt will not lose anchorage until it is pulled to the point that the neck of the reinforcing bar contracts. Therefore, equipment and methods have been sought for measuring the completeness of mortar filling directly. Thurner (1983) proposed the principle of using an ultrasonic method to determine the quality of fillings. Over a ten-year period, several instruments were developed based on this principle. However, these instruments were only capable of determining smaller gradations in relation to the bolt-extraction force and did not directly reflect the degree of mortar filling.

On the basis of Thurner's principle, the author quantitatively investigated the relationship between the amplitude of the reflected wave and the completeness of mortar filling, and also examined different measuring methods and instruments. Thus, it became possible to use the percentage of mortar filling to evaluate the quality of the grouting. Accuracy by this method can reach 10%.

Principles

The basic principle of the method is as follows: When a pulse is generated on the outer end of the bolt, the ultrasonic waves propagate along the bolt and are reflected back when they reach the inside end of the bolt. The reflected wave is detected on the outside end of the bolt. If the reinforcing bar is completely enclosed by the concrete mortar and the mortar is adhered to the surrounding rock, the ultrasonic wave will, during the course of propagation, be continuously transmitted from the reinforcing bar through the concrete mortar into the rock. Consequently, there will be great energy loss, and the reflected wave as measured at the outside end of the shaft will be of low amplitude and may not even be determinable. If there is no filling with mortar grout, then there is merely an empty shaft in which the ultrasonic wave will be propagated in the reinforcing bar with little energy loss, and the amplitude of the reflected wave received will be greater. If there is incomplete filling with mortar grout, there will be an intermediate state, and the intensity of the reflected signal will be intermediate between those previously mentioned. Therefore, the degree of

mortar filling can be determined (Bergman et al. 1983). Low-frequency waves, such as 10-kHz sonic waves, have proved sufficient for this testing.

Equipment

The equipment required for this testing includes

- a pulse generator, installed on the exposed portion of the bolt, that can generate sonic waves of 10-kHz frequency;
- a coupling device, installed at the outside end of the shaft, with water between the inside wall and the shaft body as the coupling agent; and
- a recorder that receives the signal propagated from the head and displays the length of the bolt and the degree of mortar filling (Fig. 2a–c).

Method of measurement

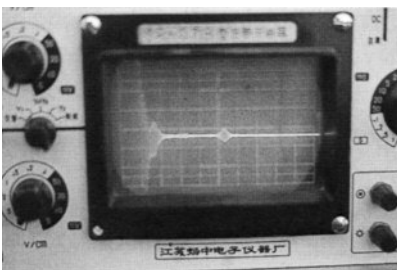
Three to four groups of standard grouted bolts were installed in different types of rock on the basis of the design parameters, with one or two grouted bolts in each group. Three groups of grouted bolts with 70%, 80%, and 90% mortar filling were tested. The degrees of filling were set as grade A for over 90% filling, grade B for 80–90% filling, grade C for 70–80% filling, and grade D for less than 70% filling. Grades can be set as desired on the basis of the design, with four as the maximum number of grades that can be set for this instrument.

The amplitude of the reflected wave is then determined on these standard grouted bolts, an average value being taken when there is more than one grouted bolt in a group (Fig. 3). These values serve as calibration standards for other grouted bolts. The calibration values are input into the instrument before performing determinations on other grouted bolts. When other determinations are made, the lengths of the grouted bolts and the degree of mortar filling can be displayed automatically by the measuring instrument.

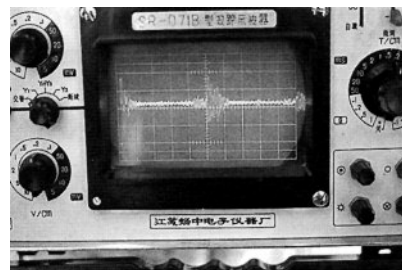
When determinations are to be made on individual grouted bolts, the outside ends of the grouted bolts should first be smoothed (they may be sawed flat) and the pulse generator attached. Then the receiving head of the coupling device is affixed to the outside end of the shaft body.

Figure 2a–c

Tests for completeness of filling: (a) drill hole is partially filled with grouting material; rock bolt is 2 m in length and 16 mm in diameter; (b) drill hole contains no grouting material; rock bolt is 2 m in length and 16 mm in diameter; and (c) readout equipment for determining completeness of grout filling.



a



b



c



Figure 3
In situ test of the degree of mortar filling.

Water is then poured to fill the inside wall of the coupling apparatus as well as any voids that may exist on the surface of the outside end of the grouting bolt.

The instrument monitors the reflected signal in wave form by means of an oscilloscope. When the operator has manually adjusted the instrument until reflected signals appear, the instrument automatically displays the length of the grouted bolt, the amplitude of the reflected wave, and the degree of mortar filling.

Results of determinations

Accuracy of measurement is a point of interest during testing procedures. The first criterion of accuracy is whether values obtained by repeated determinations of parameters for the same grouted bolt and for bolts with the same or different degrees of filling are consistent. The second criterion is whether the results determined for different grouted bolts conform to the actual circumstances of those grouted bolts.

For this purpose, the author tested large numbers of anchored bolts with known degrees of mortar filling and has also requested other researchers to prepare grouted bolts of known characteristics and to test the methods and instruments. Table 3 lists the data obtained in a tunnel project. Two bolts were inserted for each degree of filling. By referring to this table, the accuracy of the measurements for grouted bolts under the same conditions can be checked and different degrees of mortar filling can be differentiated. It can be seen that variation between the two measurements obtained from the two bolts situated in the same grout was considerably less than 10%.

Table 3 Filling tests

Bolt no.	1 & 2	22 & 25	8	10	11	18
Anchoring depth (m)	2.0	3.8	3.8	2.0	3.8	2.0
Filling (%)	100	70	100	70	65	0
Amplitude	129/132	66/163	115/118	171/175	168/171	151/154
Difference	3	3	3	4	3	3

Table 4 In situ tests at Chen village tunnel (partial results)

	Control bolts			Test bolts			
Bolt no.	9	24	25	8	11	16	22
Anchor depth (m)	3.8	3.8	3.8	3.8	3.8	3.8	3.8
Filling (%)	90	80	70	100	85	50	70
Classification	A	B	C	A	B	D	C
Depth (m)				3.6	3.7	3.7	3.6
Amplitude	125	145	160	114	168	over	156

Data shown are for bolts 22 mm in diameter.

Table 5 In situ tests at Chen village tunnel (partial results)

	Control bolts			Test bolts		
	3	4	6	12	18	15
Bolt no.	3	4	6	12	18	15
Anchor depth (m)	2.0	2.0	2.0	2.0	2.0	2.0
Filling (%)	100	90	80	90–100	90	50
Classification	A	B	C	A	B	D
Depth (m)				1.7	1.9	1.7
Amplitude	138	154	168	144	151	206

Data shown are for bolts 18 mm in diameter.

Tables 4 and 5 show the correlation between the results of these two determinations and the degree of filling of mortar in the grouted bolts (Zhong 1988, 1993). From the data presented it can be seen that the determined degrees of mortar filling conform completely to actual conditions. The maximum error for determined depth of insertion of anchors was an acceptable level of 0.2 m.

Note

- 1 It was not possible to ascertain from the author the generic chemical nature of the additive, described as being of a "TS" type. Ed.

References

- Bergman, G. A., N. Krauland, J. Martna, and T. Daganus
1983 Nondestructive field test of cement-grouted bolts with the boltometer. In *Proceedings of the 5th International Congress on Rock Mechanics, Melbourne, Australia, 1983*. Rotterdam: A. A. Balkema; Salem, N. H.: Merrimack Book Service.
- Thurner, H. F.
1983 Detection of invisible faults on rock bolts in situ. In *Rock Bolting: Theory and Application in Mining and Underground Construction. Proceedings of the International Symposium on Rock Bolting, Abisko, August–September 1983*, ed. Ove Stephansson. Rotterdam and Boston: A. A. Balkema.
- Zhong Shihang
1988 Excavation and supporting of the tunnel running through the F1–F10 faults and converging water to the city Tainjing from Luan River source. In *Proceedings of the International Symposium on Engineering in Complex Rock Formations, Beijing, China, 3–7 November 1986*, ed. Li Chengxiang and Yang Ling. China: Science Press; Oxfordshire and New York: Pergamon Press.
- 1993 The progress of measurement techniques on tunnel support (in Chinese). *Report on Advanced Technology in Railroad Construction, Railroad Tunnels and Underground Construction (in Chinese)*, comp. the Railway Tunnel and Underground Projects Science and Technology Information Center, Ministry of Railways. Beijing: Railway Publishing House.

Techniques for Reinforcement of the Maijishan Grottoes

Yi Wuzhi and Lang Xiangui

THE MAIJISHAN GROTTOES, located 45 km southeast of Tianshui, Gansu Province, is one of the most famous grotto sites in China. Dating from about 400 C.E., the site consists of 194 caves housing more than 7,800 sculptural objects and 1,000 m² of wall paintings. From late 1975 to early 1994, a joint project for the restoration and consolidation of these fragile grottoes was undertaken (see acknowledgments). Four different techniques were tested and applied at the site: rock bolting, grouting, structural support, and spraying of concrete on the rock surface to prevent weathering.

Geology, Geomorphology, and Deterioration of the Maijishan Grottoes

Shaped like a haystack, Maijishan mountain is 142 m high (Figs. 1, 2). The east, west, and south sides are barren and steep with a slope of 95°. The bedrock is exposed and the lower part of the cliff has talus deposits. The Maijishan stratum, of Upper Tertiary period, is a purplish and brick-red conglomerate interspersed with thin layers of sandstone and mudstone loosely cemented by fine red clay containing calcium and iron (Huang 1976).

The severe, extensive deterioration of the Maijishan caves is the result of weathering, cracks caused by stress relief, and seismic activity. Various types of damage include cracking, collapse, flaking, and spalling due to moisture seepage, and repeated excavation of grottoes, all of which have left the cliff surface with many weathered, overhanging rocks (State Cultural Relics Museum 1964).

Technical Research on Stabilization of the Grottoes

Based on the initial condition survey of the caves, the stabilization plan for the Maijishan grottoes was initiated in 1960. Various organizations, including the State Cultural Relics and Museum Institute, recommended reinforcement of the grottoes as the only way to preserve these cultural treasures. In 1974, after several years of extensive investigation, the Gansu Provincial Construction Survey and Design Bureau proposed the use of steel rock bolts and concrete retaining walls to reinforce the cliff on the



Figure 1
Maijishan grottoes after the 1984 stabilization.

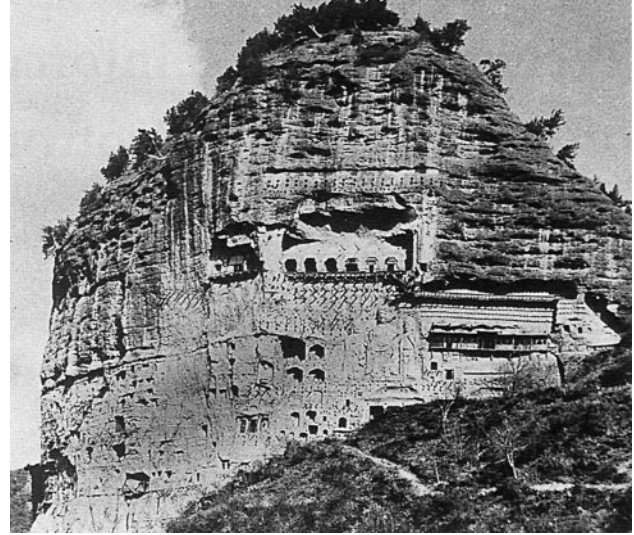


Figure 2
An early view of the Maijishan grottoes.

west side and the use of steel-and-concrete frame structures to support the roof (Gansu Construction Survey 1975).

At the end of 1975, the authors conducted preliminary field testing of a rock bolting technique using steel and concrete grouting. The success of these trials demonstrated the possibility of designing a strategy employing new methods (Yi and Lang 1979). By the end of 1983, the team completed research, design, and application of the four techniques detailed below: sprayed concrete, rock bolting, grouting, and structural support.

Tests of sprayed concrete

To prevent further weathering of the poorly cemented conglomerate, concrete was sprayed on the surface of the rock. A pull test was performed on five of the areas treated. In all five cases, breakage occurred at the inner layer of the rock, not at the concrete-conglomerate interface, demonstrating that concrete adheres well to the conglomerate.

Tests of rock bolting

The main objective of this experiment was to fasten the fragile and precariously hanging cliff rocks to the firmer substrata with steel rock bolts. To ensure the safety of the cultural relics in and outside the caves, as well as of personnel, successful drilling, grouting, and bolt anchoring methods were essential. First, a series of holes, 12–60 mm in diameter, was drilled to a depth of 3–15 m using an electric rock drill with a guiding track. Techniques and equipment were also developed for bolting after grouting.

Two kinds of rock bolting tests were performed: (1) tensile strength of steel rods bolted and grouted into the cliff face, and (2) shear strength of the conglomerate with concrete grouting and steel rock bolts.

Sixty-six types of rods were tested in situ for their tensile strength. Commercial cement mortar and no. 16 manganese spiral steel, 16–32 mm in diameter, were found to provide a good anchoring effect. This steel anchor has a maximum tensile yield strength when the bolting length is twenty-five times the diameter of the rod. After unfavorable factors were taken into account, such as the property of the rock and the quality of grout filling, the bolting length was set at thirty to fifty times the rod diameter.

To obtain test results that approximated actual conditions, bolted and unbolted conglomerate blocks were comparison tested in situ (Fig. 3), with the bolted samples anchored directly to the cliff face with horizontal and inclined rods. A hydraulic jack was used to shear the blocks. Results were as follows:

First, both horizontal and inclined rods produced a remarkable improvement in the crack-resistance and ultimate-rupture loads of the conglomerate (Table 1). Blocks reinforced with two steel rods of 20 mm diameter showed average increases of 36% in crack-resistance load and 100% in ultimate-rupture load.

A second important effect of the steel-rod reinforcement was improvement in the sudden shear rupture characteristics of the conglomerate. Unbolted blocks ruptured under a 10 t load, whereas the bolted blocks only fractured. These tests indicated that bolted blocks can sustain 21–55% more load than unbolted blocks.

Bolting also increased the maximum shear displacement of the conglomerate. Tests found the shear displacement of the bolted blocks to be five to nine times that of the unbolted conglomerate before rupture.

In summary, conglomerate reinforced with steel rock bolts in combination with cement grouting showed higher tensile and shear strengths than unconsolidated conglomerate.

Tests of crack grouting

In 1983, Li Zuixiong successfully tested a high molar-ratio ($K_2O:SiO_2$) potassium silicate consolidant. Li and the authors studied the characteristics

Figure 3
Plan of the shear testing site of the Maijishan conglomerate with and without anchor bolts.

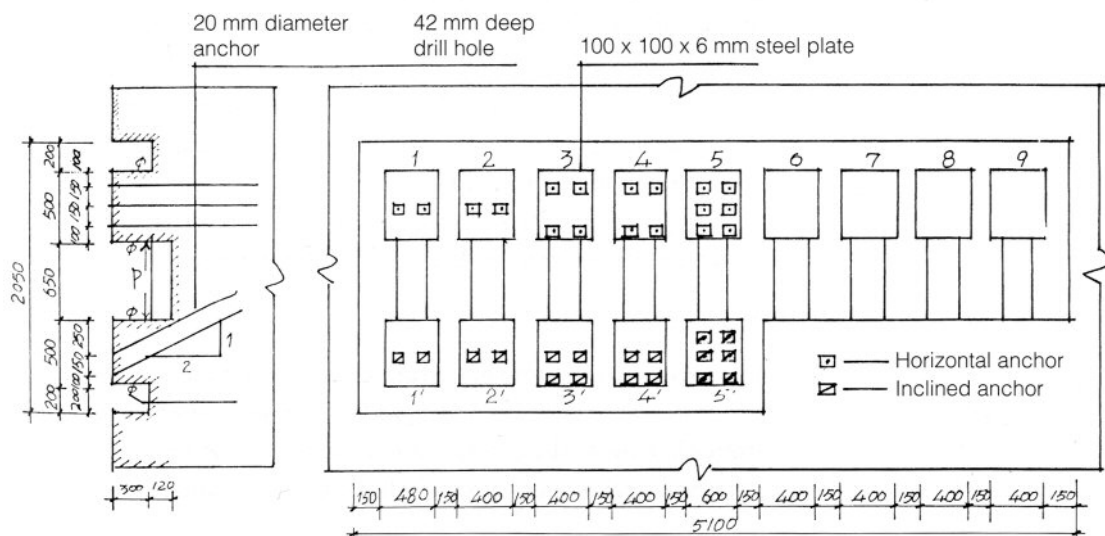


Table 1 On-site shear tests of the conglomerate with and without anchors

Sample Type	Sample No.	Shear rupture		Maximum shear		Maximum		%		Fracture Characteristics
		Load N_T (kN)	Displacement ΔT (mm)	Load N_p (kN)	Displacement Δp (mm ²)	Shear Rt (N mm ⁻¹)	Rt Rg ⁻¹	N_T	N_p	
Conglomerate	6	140	0.16	140	0.16					Brittle
Conglomerate	7	100	0.12	100	0.12					Brittle
Conglomerate	8	140		140				100	100	Brittle
Conglomerate	9	180	0.18	180	0.18					Brittle
with 2 20-mm HA ^a	1	200	0.37	280	1.77	445.8	1.29	143	200	3 mm shear fracture
with 2 20-mm HA	2	180	0.31	280	1.66	445.8	1.29	129	200	3 mm shear fracture
with 4 20-mm HA	3	280	0.38	340	1.57	270.7	0.783	200	242	2.5–4 mm shear and tension cracks
with 4 20-mm HA	4	280	0.39	350	1.01	278.6	0.808	200	250	2.5–4 mm shear and tension cracks
with 6 20-mm HA	5	280	0.47	355	1.04	188.4	0.545	200	253	3 mm shear and tension cracks
with 6 20-mm HA	5'	280	0.51	350		185.7	0.537	200	250	3 mm shear and tension cracks
with 2 20-mm IA ^b	1'	320	0.29	>360				228	>257	2 mm shear fracture
with 2 20-mm IA	2'	320	0.45	420	1.65	598.0	1.730	228	300	2 mm shear fracture
with 4 20-mm IA	4'	380	0.505	>500		>356		271	>357	

^a HA = horizontal anchors

^b IA = inclined anchors

and application of potassium silicate mixed with the fine red clay of the Maijishan conglomerate to form a composite for grouting crevices (Li and Yi 1983).

Research on the Maijishan cliff showed that the strength of the potassium silicate consolidant and that of the composite with red clay were clearly greater than that of the conglomerate. Tests of conglomerate rock cemented by potassium silicate and by the composite indicated much greater tensile strength than that of similar test pieces grouted with a high-polymer emulsion or epoxy resin. Because the potassium silicate component was able to penetrate into and solidify the strength of the clay, the two potassium silicate-based mortars not only filled the cracks of the Maijishan conglomerate to which it was applied but also penetrated and consolidated the surrounding rock.

These results provided the basis for the design and application of the consolidation plan for the Maijishan grotto site.

Structural Stabilization Techniques

In addition to repairing and maintaining the temples, pavilions, and other structures, the restoration of the Maijishan grottoes focused on the strengthening of the cliff face and construction of new wooden walkways (Yi 1984). Techniques of rock bolting, grouting, and surface spraying with

concrete, with the addition of structural supports, were applied to stabilize the cliff face, as follows:

Sprayed concrete

Concrete was sprayed onto the cliff face with and without the installation of a 6–8 mm diameter steel reinforcing net laid on the surface. These two types of operations had four purposes: (1) to fill all the crevices, (2) to protect the cliff face from further weathering, (3) to stabilize dangerous rocks, and (4) to restore the cliff face and eaves of the corridors.

High-pressure spraying of concrete was used to fill more than a thousand small holes created by water erosion and old walkway posts, and large crevices on the cliff face of the grottoes. The holes ranged from 20 to 30 cm in diameter and were about 50–60 cm deep.

To provide protection from further erosion, the cliff face was sprayed with concrete over a steel reinforcement net. This has been shown to effectively slow weathering. Sprayed concrete has also effectively limited the displacement of the surrounding rock, thus preventing the loosening, spalling, and collapse. This technique was employed as a preliminary, immediate measure for the stabilization of the strata.

Because concrete sprayed under high pressure can reach a thickness of 10–15 cm, collapsed bedrock on the cliff face, corridors, and eaves could also be restored to their original shapes by applying the concrete over a steel reinforcement net in combination with rock bolting.

Rock bolting and grouting

For further structural reinforcement, mortar was used in combination with spiral steel bolting rods to fasten layers of fractured or earthquake-damaged rocks onto the more stable substrata. Cracks inside the caves were treated with sealing and grouting methods, according to their individual condition. Potassium silicate and the added clay composite were used for this purpose.

Structural support

In addition to spraying concrete, rock bolting, and grouting, a steel-and-concrete structure was built to support the huge unstable roof rock between the Seven Buddha pagoda and Niuer Tang (hall). The structure is 1.5 m thick, 3.5 m high, and 3.5 m wide. Six steel rods 32 mm in diameter, spaced 700 mm apart, were horizontally anchored 6 m deep into the bedrock. In addition, several steel rods were obliquely anchored 15 m deep.

Characteristics of structural stabilization techniques

Compared with the previous reinforcement method of retaining pillars, the new techniques of concrete spraying, rock bolting, grouting, and structural support used at the Maijishan grottoes demonstrated a range of valuable characteristics, as follows:

1. **Thinness:** The retaining pillars, which are about 0.5–10 m thick, were reinforced by spraying concrete and rock bolting. When steel bolts 3–15 m long were used to anchor the fractured rocks, a concrete coating with a thickness of only 50–150 mm was needed.
2. **Firmness:** Steel bolts 3–15 m in length used to strengthen the cliff face effectively increased the internal strength of the rocks. These rods function like ribs in a body.
3. **Depth:** Steel rods anchored deep into bedrock remarkably increased the cohesion and stability of the rock.
4. **Adaptability:** In addition to strengthening, these techniques can also be applied to the restoration of the site (collapsed bedrock, corridors, and eaves).
5. **Speed:** High-speed, high-efficiency electric machines were used to carry out drilling, grouting, and spraying.
6. **Economy:** Much less material was needed for this design when compared to that of the construction of a typical retaining pillar.
7. **Aesthetics:** An appropriate amount of red clay was added to the concrete coating to match the original surface color. Thus, steel rods anchored into the rocks do not affect the appearance of the grottoes or the cliff face.

Conclusions

In a 1984 evaluation, conservation experts and scholars stated, “Loosely cemented conglomerate, the steep slope, and the huge rocks hanging inside the caves have made the consolidation of the Maijishan grottoes a difficult and dangerous operation” (Yi and Lang 1984).

The present comprehensive approach to the consolidation of the Maijishan grottoes—concrete spraying, grouting, rock bolting, and construction of a structural support—all without substantially changing the appearance of the caves, has opened a new avenue for the conservation of grotto sites (Figs. 4, 5). This is an outstanding example of how advanced technology can be applied in the protection of threatened cultural heritage.

Acknowledgments

The research, design, and implementation of this project were carried out under the guidance of the State Bureau of Cultural Relics, the State Cultural Relics Museum and Research Institute, and the Gansu Provincial Culture Department from the end of 1975 to the beginning of 1994. This is a joint effort among specialists from the Gansu Provincial Architecture Institute; the Gansu Construction Survey and Design Institute; the Fifth Construction Engineering Company; and the Maijishan Consolidation Office, a temporary office in charge of project design and supervision. The authors would like to take this opportunity to express their sincere gratitude to the leading officers, experts, and all the engineering crew members who assisted in this project.

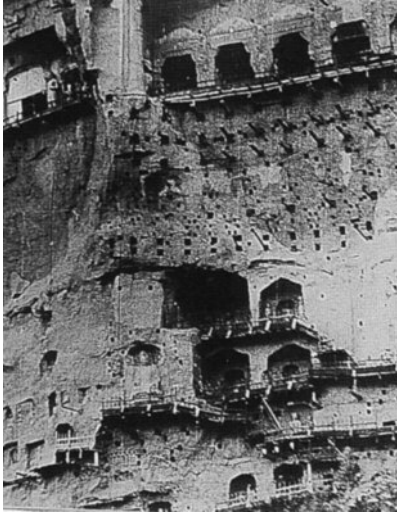


Figure 4

An early view of Maijishan Grotto 15 to the fifth section.



Figure 5

Grotto 15 to the fifth section after stabilization.

References

- Gansu Construction Survey and Design Institute
1975 *The Preliminary Design for the Repair and Stabilization of the Maijishan Grottoes* (in Chinese). Lanzhou: Gansu Construction Survey and Design Institute.
- Huang Yuding
1976 *Report on the Geological Survey for the Maijishan Stabilization Project* (December) (in Chinese). Xian: Shanxi Prospecting Institute.
- Li Zuixiong and Yi Wuzhi
1983 *Feasibility Study on the Application of CPS Inorganic Compound to Grout the Crevices in the Maijishan Conglomerate* (in Chinese). Lanzhou: Gansu Museum and the Gansu Architectural Research Institute.
- State Cultural Relics Museum and Research Institute
1964 *Survey Report on Maijishan Grottoes* (July) (in Chinese). Xian: State Cultural Relics Museum and Research Institute.
- Yi Wuzhi
1984 *The Techniques of the Spraying, Grouting, Rock-Bolting and Supporting Techniques for the Stabilization of Maijishan Grottoes* (April) (in Chinese). Tenshui: Maijishan Stabilization Office, with the assistance of the Gansu Survey and Design Institute, the Gansu Fifth Construction Company, and the Gansu Architectural Research Institute.
- Yi Wuzhi and Lang Xiangui
1979 *Research and Experiments on Spraying Concrete and Rock-Bolting Stabilization Techniques* (April) (in Chinese). Lanzhou: Gansu Architectural Research Institute.
- 1984 *Research and Experiments on Spraying, Grouting, Rock-Bolting and Supporting Stabilization Techniques* (April) (in Chinese). Lanzhou: Gansu Architectural Research Institute.

Chemical Consolidation of Conglomerate and Sand at the Mogao Grottoes

Li Zuixiong, Neville Agnew, and Po-Ming Lin

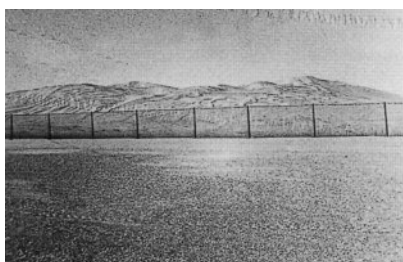


Figure 1
Gravel plateau above the Mogao grottoes, connected to the Mingsha mountain in the west. A windbreak fence was built in front of the mountain.

THE MOGAO GROTTOES were excavated in a north-south-oriented cliff face on the west bank of the Daquan River. The cliff face is 1,680 m long and approximately 20 m high. At the base of the cliff is a relatively flat sand-and-gravel ground. The cliff is about 90 m at its closest point to the Daquan River and about 180 m at the farthest point from it. Trees have been planted on the flat, elongated area in front of the cliff. The caves are excavated in the south 1,000 m of the cliff face. In the northern area, except for a few caves that are decorated with murals and polychrome statues, most of the caves are undecorated and served as living quarters for craftsmen, monks, and pilgrims. Toward the top of the cliff in the southern region is a 35° erosional slope 30 m in width partly covered in sand and gravel with exposed surfaces of conglomerate. At the top of the slope is a $3,000 \times 800$ m plateau composed of sand and gravel, leading to the Mingsha mountain in the west (Fig. 1).

This region is characterized by large sand dunes, and winds blow from several directions seasonally. The westerly winds bring sand from the dunes of the Mingsha mountain, causing erosion of the cliff rock and damage to the grotto areas.

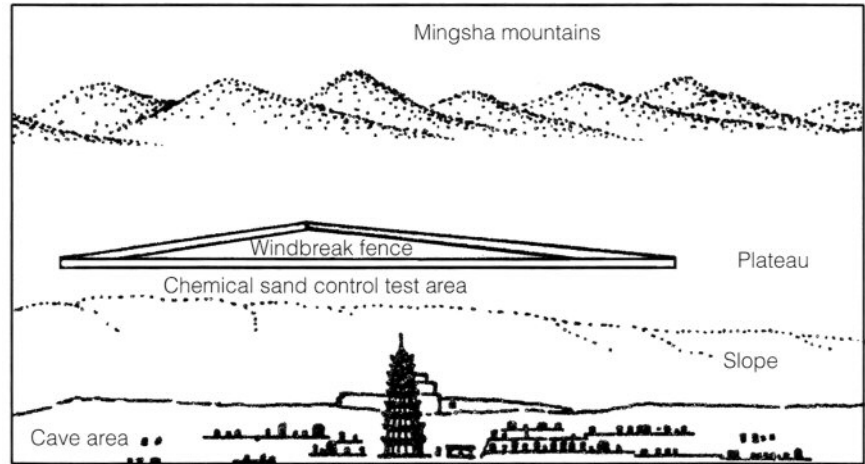
On the basis of estimates, $3,000 \text{ m}^3$ of sand accumulated annually in front of the cliff face before the installation of the windbreak fence. The sand blocked walkways and entrance doors, and fine dust infiltrated the grottoes, settling on the statuary and wall paintings. Removal of such a large sand accumulation required considerable annual expenditures of money.

A knitted synthetic fabric windbreak fence in an A shape (as viewed from above) was installed on the top of the cliff to control the windblown sand carried by the westerly winds. The apex of the triangular windbreak fence is about 70 m from the Mingsha mountain and is pointed toward it; its base is about 800 m in length. It is parallel to the cliff face and positioned about 200 m from it. All the southern caves are enclosed in the area protected by it (Fig. 2).

Since its erection, the windbreak fence has effectively prevented sand blowing from the Mingsha mountain from entering the grotto area.

Figure 2

Schematic drawing showing the locations of the A-shaped windbreak fence and chemical consolidation test area.



This has resulted in the sand carried by the wind being deposited around the windbreak fence or diverted to outside the grotto area, thus reducing the sand deposit in the grotto area by 60%. However, since the installation of the windbreak fence, the balance of supply of sand to the cliff face has been disturbed. Wind has stripped the 30° slope and plateau behind it of its residual sand, exposing the weak conglomerate of the cliff to more rapid erosion than it experienced previously (Fig. 3). Analysis of the sand grains collected from sand traps placed on the walkways and around the grotto area shows that after the installation of the windbreak fence, coarser sand grains and even pebbles were deposited (Ling et al. 1993). The upper layers of the Quaternary argillaceous conglomerate cliff rock are loosely cemented and easily eroded by wind, causing pebbles to fall from the top of the cliff. This is not only dangerous to pedestrians on the walkways below, but thinning of the rock of the roofs of some of the upper-level caves—a phenomenon already well advanced—will further endanger these caves. It is presently considered that it will probably be necessary to chemically consolidate the sand in front of the windbreak fence, and the exposed rock of the cliff slope. In fact, the latter is the principal objective of the testing described in the present paper because of the ease of erosion of the exposed rock on the 30° slope. With the installation of the windbreak fence completed, testing of chemical consolidation became the next priority, the use of both the windbreak fence and chemical consolidation being planned as a comprehensive sand-control system.



Figure 3

Severely eroded strata at the Mogao grottoes.

Experimental Work

Sand sample analysis

Analysis of sand granularity

Sand samples were collected for analysis from three sites. Two samples collected from the chemical consolidation test area located east of the windbreak fence were a mixture of coarse sand, gravel, and clay. The third sample, collected on the slope north of the Nine-Story Pagoda, consisted

of homogeneous, fine-grained sand. The fourth sample, collected from the sand deposited along the shelter north of the Nine-Story Pagoda, was also fine and homogeneous. Results are presented in Table 1.

Mineralogical analysis of sand samples

The sand samples for mineralogical analysis were collected from the chemical consolidation test area on the eastern side of the windbreak fence. Results are given in Table 2.

Consolidants tested

Two types of binding agents, an inorganic one and synthetic organic polymers, were used for chemical consolidation tests on the top of the cliff of the Mogao grottoes. The inorganic material was a high-molar potassium silicate (PS)¹ (Li 1985; Nishiura and Li 1988). Three types of organics were used: (1) Primal AC-33, an aqueous emulsion composed of 40% methacrylates and 60% acrylates (abbreviated AC); (2) a polyvinyl acetate emulsion, Aerospray 70 Binder (abbreviated AS); and (3) a mixture composed of copolymer of methacrylates and acrylate (40%), polyethoxylated ethanol (1%), silicates (3.5%), 12.3% polymethacrylates, 42% acrylates, and 1% organic silicate emulsion, to which 0.2% polyethoxylated ethanol was also added; it is commonly called Soil Seal (abbreviated SS).

Determination of the permeation of consolidants on sand

Two types of sand were selected to test the depth of penetration of consolidants. One was from the chemical consolidation area on the eastern side of the windbreak fence (designated A), the other was from the fine-grained deposit on the north side of the Nine-Story Pagoda (designated B). Samples were introduced into transparent cylindrical tubes (45 × 300 mm). Samples were packed by the same method so that the compaction would be essentially similar. Consolidants were diluted to suitable concentrations and dripped onto the top of the samples at the same speed; the permeation rates were recorded (Fig. 4; Table 3).

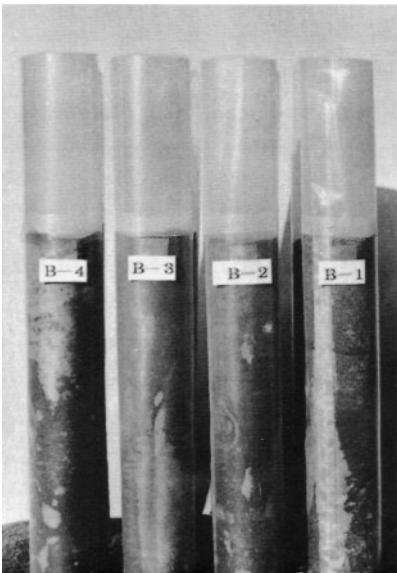


Figure 4
Sand samples for consolidant permeation test
(45 × 300 mm).

Determination of the water-absorption capacity of consolidated sand samples

Determinations were made according to standard methods for rock in which a cylindrical sample (50 × 100 mm) is soaked in water for forty-eight hours and reweighed. It is important that water be able to pass quickly through the consolidated sand and rock covering the cliff top and the slope of the Mogao grottoes; if the consolidated sand has a very low water permeability, most of the rainwater will not be able to permeate the sand and will collect and run down the slope, accelerating erosion and possibly endangering the grottoes over time.

A mold was made, and the sand from groups A and B were made into cylindrical samples 50 mm in diameter and 100 mm in height. Three samples from each group were consolidated using 1:10 water solutions of

Table 1 Sand granularity analysis: particle size and percentage

	Sample no. 1	Sample no. 2	Sample no. 3	Sample no. 4
Mean size (mm)	Percentage	Percentage	Percentage	Percentage
15.0	5.32			
10.0	2.21	2.18		
7.00	2.35	9.09		
4.00	3.78	11.45		
2.00	4.89	15.12		
1.00	6.15	15.35		
0.50	2.24	1.85	0.90	1.32
0.40	1.05	0.43	3.75	1.03
0.315	2.31	0.94	10.82	2.57
0.25	5.13	2.64	20.53	6.60
0.200	2.16	1.33	4.42	1.73
0.160	8.23	3.91	17.86	8.45
0.125	14.88	9.02	23.34	28.08
0.10	12.58	8.55	10.98	23.23
0.08	7.2	4.62	3.32	8.74
0.063	11.84	8.52	3.26	13.76
<0.063	7.68	5.00	0.82	4.50

Sample 1 collected from 2 to 5 cm depth at the chemical consolidation test site, east of the windbreak fence.

Sample 2 collected from the surface 0 to 2 cm at the chemical consolidation test site, east of the windbreak fence.

Sample 3 collected from the surface north of the Nine-Story Pagoda.

Sample 4 collected from the slope surface north of the Nine-Story Pagoda.

Table 2 Petrological analysis of the sand

		Heavy minerals (Density > 2.85)				Light minerals (Density < 2.85)			
Unstable minerals		Relatively stable minerals		Stable minerals		Very stable minerals		quartz	46.50
augite	7.00	diopside	10.00	black metal ore	6.00	limonite	3.50	orthoclase	6.25
enstatite	1.00	tremolite	4.50	titanite	0.25	leucoxene	1.50	plagioclase	19.00
hornblende	47.00	actinolite	1.00			zircon	0.50	weathered plagioclase	6.00
grunerite	2.00	epidote	4.75			tourmaline	0.75	chalcedony	0.25
lamprobolite (basaltic hornblende)	0.75	zoisite	0.75			limonite	7.50	carbonates	1.50
		allanite	0.50					rock debris	20.50
		chlorite	0.75						
Subtotal	57.75	Subtotal	22.25	Subtotal	6.25	Subtotal	13.75	Total	100.00

Table 3 Permeation tests on sand

Sample no.	Consolidant	Concentration (in water)	Permeation depth/time	Total volume (ml)	Time (minutes) ^a
A-1	AC	1:10	9 cm / 10 min	250	50
A-2	AS	1:10	9 cm / 10 min	200	70
A-3	SS	1:10	11 cm / 10 min	215	45
A-4	PS	10%	7 cm / 10 min	200	50
B-1	AC	1:10	13 cm / 5 min	210	30
B-2	AS	1:10	13 cm / 5 min	250	20
B-3	SS	1:10	12 cm / 5 min	250	45
B-4	PS	10%	12 cm / 5 min	250	20

^a Time required for consolidant to penetrate the entire sample

AC, AS, or SS, and PS at a concentration of 10% in water (Fig. 5). After curing, water absorption tests were carried out. Results are given in Table 4 (Figs. 6, 7).

Table 4 Water absorption test of consolidated sand samples (continued on next page)

Sample no.	Cons.	Conc.	Dry wt. (g)	Wet wt. 5 min (g)	A.W. ^a (g)	A.R. ^b (%)	Wet wt. 10 min (g)
1	AC	1:10	362.00	362.80	0.80		363.90
A-1 2	AC	1:10	369.00	371.20	2.20	0.39	372.70
3	AC	1:10	360.30	361.70	1.40		362.50
1	AS	1:10	382.00	384.20	2.20		387.50
A-2 2	AS	1:10	364.00	366.50	2.50	0.81	370.05
3	AS	1:10	365.70	370.01	4.31		372.90
1	SS	1:10	353.00	354.50	1.50		356.00
A-3 2	SS	1:10	356.50	357.90	1.40	0.38	359.00
3	SS	1:10	369.30	370.50	1.20		372.20
1	PS	10%	313.50	367.00	53.50		368.00
A-4 2	PS	1:10	314.10	369.00	54.90	16.38	369.40
3	PS	1:10	329.00	377.00	48.00		378.00
1	AC	1:10	317.50	321.40	3.90		322.30
B-1 2	AC	1:10	310.00	313.50	3.50	1.33	315.00
3	AC	1:10	307.60	312.30	4.70		314.00
1	AS	1:10	303.50	321.50	18.00		328.00
B-2 2	AS	1:10	312.00	334.10	22.10	5.86	339.50
3	AS	1:10	328.00	343.00	15.00		352.50
1	SS	1:10	321.80	331.70	9.90		337.30
B-3 2	SS	1:10	323.20	327.10	4.00	2.54	335.50
3	SS	1:10	323.20	334.00	10.80		348.50
1	PS	10%	339.80	386.70	46.90		390.50
B-4 2	PS	1:10	323.30	365.50	42.20	13.06	375.20
3	PS	1:10	338.00	379.70	41.70		384.00

^a A. W. = weight of absorbed water

^b A. R. = water absorption rate

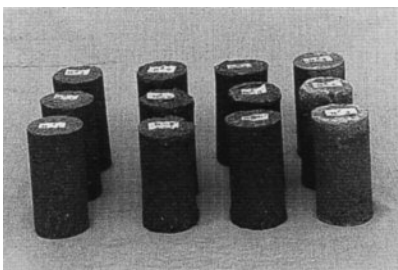


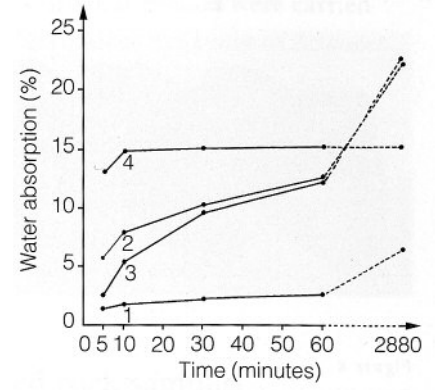
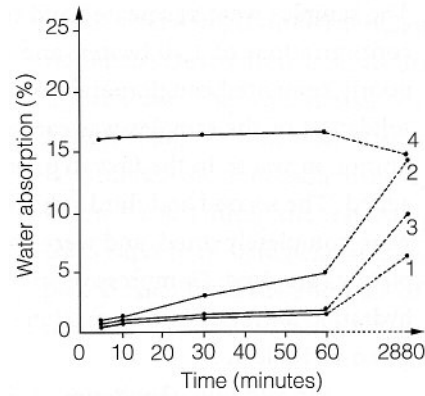
Figure 5
Sand samples for water absorption test
(50 × 100 mm).

Figure 6

Water absorption of consolidated group A sand: 1 = AC; 2 = AS; 3 = SS; 4 = PS.

Figure 7

Water absorption of consolidated group B sand: 1 = AC; 2 = AS; 3 = SS; 4 = PS.



Determination of the compressive strength of consolidated rock

Rock collected from severely weathered areas in the northern region of the Mogao grottoes was made into 50 × 50 × 50 mm samples (Fig. 8).²

Table 4 continued

Sample no.	A.W. (g)	A.R. (%)	Wet wt. 30 min (g)	A.W. (g)	A.R. (%)	Wet wt. 1 hr (g)	A.W. (g)	A.R. (%)	Wet wt. 48 hrs (g)	A.W. (g)	A.R. (%)
1	1.90		364.30	2.30		365.30	3.30		380.50	18.50	
A-1 2	3.70	0.71	374.50	5.50	1.04	376.50	7.50	1.46	399.50	30.50	6.88
3	2.20		364.00	3.70		365.50	5.20		386.50	26.20	
1	5.50		393.00	9.00		400.00	18.00		437.00	55.00	
A-2 2	6.05	1.69	376.00	12.00	2.91	384.50	20.50	4.94	414.30	50.30	14.34
3	7.20		377.00	11.30		382.10	16.40		419.80	54.10	
1	3.00		357.50	4.50		359.30	6.30		389.20	36.20	
A-3 2	2.50	0.78	360.00	3.50	1.13	362.10	5.60	1.65	390.50	34.00	9.86
3	2.90		373.50	4.20		375.20	5.90		405.50	36.20	
1	54.50		368.50	55.00		368.50	55.00		373.00	30.60	
A-4 2	55.30	16.62	369.70	55.60	16.71	369.70	55.60	16.76	373.50	59.40	16.97
3	49.00		378.30	49.00		378.50	49.50		382.50	53.50	
1	4.80		324.00	6.50		325.00	7.50		337.30	19.80	
B-1 2	5.00	1.73	316.20	6.20	2.20	317.00	7.00	2.50	326.90	16.90	6.32
3	6.40		315.50	7.90		316.50	8.90		330.00	22.40	
1	24.50		335.00	31.50		340.00	36.50		369.50	66.00	
B-2 2	27.50	8.11	346.90	34.90	10.26	353.30	41.30	12.54	383.00	71.00	22.09
3	24.50		361.90	33.90		368.50	40.5		399.40	71.40	
1	15.50		346.00	24.20		350.00	28.20		383.20	61.40	
B-3 2	12.30	5.48	355.20	32.00	9.65	370.00	46.80	12.34	396.20	73.00	22.43
3	24.30		360.50	37.30		367.80	44.60		406.00	82.80	
1	50.70		391.20	51.40		391.20	51.40		391.00	51.20	
B-4 2	51.90	14.86	376.20	52.90	15.03	376.80	53.50	15.14	377.00	53.90	15.56
3	46.00		384.00	46.00		384.50	46.50		388.50	50.50	

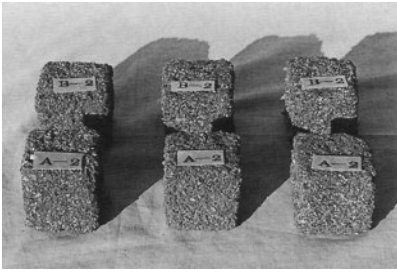


Figure 8
Consolidated rock samples prepared for property tests (50 × 50 × 50 mm).

The samples were permeated and consolidated with AC, AS, and SS in concentrations of 1:10 (water) and with 10% PS. Because the cliff rock is poorly cemented conglomerate of low strength, the permeation and consolidation of the samples was carried out in several steps to avoid disintegration in water. In the first step, only a small amount of consolidant was added. The second and third steps were not carried out until the samples were completely dried, and were continued until the samples were completely saturated. Compressive strength was determined using a Newton hydraulic universal testing machine (model WE-10A, 1004). Test results are given in Table 5.

In addition, the compressive strength of consolidated sand was determined. Samples of the same size were treated similarly to the rock samples in preparation for testing. Results are given in Table 6.

Wind-tunnel erosion tests on cliff conglomerate

Samples of approximately 50 × 50 × 50 mm were taken from weathered rock from the northern region of the grottoes. Samples were consolidated using AC, AS, and SS in concentrations of 1:10 (water), and with 10% PS, as previously.

Table 5 Compressive strength of consolidated weathered rock

Sample no.	Consolidant	Load (kN)					Average	Compressive strength (MPa)	Note
		1	2	3	4	5			
A ₀ 1–5	—	0.50	0.45	0.20	0.10	0.35	0.32	0.13	Unconsolidated
A 1–3	AC 1:10 (water)	9.20	10.20	14.10			11.17	4.47	Consolidated
B 1–3	AS 1:10 (water)	3.50	6.70	2.20			4.13	1.65	Consolidated
C 1–3	SS 1:10 (water)	1.35	3.00	1.00			1.78	0.17	Consolidated
D 1–3	PS 10%	31.50	29.00	32.30			30.93	12.37	Consolidated

Table 6 Compressive strength of consolidated cylindrical sand (50 × 50 mm cross section)

Sample no.	Consolidant	Load (kN)				Average	Compressive strength (MPa)
		1	2	3	Average		
A-1	AC 1:10 (water)	3.90	2.30	3.20	3.13	1.20	
B-1	AC 1:10 (water)	1.50	1.60	1.30	1.47	0.60	
A-2	AS 1:10 (water)	10.60	15.90	13.80	13.43	5.40	
B-2	AS 1:10 (water)	1.50	1.80	0.90	1.40	0.60	
A-3	SS 1:10 (water)	1.40	1.70	1.20	1.43	0.60	
B-3	SS 1:10 (water)	1.20	1.00	1.20	1.13	0.40	
A-4	PS 10%	16.70	17.60	31.00	21.77	8.70	
B-4	PS 10%	19.10	10.90	6.70	12.23	4.90	

The wind-tunnel simulation tests of wind erosion were carried out at the Desert Research Institute of the Chinese Academy of Sciences in Lanzhou. The wind tunnel is 38.78 m in length, the testing segment length being 16.23 m with a cross-sectional area of $1 \times 0.6 \text{ m}^2$. Wind speed is continuously adjustable from 2 to 35 m s^{-1} , and turbulence intensity is below 0.4%. During the test, samples were set horizontally on sample trays capable of being elevated to any desired position. Samples were placed 12 m from the entrance of the tunnel in the wind direction. Test results are shown in Table 7 (Figs. 9, 10).

Freeze-thaw tests of consolidated rock samples

Rock samples similar to those used in previous tests were used for freeze-thaw tests. Because of the high porosity and high water absorption of the conglomerate, the samples disintegrated easily when frozen and thawed. The conditions of the samples in different freeze-thaw cycles were recorded, but the weight losses were not recorded. Testing was continued until all the samples had disintegrated. The number of freeze-thaw cycles was recorded, and rough estimates were made of the resistance to freezing and thawing of the weathered rock samples and the samples after consolidation.

Freeze-thaw tests were performed on four groups of samples (three samples in each group) after consolidation using AC, AS, and SS at concentrations of 1:10 (water), and of 10% PS. Samples were first heated at $105\text{--}110 \text{ }^\circ\text{C}$ to constant weight, after which they were soaked in water at $20 \text{ }^\circ\text{C}$ for four hours. They were then placed in a freezer at $-30 \text{ }^\circ\text{C}$ for four hours. Repeated cycles of freezing and thawing consisted of thawing for four hours ($20 \text{ }^\circ\text{C}$ water) and freezing for four hours ($-30 \text{ }^\circ\text{C}$), with each eight-hour period being counted as one cycle.

A minute crack developed in one of the 10% PS-consolidated samples in the third freeze-thaw cycle, at which time the other two samples were still intact. In the fifth freeze-thaw cycle, minute cracks also appeared in the other two. In the eleventh freeze-thaw cycle, there was expansion of the cracks in all three. During the seventeenth cycle, the corners of two of the samples fell off. During the twenty-eighth cycle, the two samples with chipped corners broke into two or three pieces. By the forty-fifth freeze-thaw cycle, all three rock samples virtually disintegrated.

One of the samples treated with AS developed a crack in the eighth cycle, at which time the other two samples were essentially intact. In the twelfth cycle, the crack that had already appeared expanded, a small piece broke off from the lower part of the second sample, and a minute crack also developed in the third rock sample. By the forty-fifth freeze-thaw cycle, there was clear enlargement of the cracks in all three rock samples. However, there was no evidence of disintegration.

The corners of one of the AC samples broke off at the twentieth freeze-thaw cycle. The other two samples were basically intact. In the twenty-sixth cycle, there was disintegration of the lower portion, whereas there were no changes in the other two samples. During the thirty-third cycle, distinct cracks appeared in the sample that had begun to disintegrate, and the corners fell off of the other two samples, which also showed

Table 7 Wind-tunnel erosion experiments on consolidated cliff conglomerate

Sample no.	Consolidant	Surface area (cm ²)	Duration (minutes)	Wind vel. (m s ⁻¹)	Sample wt. before (g)	Sample wt. after (g)	Weight loss (g)	Calculated weight loss (kg m ⁻² hr ⁻¹)	Notes
A ₀	untreated control	48.1	30	5	896.0	896.0	0		
A ₀	untreated control	48.1	30	10	896.0	893.5	2.5 ^a		Wind only
A ₀	untreated control	48.1	30	15	893.5	893.0	0.5	0.21	
A ₀	untreated control	48.1	15	20	893.5	892.5	1.0	0.21	
A ₀	untreated control	48.1	30	7	892.5	881.0	11.5	4.78	Wind and sand
A ₀	untreated control	48.1	20	10	881.0	682.5	198.5	123.80	(threshold vel. 6.2 m s ⁻¹)
A ₀	untreated control	48.1	6	15	682.5	436.5	246.0	512.47	
A ₀	untreated control	54.6	3	20	809.5	241.3	568.2	2081.32	
A ₁	AC 1:10	56.5	30	5	933.5	933.5	0		
A ₁	AC 1:10	56.5	30	10	933.5	933.5	0		Wind only
A ₁	AC 1:10	56.5	30	15	933.5	933.5	0		
A ₁	AC 1:10	56.5	15	20	933.5	933.5	0		
A ₁	AC 1:10	56.5	30	7	933.5	933.0	0.5	0.18	Wind and sand
A ₁	AC 1:10	56.5	20	10	933.0	932.0	1.0	0.53	(threshold vel. 6.2 m s ⁻¹)
A ₁	AC 1:10	56.5	6	15	932.0	931.0	1.0	1.77	
A ₁	AC 1:10	56.5	3	20	931.0	928.5	2.5	10.62	Wind only
A ₂	AS 1:10	58.9	30	10	948.0	948.0	0		
A ₂	AS 1:10	58.9	30	20	948.0	948.0	0		
A ₂	AS 1:10	58.9	30	7	948.0	948.0	0		
A ₂	AS 1:10	58.9	20	10	948.0	947.0	1.0	0.51	Wind and sand
A ₂	AS 1:10	58.9	11	15	947.0	945.5	1.5	1.39	
A ₂	AS 1:10	58.9	7	17	945.5	943.0	2.5	3.64	
A ₂	AS 1:10	58.9	8	20	943.0	936.0	7.0	8.91	
A ₃	SS 1:10	57.3	30	10	902.0	902.0	0		Wind only
A ₃	SS 1:10	57.3	30	20	902.0	902.0	0		
A ₃	SS 1:10	57.3	30	7	902.0	902.0	0		
A ₃	SS 1:10	57.3	20	10	902.0	902.0	0	0.52	
A ₃	SS 1:10	57.3	11	15	901.0	901.0	0		Wind and sand
A ₃	SS 1:10	57.3	7	17	901.0	900.0	1.0	0.52	
A ₃	SS 1:10	57.3	8	20	900.0	900.0	0		
A ₄	PS 10%	52.0	30	5	917.5	917.5	0		
A ₄	PS 10%	52.0	30	10	917.5	917.5	0		Wind only
A ₄	PS 10%	52.0	30	15	917.5	917.5	0		
A ₄	PS 10%	52.0	15	20	917.5	917.5	0		
A ₄	PS 10%	52.0	30	7	917.5	916.7	0.8	0.31	Wind and sand
A ₄	PS 10%	52.0	20	10	916.7	916.7	0		(threshold vel. 6.2 m s ⁻¹)
A ₄	PS 10%	52.0	6	15	916.7	916.5	0.2	0.38	
A ₄	PS 10%	52.0	3	20	916.5	916.5	0		

^apossible error in measurement

Figure 9

Abrasion loss of consolidated rock sample in the wind tunnel test (wind only): C = unconsolidated; D = AC; A = AS; S = SS; P = PS.

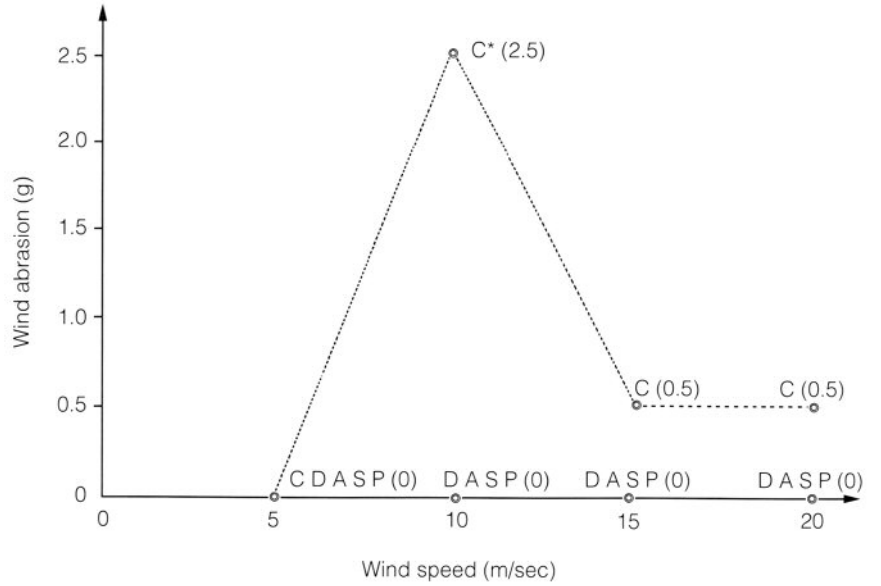
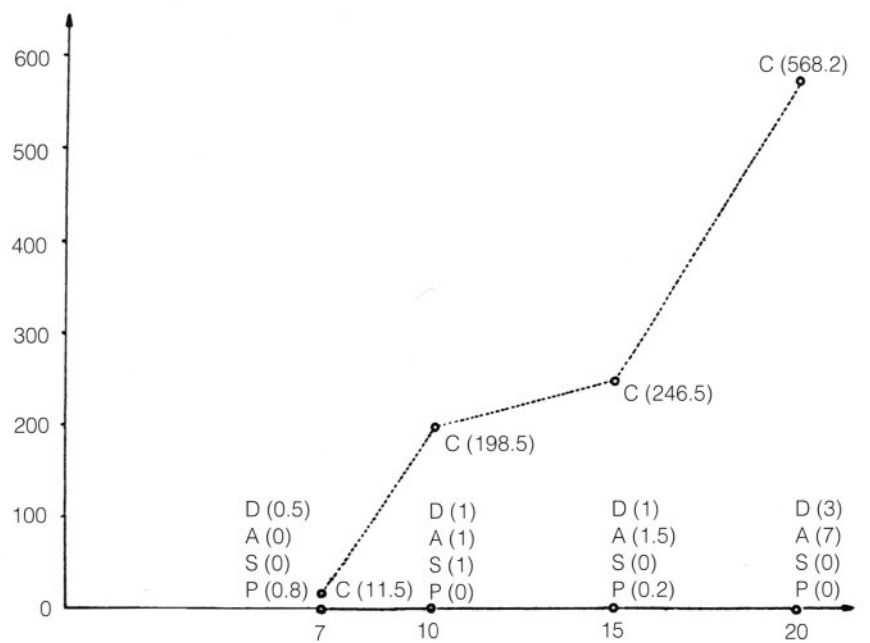


Figure 10

Abrasion loss of consolidated rock sample in the wind tunnel test (wind plus sand): C = unconsolidated; D = AC; A = AS; S = SS; P = PS.



some disintegration. By the forty-third freeze-thaw cycle, all three samples had basically disintegrated.

Water resistance of consolidated sand samples

The sand samples consolidated with AC, AS, and SS at a ratio of 1:10 (water), and 5% PS were soaked in water to determine their water resistance. The 5% PS-consolidated sand sample was soaked in water for as long as sixteen months with no sign of disintegration. The AC, AS, and SS consolidated samples all showed signs of disintegration after two weeks; after two to three months, all had swelled and softened.

On-site chemical consolidation tests

The natural conditions at the cliff top allowed on-site chemical consolidation tests to be performed on the sand-covered area east of the windbreak fence and 150 m from the cliff face. The covering sand here consists primarily of mixed coarse and fine sand, together with small amounts of gravel and clay, and was the same as the group A sand samples used in the permeation tests described above.

The test area was divided into 2×2 m squares, after which the solutions of AC, AS, SS, and PS were sprayed on the surface. The squares were treated in two ways. In one case, the consolidant was sprayed directly onto the dry sand; in the other, water was first sprayed onto the dry sand so as to moisten it to a depth of about 1–2 cm, and the consolidant was then applied. The objective of this procedure was to ascertain whether pre-melting would be an advantageous procedure.

PS of high modulus has frequently been used in the past for consolidation of both weathered conglomerate and weathered adobe buildings with good protective effects. The general method was first to spray low concentrations of PS, with a second application after the first had dried. Consolidation by this method may be carried out three or four times or more with increasing concentration to a final one not exceeding 5%. The number of treatments is determined primarily by the porosity and the required consolidation strength. In this way, the depth of penetration of consolidant is maximized. If the conglomerate or other rock is of very high porosity, the final PS spray concentration may be as high as 10%. In this test, the PS concentration was 5% and the spray volume was controlled at 2, 4, and 6 l m^{-2} .

Consolidation tests using an adhesive made by mixing potassium silicate and sodium silicate (abbreviated NaS) in 3:1 ratio were also performed. Results are presented in Table 8.

Three concentrations of AC were used in conducting on-site spraying and consolidation tests. Specifically, AC:water ratios of 1:10, 1:20, and 1:30 were used. Volumes used were 1.15, 2.30, 3.45, 4.60, and 5.75 l m^{-2} (Table 9).

The concentrations of AS and SS were the same as the AC concentrations, i.e., 1:10, 1:20, and 1:30. The spray volumes of AS were 4.60 and 5.75 l m^{-2} , and the spray volumes of SS were 2.30, 3.45, 4.60, and 5.75 l m^{-2} (Tables 10 and 11).

Hardness tests of consolidated sand

Six months after consolidation, surface hardness tests of the consolidated sand were carried out. At present, there is no standard method of performing surface hardness tests of consolidated sand. We used a simple puncture method and the resilience method with a Schmidt hammer to conduct comparative tests.

The puncture test used a steel pipe 2 cm in diameter and 111 cm in length, to which a sharp-tipped steel head had been attached, and mass

612.5 g. As shown in Figure 6, the steel pipe was held vertically and dropped from a height to the tip of 60 cm. The depth of penetration was measured. Three determinations were made on each test square. Results are given in Tables 8–11 and in Figure 11.

The Schmidt hammer (Chinese HT-225 “resilience meter”), the surface hardness meter most widely used at present, was used on the consolidated sand. Its impact kinetic energy is 0.225 kg·m, and it is commonly used to test concrete. As stated above, there is no standard method for determining the surface hardness of consolidated sand, and the Schmidt hammer tests were performed for reference purposes. For this reason, when the determinations were made on the test squares, the maximum and minimum resilience values were eliminated and the six most frequent resilience values taken. These values were not used for calculating hardness; rather, the aforementioned four types of consolidated sand were compared on the basis of the resilience values, after which the hardness of the consolidant surface was compared.

Determination of the penetration depth of the consolidant

The depth to which the consolidant penetrated was roughly estimated after completely drying by removing a block of consolidated sand and measuring its thickness. In part because spraying was done by hand, the depth of penetration was not uniform. Three points were selected for each test square for measurement of penetration depth. Results are given in Tables 8–11 and Figure 12.

Table 8 On-site sand consolidation test

Sample no.	Consolidant	Conc. (%) (in water)	Quantity (l m ⁻²)	Thickness of wetted sand layer (mm)	Average penetration (mm)	Puncture test averages (mm)	Schmidt hammer test averages (mm)	Appearance after one year
PS-1		5	6	1	40	2	11	No visible change
PS-2		5	4	1	32	5	11	
PS-3	PS	5	2	1	15	41	No rebound	
PS-4	(molar ratio	5	6	0	33	6	11	
PS-5	= 3.6)	5	4	0	21	18	No rebound	
PS-6		5	2	0	12	18	No rebound	
PS-NaS-1		15	6	0	37	8	No rebound	Salt efflorescence on the surface
PS-NaS-2		15	4	0	33	11	No rebound	
PS-NaS-3		15	2	0	12	32	No rebound	
PS-NaS-4	PS:NaS	7	6	0	35	12	No rebound	
PS-NaS-5	(3:1)	7	4	0	32	29	No rebound	
PS-NaS-6		7	2	0	14	39	No rebound	
PS-NaS-7		3.5	6	0	40	14	No rebound	
PS-NaS-8		3.5	4	0	30	19	No rebound	
PS-NaS-9		3.5	2	0	20	36	No rebound	

Table 9 On-site AC consolidated sand test

Sample no.	Dilution	Quantity (l m ⁻²)	Thickness of wetted sand layer (mm)	Average penetration (mm)	Puncture test averages (mm)	Schmidt hammer test averages (mm)	Appearance after one year
AC-1	1:30	5.75	0	10	30	No rebound	Consolidation darkened the sand slightly
AC-2	1:30	4.60	0	13	22	No rebound	
AC-3	1:30	3.45	0	13	28	No rebound	
AC-4	1:30	2.30	0	9	36	No rebound	
AC-5	1:30	1.15	0	5	41	No rebound	
AC-6	1:20	5.57	0	18	12	No rebound	
AC-7	1:10	5.75	0	33	8	No rebound	
AC-8	1:30	5.75	10	12	34	No rebound	Consolidation darkened the sand slightly
AC-9	1:30	4.60	10	18	16	No rebound	
AC-10	1:30	3.45	10	19	22	No rebound	
AC-11	1:30	2.30	10	15	32	No rebound	
AC-12	1:30	1.15	10	9	34	No rebound	
AC-13	1:20	5.57	10	20	11	No rebound	
AC-14	1:10	5.75	10	27	9	No rebound	
AC-15	1:30	5.75	20	10	24	No rebound	
AC-16	1:30	4.60	20	20	14	No rebound	
AC-17	1:30	3.45	20	20	20	No rebound	
AC-18	1:30	2.30	20	12	25	No rebound	
AC-19	1:30	1.15	20	10	43	No rebound	
AC-20	1:20	5.57	20	33	13	No rebound	
AC-21	1:10	5.75	20	33	8	No rebound	

Table 10 On-site AS consolidated sand test

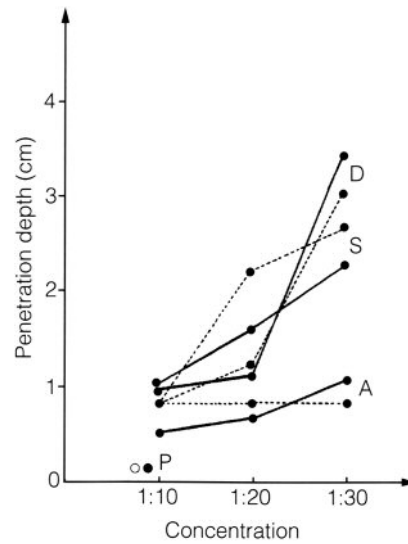
Sample no.	Dilution	Quantity (l m ⁻²)	Thickness of wetted sand layer (mm)	Average penetration (mm)	Puncture test averages (mm)	Schmidt hammer test averages (mm)	Appearance after one year
AS-1	1:30	5.75	0	25	8	10	Consolidation darkened the sand slightly
AS-2	1:30	4.60	0	18	26	No rebound	
AS-3	1:20	5.75	0	23	8	10	
AS-4	1:20	4.60	0	25	8	No rebound	
AS-5	1:10	5.75	0	22	7	11	
AS-6	1:10	4.60	0	21	9	No rebound	
AS-7	1:30	5.75	10	23	14	No rebound	Consolidation darkened the sand slightly
AS-8	1:30	4.60	10	23	11	No rebound	
AS-9	1:20	5.75	10	23	7	10	
AS-10	1:20	4.60	10	27	6	10	
AS-11	1:10	5.75	10	27	3	11	
AS-12	1:10	4.60	10	23	10	10	
AS-13	1:30	5.75	20	25	7	10	
AS-14	1:30	4.60	20	23	20	No rebound	
AS-15	1:20	5.75	20	23	8	11	
AS-16	1:20	4.60	20	23	19	No rebound	
AS-17	1:10	5.75	20	33	6	11	

Table 11 On-site SS consolidated sand test

Sample no.	Dilution	Quantity ($l\ m^{-2}$)	Thickness of wetted sand layer (mm)	Average penetration (mm)	Puncture test averages (mm)	Schmidt hammer test averages (mm)	Appearance after one year
SS-1	1:30	5.75	0	32	27	No rebound	Consolidation darkened the sand slightly and a small amount of blue-green deposit appeared on the surface
SS-2	1:30	4.60	0	33	32	No rebound	
SS-3	1:30	3.45	0	25	32	No rebound	
SS-4	1:30	2.30	0	18	33	No rebound	
SS-5	1:20	5.75	0	33	22	No rebound	
SS-6	1:20	4.60	0	37	17	No rebound	
SS-7	1:20	3.45	0	27	26	No rebound	
SS-8	1:20	2.30	0	18	25	No rebound	
SS-9	1:10	5.75	0	43	8	10	
SS-10	1:10	4.60	0	32	8	No rebound	
SS-11	1:10	3.45	0	25	19	No rebound	
SS-12	1:10	2.30	0	17	24	No rebound	
SS-13	1:30	5.75	10	37	27	No rebound	
SS-14	1:30	4.60	10	33	20	No rebound	
SS-15	1:30	3.45	10	23	35	No rebound	
SS-16	1:30	2.30	10	20	31	No rebound	
SS-17	1:20	5.75	10	32	15	No rebound	
SS-18	1:20	4.60	10	37	32	No rebound	
SS-19	1:20	3.45	10	28	25	No rebound	
SS-20	1:20	2.30	10	27	37	No rebound	
SS-21	1:10	5.75	10	42	8	9	
SS-22	1:10	4.60	10	38	10	10	
SS-23	1:10	3.45	10	28	15	No rebound	
SS-24	1:10	2.30	10	25	14	No rebound	
SS-25	1:30	5.75	20	37	19	No rebound	
SS-26	1:30	4.60	20	25	17	No rebound	
SS-27	1:30	3.45	20	27	27	No rebound	
SS-28	1:30	2.30	20	20	29	No rebound	
SS-29	1:20	5.75	20	40	15	No rebound	
SS-30	1:20	4.60	20	32	17	No rebound	
SS-31	1:20	3.45	20	25	24	No rebound	
SS-32	1:20	2.30	20	18	25	No rebound	
SS-33	1:10	5.75	20	37	11	9	
SS-34	1:10	4.60	20	42	10	No rebound	
SS-35	1:10	3.45	20	28	14	No rebound	
SS-36	1:10	2.30	20	20	20	No rebound	

Figure 11

Puncture test: D = AC; A = AS (dry); S = SS;
P = PS (prewettted).



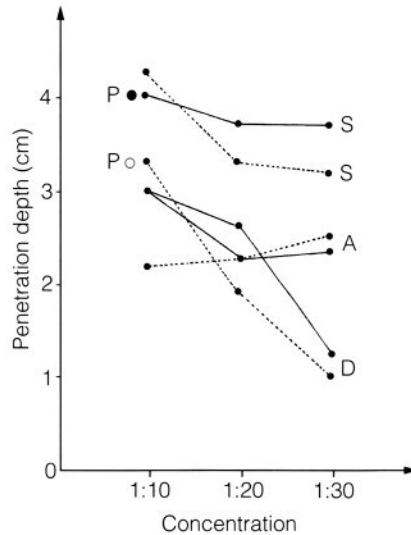
Test Results and Discussion

Results show that the 1:10 AC, AS, and SS, and the 5–10% PS all exhibit good penetration capacity in both fine sand and the sand-gravel-clay mixtures. By comparison, the ability of these four types of consolidant to penetrate fine sand was greater than that of mixed sand. The loose sand requiring chemical consolidation in the Mogao grotto region is primarily the fine-grained windblown sand from the Mingsha mountain. However, since the installation of the wind fence, the fine-grained sand on the surface has been largely removed so that most of the sand remaining on the exposed surface consists of pebbles and coarse-grained sand. When the wind is not strong, sand is not readily blown from this type of surface. The sand deposits on the cliff slope and the conglomerate itself requires consolidation to combat erosion, which has accelerated since construction of the fence. All four of the consolidants exhibit ideal penetration for the purposes of these consolidation objectives, but each performs very differently.

Results show that sand samples consolidated with 10% PS had the highest water absorption rate. Within five minutes, the water absorption of the group A samples was 16.38% and that of the group B samples was 13.06%, with saturation being achieved in ten minutes. With AC, AS, and SS, samples had a slow absorption rate after the first five minutes. This was especially the case for the group A mixed sand samples. Water absorption for the group B samples was slightly higher. With AS it reached 5.86%; for group B samples after treatment with AS and SS for thirty minutes it was 10.26% and 9.65%, respectively. After soaking for forty-eight hours, the samples consolidated with AS and SS had the highest water absorption. Absorption in group B was even higher, that for the group A samples being 14.34% and 9.86%, respectively, and for the group B samples 22.09% and 22.43%, respectively. The reason for this could be that the intergranular films formed with AS and SS swelled after the consolidated sand had been soaked for a long period.

Figure 12

Penetration depth of the consolidants
(at 5.75 l m^{-2}): D = AC; A = AS; S = SS;
P = PS. Solid line: prewetted sand. Dashed
line: dry sand.



PS is a binding material that exhibits good penetration on sand and rock, but, even more important, chemical bonding may occur among the silicate and the quartz and mineral components of sand and rock during the cementing process. PS does not appear to form a protective film on the surface and does not fill the pores of the rock; therefore, there is a high permeation rate and high water absorption. AC, AS, and SS are high-molecular organic polymers that readily form films and, when the concentration is high, tend to fill pores. Consequently, the water penetration rate is greatly decreased. As stated earlier, the permeability of the consolidated sand is a very important consideration at Mogao. In the past, wall paintings in caves were destroyed by rainwater that flowed into the caves. If the water permeation rate of the consolidated sand on the slope above the cliff were to decrease greatly after chemical consolidation, the runoff during heavy rains might enter the caves and further endanger the wall paintings. For this reason, in the event of large-scale interventions implemented in the future, a suitable drainage system should be installed on the top of the cliff face.

Water resistance tests of the consolidants showed that the 5% PS exhibited excellent water permeability and very strong water resistance. The water resistance of the AC, AS, and SS consolidated samples was lower.

Compressive strength tests indicated that the weathered conglomerate and consolidated sand treated with 10% PS had the highest values (12.37 and 8.70 MPa, respectively). Samples having the next highest strengths were the samples consolidated with AC and AS at a ratio of 1:10 (4.47, 1.65, 1.20, and 1.65 MPa, respectively). Those consolidated with SS were much lower, being 0.17 and 0.60 MPa—values only slightly higher than 0.11 MPa, the compressive strength of the unconsolidated material.

Wind-tunnel simulation tests of wind erosion of the consolidated rock samples indicate that the weak, semicemented argillaceous

conglomerate of the cliff was extremely susceptible to wind erosion. When the wind speed reaches 10 m s^{-1} , even a wind not carrying sand can bring about rock erosion. When the speed of a “clean” wind was greater than 15 m s^{-1} , there was a distinct erosion effect at a rate of $0.21 \text{ kg m}^{-2} \text{ hr}^{-1}$. The wind-erosion effect of a sand-carrying wind was even greater. When the velocity of the sand-carrying wind reached 7 m s^{-1} , there was distinct erosion of the rock. When the velocity of the sand-carrying wind reached 10 m s^{-1} , there was a startling increase with an erosion rate as high as $123.80 \text{ kg m}^{-2} \text{ hr}^{-1}$. When the velocity of the sand-carrying wind was 20 m s^{-1} , three-fourths of a $50 \times 50 \times 50 \text{ mm}$ rock sample was eroded within three minutes (Fig. 13). After the cliff rock had been consolidated with AC, AS, and SS, and with PS, it displayed a relatively ideal resistance to wind erosion. Comparatively, the samples exhibiting the best resistance were those consolidated with SS and PS. The erosion rates of these two were close to zero when the wind velocity reached 20 m s^{-1} even when loaded with sand. The high compressive strength and the high wind-erosion resistance of the PS consolidated samples are consistent. Conversely, the compressive strength of samples consolidated with a 1:10 water solution of SS was low, whereas their wind-erosion resistance was high. This appears to be because SS exhibits high flexibility after solidification.

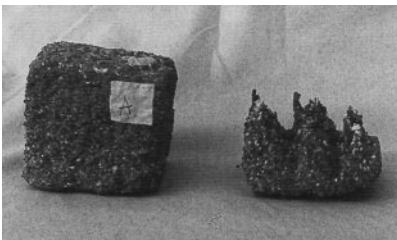


Figure 13
Rock samples before and after the wind-tunnel test.

Freeze-thaw tests showed that samples consolidated with AC, AS, and SS, and with 10% PS, had good resistance; AS exhibited especially good resistance. Although the compressive strengths of the samples consolidated with AC, AS, and SS were comparatively low, their resistance to freezing and thawing was high. This is probably because these three organic polymers readily form films that coat the surfaces of rock grains and fill pores to some degree. Thus, they limit the uptake of moisture over a short period. Conversely, the rapid absorption by PS samples causes lowered resistance to freezing and thawing.

Because the climate of Mogao is that of an arid desert with an annual precipitation of only tens of millimeters, the water content of the rock is very low. Therefore, the resistance to freezing and thawing after consolidation is not a primary consideration in evaluating consolidants.

The on-site consolidation tests on the eastern side of the wind-break fence at the top of the cliff have shown that AC, AS, and SS, with PS, provided essentially similar permeation results. Best results of hardness tests of the surface of the consolidated sand were obtained with AS and 5% PS. An amount of spray of $5\text{--}6 \text{ l m}^{-2}$ was best. When the amount of PS sprayed was less than 4 l m^{-2} , the surface hardness of the consolidated sand was significantly reduced. When the amount of AS sprayed was less than 4.60 l m^{-2} , the surface hardness of the consolidated sand was also significantly reduced. When the concentration of PS was less than 5% and when the concentration of AS was lower than 1:20 (equivalent to 5%), consolidation strength was clearly reduced. When sodium silicate was mixed with PS, there was no change in strength for six months. Over a longer period of time, the surface showed white efflorescence of salts and gradually softened, especially after rain or snow. Therefore, it is not appro-

priate to admix sodium silicate with PS for consolidation. The surface hardness of consolidated sand treated with AC and SS was low; when the concentration was below 1:10 (water), the consolidation hardness was even lower.

Results obtained by moistening the dry sand 1–2 cm prior to spraying the consolidants and then immediately spraying the consolidants increased the consolidating strength of the PS and AS.

In addition, from determinations of the surface hardness by a simple puncture test and using the Schmidt hammer, it can be seen that sand treated with AS and 5% PS has high hardness.

Conclusion

Laboratory and on-site tests of AC, AS, SS, and PS demonstrated that PS, AS, and AC are all comparatively good consolidants. However, under the conditions of the Mogao area, the organics did not perform overall as well as PS, which showed high weather and ultraviolet resistance. At the same time, the PS consolidated sand exhibited rapid water permeation. The area requiring consolidation at Mogao has been initially estimated to be about 70,000 m², including the top of the cliff and the weathered cliff face. Thus, some 300 t of consolidant will be required if the decision is made to undertake such a large-scale intervention. In any event, PS would be the material of choice. It is low cost (by comparison with organic resins), chemically and environmentally inert, and locally available, though the high molar ratio material preferred must be special ordered from the manufacturer.

Future objectives include continued improvement of the technology of chemical consolidation as well as consolidation of effective anchoring consolidated surfaces to prevent slipping in a seismic event. Much still needs to be done, and a small-scale test intervention is planned in an appropriate area. Only after evaluation of this test will further consideration be given to large-scale work.

Acknowledgments

Special thanks go to associate professors Zhang Mingquan and Zhang Huliang from the Geology Department of Lanzhou University and Wang Xiudong from the Dunhuang Academy for their assistance in the performance and analysis of this experimental work.

Notes

- 1 The high-molar potassium silicate used in this study was provided by the Lanzhou Oil Refinery, and all the organic consolidants and monitoring instruments were provided by the Getty Conservation Institute.
- 2 The authors were unable to cut the conglomerate into regular samples by machine because the cementation was loose. All that could be done was to prepare samples of close to 50 × 50 × 50 mm by hand shaping.
- 3 The adhesive was calculated after dilution.

References

- Li Zuixiong**
- 1985 Application of the PS-C in the consolidation of weathered sandstone (in Chinese). *Dunhuang Yanjiu* 2:148–56.
- Ling Yuquan, Qu Jianjun, Fan Jinshi, Li Yunhe, Neville Agnew, and Po-Ming Lin**
- 1993 Research into windblown sand damage on the top of the Mogao grottoes (in Chinese). *Grotto Conservation (Dunhuang Yanjiu special edition)* 1:134–46.
- Nishiura, Tadateru, and Li Zuixiong**
- 1988 Experimental study of the consolidation of fragile porous stone with potassium silicate for the conservation of cave temples in China. In *The Conservation of Far Eastern Art: Preprints of the Contributions to the Kyoto Congress, 19–23 September 1988*, ed. J. S. Mills, P. Smith, and K. Yamasaki, 108–12. London: International Institute for the Conservation of Historic and Artistic Works (iic).

Research into the Control of Damage by Windblown Sand at the Mogao Grottoes

Ling Yuquan, Qu Jianjun, Fan Jinshi, and Li Yunhe

WINDBLOWN SAND has long posed a severe problem at the Mogao grottoes. Carried by prevailing seasonal winds from the extensive dunes on the plateau above the grottoes, the sand erodes the cliff slopes and accumulates at the base of the grottoes. Some 2,000 m³ of sand are swept up and removed annually. Moreover, sand and accompanying dust infiltrate the grottoes themselves, where they obscure the ancient sculptures and wall paintings.

Previously, experimental windbreaks of brush and reed have failed to control this problem. In 1989, the Lanzhou Desert Research Institute of the Chinese Academy of Sciences, the Dunhuang Academy, and the Getty Conservation Institute initiated a study of the problem to develop preventive measures. The Desert Research Institute designed a 3.7 km wind fence, in an A-shaped configuration. The design was based on seasonal and diurnal wind velocity and direction data gathered from the Getty Conservation Institute's solar-powered meteorological station on the cliff top and from sand traps used to determine quantity and particle size. The stability of the dunes with respect to growth and movement was also investigated. Data indicated that seasonal wind changes would disperse the accumulation of sand at the fence. For construction of the fence, the Getty Conservation Institute provided an ultraviolet-stabilized, knitted aerotextile, which reduced wind velocity by approximately 50%, and the Dunhuang Academy erected the fence in 1990. Although some reconfiguration of the fence has been necessary where heavy sand accumulation has not been subsequently dispersed, the fence has reduced sand at the cliff base by about 62%. In time, this efficiency is expected to increase, as the present accumulation is believed to derive from residual sand between the fence and the cliff edge. The fence is expected to have a life of at least fifteen years, by which time the vegetation windbreak now being planted, with a drip irrigation system, should be well established.

Background

The Mogao grottoes are a national protected site of the first rank and are also a world famous treasure-house of ancient Chinese art. It has been

called the “art gallery of the world” and “a museum on walls.” The murals and polychrome statues inside this immense group of caves, and especially the information content of the murals, embrace a broad range of complicated themes. They occupy an extremely important position in Chinese and world art history.

It has been sixteen hundred years since the initial excavations were made at Mogao. During this period, the effects of natural and human factors have caused damage of differing degrees to the caves, murals, and statues. Windblown sand is one of the most damaging factors. Erosion or denudation by windblown sand has left many of the caves with thin roofs and poses a direct threat to the conditions of preservation and to the environment of the murals. Accumulation of sand has resulted in pressure on the roofs. Sand accumulation on the walkways blocks traffic. Sand and dust have also abraded the murals.

In the early 1960s, a plan to control sand was formulated and small-scale sand-control experiments were initiated. However, there was insufficient recognition of the severity of the damage brought about by windblown sand, and not enough serious consideration was given to the importance of controlling windblown sand. Furthermore, because the methods taken for controlling sand were inappropriate, and because of lack of funding, the sand control experiments could not be continued. For example, the local dry brush fence built on the edge of the cliff top led to accumulation of sand on top of the cliff, creating a new source of sand near the cliff face and a latent danger. Another instance was the digging of sand-control ditches on the top of the cliff. The ditches were quickly filled by sand carried by the westerly wind. The principal reasons for these failures were that there was insufficient understanding of the patterns of wind and sand movement and poor awareness of the severity of the damage that they bring about. Therefore, for many years a passive approach was taken, and sand that had accumulated in front of the caves was removed by hand. After the World Heritage Committee of Unesco listed the Mogao grottoes as a World Heritage Site in 1987, research on damage to the Mogao grottoes by windblown sand was given serious consideration and support by leaders in various departments and at various levels. In July 1989, the Dunhuang Academy and the Lanzhou Desert Research Institute of the Chinese Academy of Sciences with the Getty Conservation Institute initiated experimental research on sand control using knitted polyethylene textile as the windbreak fence material.

The research was carried out in two stages. The first stage, from October 1989 to September 1990, involved making a topographic map (scale 1:1,000) of a 2 km² test area, then monitoring and studying the patterns of wind and sand movement using meteorological data and information collected from sand traps. The second stage began in October 1990 with the construction of the windbreak fence and continued until the end of 1992. The main objectives during this stage were to monitor the effectiveness of the fence on the basis of patterns of windblown sand activity and calculations of the intensity of the activity.

Natural Setting



Figure 1
Satellite image of the Mogao grottoes area.

Location

The Mogao grottoes are located on the southeastern margin of the Dunhuang oasis 25 km from the city of Dunhuang. The Sanwei mountains are to the east, the Mingsha sand dunes to the west, with the Daquan River valley between and the vast Gobi Desert to the north (Fig. 1).

The caves were excavated in the cliff on the west bank of the Daquan River (Fig. 2). The stratum in which the caves were excavated is the alluvial and pluvial Jiuquan conglomerate in which there is argillaceous and calcareous cementation. This is a recent geological formation, and the rock is poorly cemented. Thus, it weathers and is eroded rapidly by the wind.

This region is at the western end of the Hexi corridor in the hinterland of northwestern China and is constantly under the influence of the Mongolian high pressure system. The climate is characterized by extreme aridity, low precipitation, great seasonal temperature variation, and frequent windblown sand activity. The average annual atmospheric temperature at Mogao is 10.3 °C. The highest temperature ever recorded at the grottoes was 40.6 °C on 27 July 1965 and the lowest absolute temperature was -21.5 °C on 23 December 1965. The average annual precipitation level is 23.2 mm and annual evaporation is 3,479 mm, 150 times the precipitation level; and the average relative humidity is 32%.

Wind conditions

The Mogao grottoes are situated in a windy region having an annual average wind velocity of 3.5 m s⁻¹. However, it is a region in which there is great variation in wind direction (Fig. 3). The south wind is the most common and accounts for 31% of the wind frequency. The southerly winds, including the south-southeast and south-southwest winds, account for 47.9% of the wind frequency. However, the wind speeds are not very great. For example, 39% of the south winds have a wind speed less than that required for saltation of sand (5.0 m s⁻¹ at a height of 2 m), whereas only 1.5% of the winds have a velocity higher than 8.0 m s⁻¹, and 59.2%

Figure 2
Overall view of the Mogao grottoes.



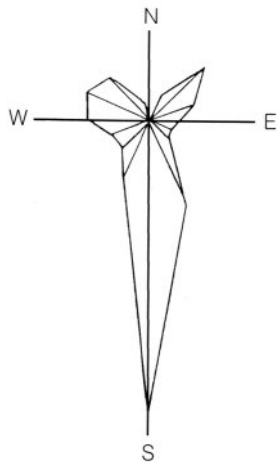


Figure 3
Wind rose at the Mogao grottoes (1990–91).

have a velocity greater than 5.0 m s^{-1} and less than 8.0 m s^{-1} . Wind-tunnel experiments in Lanzhou have demonstrated that winds with velocities in this range have a very limited sand transport capacity. They can barely move the sand on the surface of the dunes to form ripples. They have even less effect on the sand and gravel of the Gobi Desert. The next prevailing wind is the westerly wind. The frequency of the westerly winds (south-west, west-southwest, west, west-northwest, and northwest) is 28.1%. However, they account for 31.9% of the sand-transport capacity. Most (70.8%) of the westerly winds are less than the saltation speed, and 23.4% have wind speeds greater than 5.0 m s^{-1} and less than 8.0 m s^{-1} , accounting for 28.9% of sand-transport capacity. The frequency of wind speeds greater than 8.0 m s^{-1} amounts to 5.8% on average and accounts for 71.1% of the sand-transport capacity. In other words, the common southerly winds are weaker, and the westerly winds are stronger. Thus, the westerly winds are the principal cause of sand accumulation and damage in front of the grottoes. The frequency of the easterly winds is only 14.8%, and they account for 27.5% of the sand-transport capacity. The major damage caused by the easterly winds is erosion and denudation of the cliff face. It also has an effect, that cannot be undervalued, of inhibiting the eastward drift of sand at the top of the cliff.

The formation and characteristics of this type of average flow field is affected by the large-scale topography—such as the dynamic and thermal action of the Qinghai-Xizang plateau (Luo 1982) and the Qilian and Tian mountains—as well as small-scale landforms, the Sanwei and Mingsha mountains, and the desert and surface of the Gobi (Ling 1988). Specifically speaking, the strong west winds are dominated primarily by the circulation of the prevailing westerly wind and large-scale weather patterns. The weak, frequent southerly winds derive from local currents or from the Qilian mountains. There were some obvious patterns in the seasonal and daily variations of the southerly winds, which are more common in evenings and in the winter months (from October to February). Although the winds are weak, they display considerable directional stability.

This typical circulation pattern shaped the unique landform of the Mingsha mountain and led to the formation of a group of relatively stable but complex sand dunes. There were clear seasonal variations, with coarse sands covering the upper-middle section of the slope in the dominant wind direction.

On the basis of site inspection and research, it was discovered that the sand in this region is primarily derived locally—that is, under the action of winds of different frequencies, of different strengths, and of multiple directions, local sands were transported back and forth in the area.

Patterns of Sand Movement in the Mogao Grottoes Region

Characteristics of sand movement

From an overall standpoint, sand movement in this region belongs to the category of sand flow from the Gobi Desert. Specifically, intense saltation of sand grains raises the height of sand transport and makes the amounts



Figure 4
Patterns of sand accumulation in different directions around a plant.

of sand carried in the upper and lower layers relatively uniform. Under such conditions, sand is transported and tends not to accumulate. However, winds from different directions, of different frequencies and different intensities, alter the characteristics of the sand movement, making it more complex. For example, there can be sands of different granularity accumulated in different shapes in different directions around a plant (Fig. 4). Accumulation of sand can only undergo changes in shape but cannot continuously increase in volume. Sand ripples and dunes are no exception to this. There are also severe limitations imposed by multiple changes of wind direction. In Figure 4, the formation of coarse sand ripples at the leeward side under the action of the strong west wind can clearly be seen. The sand was from a sand and gravel surface. Not only is the area of accumulation large but the height and width of the ripples are also large. Sand formed by southerly winds is very fine-grained and displays a small area of accumulation, and the height and width of the ripples are small. This sand originates from drifting sand dunes. The east wind has a reverse transport capacity in respect to sand accumulated at the tops and sides of the cliffs and can form accumulations of sand behind vegetation. The scale and granularity of the sand deposits are smaller than those deposited by the west wind but larger than those deposited by the south wind. There are clear seasonal variations in the shape of sand accumulation, and the changes are completely congruent with the pattern of changes in average flow fields.

Pattern and intensity of windblown sand activity

To further understand the patterns of movement of the wind-driven sand, we selected three profiles for monitoring the distribution, movement, and deposition of sand on the top of the cliff and at the cliff base and conducted more than two years of monitoring and research. The directions of the monitored profiles are the same as the wind directions.

The amount and rate of sand transport was monitored at a height of 0–20 cm, and the average wind velocity was monitored at heights of 0.2 and 1.5 m above the ground surface. Five observation points were established for each profile, and comparative monitoring was performed simultaneously.

At the same time, five sand traps were set up in front of the grottoes (Caves 152, 256, 404, 208, and 154) at different locations to measure the daily sand accumulation from 1800 to 0800 hours. These times were established to avoid disturbance by visitors during the day.

A small sand dune was also selected, and studies were made of change in its shape and rate of movement, with contour lines mapped each time after a gusty wind. Determinations were also made of shifts in the ridge using marker sticks.

Monitoring results

Characteristics of windblown sand distribution from the sand drift to the top of the cliff during west or northwest winds can be seen in Tables 1–3.

Note that the sand-transport rate increased rapidly with increasing average wind velocity. The relationship between the transport rate (q) and the threshold deflation velocity (V_t) is as follows (Ling 1992):

$$q = 8.95 \times 10^{-1} (V - V_t)^{1.9}$$

where V_t is the sand grain deflation velocity. V_t is 5.0 m s^{-1} (at a height of 2 m) for sand grains of 0.125–0.250 mm in size. The roughness of the ground surface in the Gobi Desert is 0.115 cm, which is much higher than that of drifting sand (average roughness at the surface of the shifting sand being 0.005 cm). Therefore, the threshold grain-deflation velocity in the Gobi Desert is undoubtedly high. Theoretically, grain-deflation velocity is proportional to the square root of the diameter of the sand grain, that is, $V_t \propto d^{1/2}$. For the same wind velocity, the sand-transport rate is lower in the Gobi Desert than that in an area of shifting sand. However, as a result of long-term transport by southerly winds, the ground surface of the Gobi Desert is covered with numerous small sand dunes, and the threshold deflation velocity is thus close to that of drifting sand. To calculate the maximum possible rate of sand transport, the authors used 5.0 m s^{-1} as the average threshold deflation velocity. As shown in Table 1, when the average wind velocity was about 6.0 m s^{-1} , the sand-transport rate was about the same at all five observation points along the profile. When the average wind velocity increased to 8.0 – 9.0 m s^{-1} , there was a marked change in the sand transport rate and a high rate (relative to the sand and gravel of the Gobi Desert) was observed at observation point no. 3. This was because of the sandy character of the drifting sand transported by the westerly wind. After carrying sand for 500–700 m, the westerly winds deposited part of their load in the depression around observation point no. 3. Following this, some of this sand was carried to a sand and gravel plateau about 5 m lower than the previous ground surface. It was then carried another 200 m to the top of the cliff or near the cliff face. The abrupt change in the landforms led to separation of the flow into layers and deposition of sand in separate regions.

Table 1 Characteristics of windblown sand with a west or northwest wind

Item and location	No. 1 Drift sand	No. 2 Gobi	No. 3 Gobi	No. 4 Gobi	No. 5 Cliff top
$V_{1.5} \text{ (m s}^{-1}\text{)}$	6.1	5.8	6.3	6.5	6.4
$q \text{ (g cm}^{-1} \text{ min}^{-1}\text{)}$	0.501	0.344	0.386	0.305	0.366
$V_{1.5} \text{ (m s}^{-1}\text{)}$	9.4	8.2	8.2	8.9	8.8
$q \text{ (g cm}^{-1} \text{ min}^{-1}\text{)}$	4.429	3.960	4.228	3.161	3.459
$V_{1.5} \text{ (m s}^{-1}\text{)}$	10.4	8.9		10.3	10.7
$q \text{ (g cm}^{-1} \text{ min}^{-1}\text{)}$	9.307	5.864		6.199	7.960
$V_{1.5} \text{ (m s}^{-1}\text{)}$	12.6	11.2	12.1	15.6	14.3
$q \text{ (g cm}^{-1} \text{ min}^{-1}\text{)}$	16.750	10.300	10.825		

All five locations are on the plateau above the grottoes, at various points between the edge of the cliff and the Mingsha dunes. "Drift sand" and "Gobi" refer to the characteristics of the surface, the latter being gravel.

Table 2 Characteristics of windblown sand with a southwest wind

Item and location	No. 1 Drift sand	No. 2 Gobi	No. 3 Gobi	No. 4 Gobi	No. 5 Cliff top
$V_{1.5}$ (m s^{-1})	5.8	5.4	5.5	6.0	6.1
q ($\text{g cm}^{-1} \text{min}^{-1}$)	0.473	0.136	0.093	0.039	0.095
$V_{1.5}$ (m s^{-1})	8.5	7.2	7.5	7.8	7.8
q ($\text{g cm}^{-1} \text{min}^{-1}$)	1.960	1.586	1.132	0.717	0.509

See note to Table 1.

Table 3 Characteristics of windblown sand with an easterly wind

Item and location	No. 1 Drift sand	No. 2 Gobi	No. 3 Gobi	No. 4 Gobi	No. 5 Cliff top
$V_{1.5}$ (m s^{-1})	6.7	6.2	6.3	6.6	6.8
q ($\text{g cm}^{-1} \text{min}^{-1}$)	0.824	0.613	0.565	0.573	1.480
$V_{1.5}$ (m s^{-1})	8.3	7.7	7.8	8.0	8.8
q ($\text{g cm}^{-1} \text{min}^{-1}$)	5.312	3.143	3.614	4.601	6.798

See note to Table 1.

Sand accumulation at the base of the cliff occurs only when the slope angle is larger than the angle of repose or after a gusty wind when sand may slide down the cliff face, with great variations occurring in the granularity of the accumulated sand. Generally, there can be two peaks of annual change in sand accumulation in front of the caves. The principal peak appears in April to June, during which period the east and west winds are dominant. The next peak appears from August to October. On the basis of the observations of the distribution of sand-transport rates from the profiles, most of the sand transported at each section was the result of local deflation. Only when the wind velocity was greater than 11.0 m s^{-1} did long-distance transport of sand occur (Table 1.)

The amount of sand transport varies with height above ground and is closely related to the positioning of the sand-control installation and the height of transport of the wind-driven sand. Under ordinary conditions, the height of transport of drifting, windblown sand above the surface of the shifting sand is less than 1 m, and more than 95% of the sand is transported in a zone less than 20 cm above the ground surface. Of this, 80–90% of the sand is carried in a zone 0–10 cm above the ground surface. That is to say, drifting sand can be stabilized either by reducing wind velocity or by controlling the movement of the windblown sand. If, at the same time, we can take measures to intercept the sand on the windward side, then a protection system can be established in which an emphasis on stabilization is combined with blockage.

Wind speed is usually high on the Gobi Desert because of the open topography. At the same time, the gravel nature of the ground surface increases the rebound action of the saltating sand grains. Thus, sand

can be transported in wind higher than 1 m above the ground; but only 3–4% of the sand is transported in this way. On average, less than 80% of sand is transported in the layer 0–20 cm above the ground. There is a lack of sand sources in the Gobi, and the windblown sand flow is in a very unsaturated state. Under such conditions, protective measures suited to the circumstances are ordinarily adopted in regions in which there is a danger of damage by windblown sand.

In the sand and gravel regions of the Gobi Desert, there is a fixed source of sand, the gravel is fine, and there is not a very strong rebound action on the part of the saltation sand grains. A higher concentration of sand is carried by the air in the gravel region of the Gobi. For this reason, the characteristics of sand movement in the sandy regions of the Gobi are a combination of those in the gravel region and those at the surface of drifting sand. The results of the determinations indicate that the sand-transport rate in the 0–20 cm layer exceeds 93.32%, which is very close to that on the surface of the drifting sand, when the average wind velocity is 10.4 m s^{-1} at 1.5 m above the ground surface. However, there is a sand-transport volume of only about 1% in the layer 1 m above the ground surface and a volume of only 0.19% in the layer 210–230 cm above the ground surface. The distribution of sand in the 0–2 cm layer is relatively uniform. The windblown sand flow belongs to the category of low concentration, unsaturated sand-transport intensity.

Southwesterly windblown sand flow

It can be seen from Table 2 that the amount of sand transported from the Mingsha mountain to the top of the cliff by the southwesterly winds is much less than that carried by the northwest wind. Although there is an ample supply of sand, the average flow field limited and slowed the transportation capacity of the southerly and southwesterly winds. In addition, the Mingsha mountain itself acts as a barrier to the southwest wind. For this reason, the sand-transport rate is gradually reduced from the Mingsha mountain to the top of the cliff.

Easterly windblown sand flow

As can be seen from Table 3, there is a clear increase in windblown sand flow intensity under the actions of easterly winds. That is to say, easterly winds have a definite reverse-direction transport capacity on sand that has accumulated over long periods on the cliff top and cliff face. The findings in Table 3 reflect a back-and-forth transport of sand in this region, which creates great difficulties for sand-control installations.

Sand-Control Measures and Implementation

Design principles

The objective is to protect the Mogao grottoes from damage by wind-blown sand or to lessen the degree of damage. Specifically speaking, this means controlling the large quantity of sand carried by the westerly winds

from accumulating on top of this cliff, near the cliff face, and on the walkways below, and controlling wind erosion and abrasion of the bedrock caused by the easterly winds. At the same time, the action of the southerly winds, which are of the highest frequency, needs to be taken into consideration. Therefore, design of sand-control programs must be comprehensive and economical and be able to deal with multiple wind directions.

Design basis

The observation and research carried out in the earlier phase not only deepened an understanding of the patterns of sand drift in this region but also provided valuable scientific bases for the design of sand-control programs.

Basic theoretical calculations show that maximum sand-transport capacity of westerly winds in this area is $13 \text{ m}^3 \text{ m}^{-1} \text{ yr}^{-1}$. In other words, every year $12,000 \text{ m}^3$ of sand can accumulate along the 900 m long cave area, with a considerable portion of the sand accumulating on the cliff face and some accumulating on the walkways in front of the caves. Nearly the same amount of sand is transported in the reverse direction by the easterly winds. On this 900 m long cliff, $11,500 \text{ m}^3$ of sand can be transported from the top of the cliff toward the Mingsha dunes and be distributed over the approximately 2 km^2 sand-and-gravel portion of the plateau. The difference between the maximum amount of sand that can be transported from east to west and the maximum amount of sand that can be transported from west to east is approximately 520 m^3 .

It is important to note that the maximum possible sand-transport capacity of the southerly wind is $11,000 \text{ m}^3 \text{ m}^{-1} \text{ yr}^{-1}$. The southerly winds provide new sources of sand for transport by the easterly and westerly winds but do not cause direct damage to the caves.

In the present phase, a synthetic knitted textile windbreak fence is the principal method being used to control sand from accumulating in front of the caves. Testing is also taking place on chemical consolidation to prevent weathering of the cliff rock.

Windbreak fences are frequently used to block sand flow in a single direction. In this case, sand-blocking efficiency is generally 80–90%. If the intensity of the windblown sand is high, the windbreak fence will be buried in a few years and a new fence will need to be installed on the top of the old fence.

In view of the aforementioned circumstances, and in consideration of the characteristics of the windblown sand activity in this region, an A-shaped windbreak fence system was designed and installed in a triangular form (Fig. 5). The three sides of the triangle are at an effectively larger angle to the dominant wind directions and at a smaller angle or nearly parallel to the secondary wind directions. Thus, the fence can block sand carried in the dominant wind directions and divert the sand carried in the secondary wind directions. It is an effective and comprehensive control system that is capable of controlling windblown sand from multiple wind directions. The fact that ripples that are formed on the surface of the

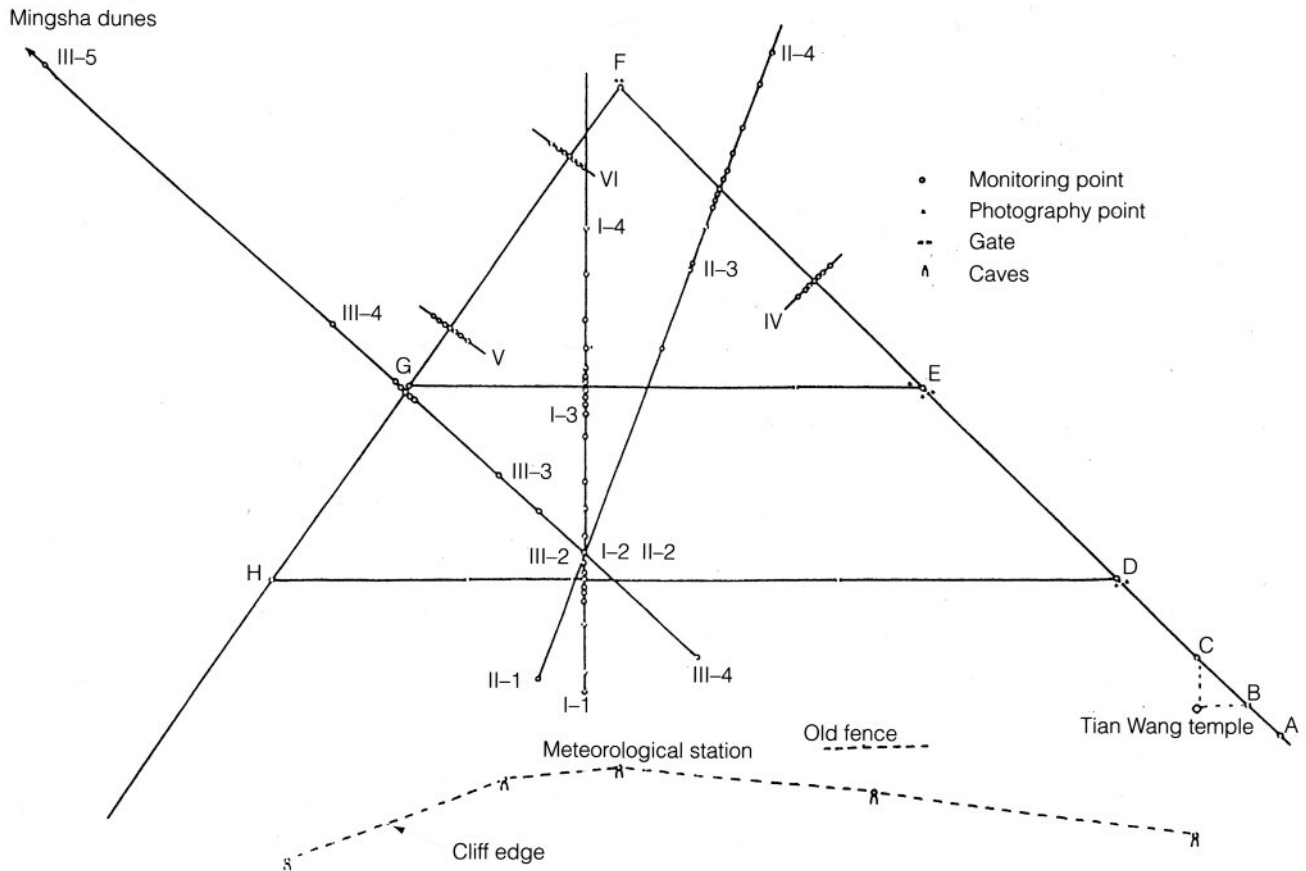


Figure 5
Plan of the synthetic textile wind fence on the plateau above the grottoes, and sand-monitoring Sections I-VI.

accumulating sand on the windward side are perpendicular to the fence provides the most convincing proof of its sand-diverting capacity.

Effectiveness of Sand Control

The windbreak fence is 1.8 m high with a void space of 20% and a resistance coefficient of 1.5. When the average wind velocity is 11.1 m s^{-1} , the windbreak fence is subject to a wind pressure of 17 kg m^{-2} . Angle steel posts were used for the fence, set with 3 m spacing. The posts were installed in a $20 \times 20 \times 30 \text{ cm}$ concrete foundation. The textile net was further reinforced with 45° wires running diagonally between posts.

To guard against sand accumulation in front of the caves, installation of the windbreak fence was completed by the end of November 1990. The amount of sand that accumulated in front of the caves during March 1991 was 75% less than that during March 1990. The sand accumulated in front of the caves cannot reflect the true effectiveness of the windbreak fence for now. The reason for this is that the gusty easterly winds cause sand accumulated on the surface of the cliff to slip down to the front of the caves. However, the following two observations show the effectiveness of the windbreak fence. First, the amount of sand in the sand traps in front of the caves was clearly decreased, the grain size became coarser, and there was a marked increase in gravel content. Second, there was decrease or disappearance of yellow layered sand on the top of the cliff and on the surface of the cliff face.

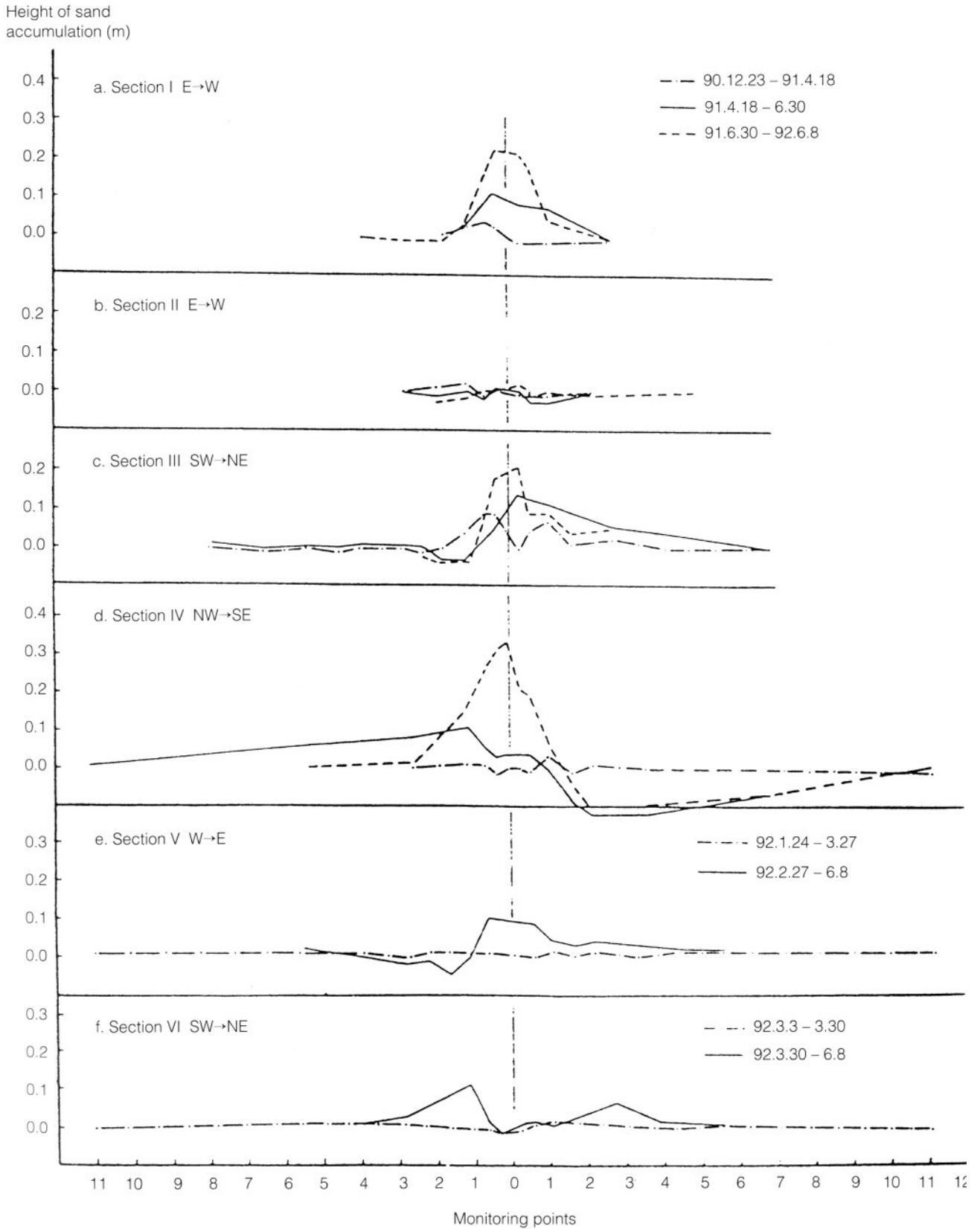


Figure 6 Sand accumulation profiles at monitoring points along Sections I-VI.

To deter sand accumulation in front of and in back of the fence, other measures were taken. In order to monitor the effectiveness of the windbreak fence, six sections were selected along the fence for study of the sand accumulation (Fig. 5). The results are shown in Figure 6. Section I

is one of sand accumulation close to the top of the cliff and parallel to the cliff face. Small quantities of sand were transported from both the east and west, which caused accumulations of sand both in front of and in back of the fence. Some of this was underground sand that had been scooped out during the installation of the fence and was later deposited around the fence. Section II was situated to the west of Section I and was close to the center of the windbreak fence system. Here there was no clear sand accumulation or erosion. Section III monitored a section of the fence aimed at preventing accumulation of sand by the southerly winds. There was severe sand accumulation in front of the fence, and there was erosion in back of the fence. Section IV was a section of the fence installed to prevent accumulation of sand by the westerly winds. In front of the fence, there was an accumulation of sand (due to the action of the northwesterly wind), and there was also erosion (due to the sand deflation action of the northeast or westerly winds). There was also clear accumulation of sand in back of the fence. From this it can be seen that the amounts of sand that accumulated inside and outside the windbreak protection system were very slightly less than the amounts that were calculated theoretically. Large amounts of

Table 4 Characteristics of windblown sand at cross Section I with a northeast wind (see also Fig. 5)

Item and location	20 m in front of no. 1	1 m in front of no. 2	1 m to the rear of no. 3	20 m to the rear of no. 3
$V_{1.5}$ (m s^{-1})	8.4	8.3	4.7	6.5
q ($\text{g cm}^{-1} \text{min}^{-1}$)	0.644	2.141	1.442	0.072

Table 5 Characteristics of windblown sand at cross Section III with a southwest wind (see also Fig. 5)

Item and location	50 m in front of no. 1	20 m in front of no. 2	1 m in front of no. 3	1 m to the rear of no. 4	20 m to the rear of no. 5
$V_{1.5}$ (m s^{-1})	6.2	5.7	4.6	2.8	4.2
q ($\text{g cm}^{-1} \text{min}^{-1}$)	0.356	0.284	0.165	0.061	0.002

Table 6 Characteristics of windblown sand at cross Section IV with a northwest wind (see also Fig. 5)

Item and location	10 m in front of no. 1	1 m in front of no. 2	1 m to the rear of no. 3	10 m to the rear of no. 4
$V_{1.5}$ (m s^{-1})	7.7	6.7	4.0	3.9
q ($\text{g cm}^{-1} \text{min}^{-1}$)	0.146	0.074	0.187	0.004

sand had been diverted. This clearly indicates the great effectiveness of the windbreak fence.

Characteristics of dynamic transport of sand

Comparisons of sand accumulated at different locations along the fence demonstrated the effectiveness of the windbreak fence. Examples are shown in Tables 4–6. As indicated in Table 4, when there were northeasterly winds in Section I, comparatively small amounts of sand transport took place 1 m in front of and in back of the fence and 20 m in back of and in front of the fence, due to insufficient sand sources, even though there was a strong wind force. The small quantity of sand transport at 20 m in back of the fence was also a result of the sand-blocking effectiveness of the fence. This is congruent with the state of sand accumulation described above. The effectiveness of this type of sand control is clearly reflected in Sections III and IV. At distances of 10 and 20 m in back of the fence, the quantity of sand transport was only 0.7–2.7% of the quantity of sand transport at the corresponding distances in front of the fence. It can be said that less than 5% of the windblown sand will be able to reach the top of the cliff after it has passed through the protection system. At present, most of the sand that has gathered in front of the caves is the product of many years of accumulation. There were very great differences in the quantity and composition of the accumulated sand, particularly under the influence of easterly winds.

In summary, comprehensive measures against damage by windblown sand are necessary, especially in the Mogao grottoes region. The diversity and complexity of windblown sand activity makes comprehensive control even more necessary. A comprehensive, overall sand-control program is dependent on a thorough understanding of the patterns of windblown sand movement.

Conclusion

Different frequencies and intensities of winds from multiple directions characterize the average flow field in the Mogao region. Serious sand accumulation and severe wind erosion are two major forms of windblown sand damage to the Mogao grottoes brought about by this type of flow field.

On the basis of test data on patterns of windblown sand activity in this region, the triangular windbreak fence was capable both of blocking the drifting sand carried in the dominant winds and of diverting fixed quantities of accumulated sand in the secondary wind directions. This multifunctional fence system has effectively controlled windblown sand (decreasing it by about 95%) and has prevented accumulation of sand in front of the caves (reducing it by about 75%).

Damage by windblown sand must be controlled in a comprehensive way. After preliminary control of sand erosion in front of the Mogao grottoes was achieved, the problem of wind erosion of the cliff face became even more pronounced. For this reason, it is also necessary to carry out effective chemical consolidation of the cliff face without delay. In

addition, further research on developing vegetation windbreak fences is a task of significance.

Maintenance—by removal of accumulated sand, as necessary—and monitoring of the windbreak fence are the keys to increasing the effective life of the fence.

Acknowledgments

The authors wish to express their thanks to Hu Wen, senior engineer of the Desert Research Institute, who carried out the systematic analysis of the meteorological data collected at Mogao. They also wish to express their gratitude to Huang Kezhong, deputy director, and Sun Rujian, former director of the Chinese National Institute of Cultural Property; Li Zuixiong, director of the Conservation Institute of Dunhuang Academy; and Neville Agnew and Po-Ming Lin of the Getty Conservation Institute for their assistance in this project. They also thank Qin Zengguo, Zhan Zhaoqi, and Hou Xing for their assistance in the installation of the windbreak fence.

References

- Ling Yuquan
- 1988 The characteristics of flow fields and their relationships to windblown sand activity in the Takla Makan desert (in Chinese). *Zhongguo Shamo* 3(8):25–27.
- 1992 Nonuniformity of Average Sand Transport Volume (Rate) Distribution: Wind Tunnel Experimental Research. Report. Lanzhou Desert Research Institute.
- Luo Siwei
- 1982 The average air circulation in the Qinghai-Xizang plateau and its neighborhood during summer and winter (in Chinese). *Gaoyuan Qixiang* 4(1):60–73.

Desert-Adapted Plants for Control of Windblown Sand

Po-Ming Lin, Neville Agnew, Li Yunhe, and Wang Wanfu

IN THE NORTHWEST of China, as in other desert regions of the world, erosion of historic and cultural sites by windblown sand is a serious problem. Sites that were long abandoned are often buried by sand and thus preserved; as, for example, the remarkable preservation of archaeological and organic remains discovered in the Takla Makan desert of Xinjiang. However, at sites open to the public, such as Mogao, the accumulation of sand needs constant removal and diverts resources and staff needed for other functions. Here sand and dust settle on the art within the grottoes, and the attrition of windblown sand has thinned the rock of the upper-level caves. Sand control is thus a matter of priority.

The problem of windblown sand is, in general, more than one of preservation of cultural heritage resources. Migrating dunes block roads and rail lines, and the Desert Research Institute (IDRAS) in Lanzhou (an institute of the Academia Sinica) has developed expertise in dealing with these problems in this area of China, and in understanding the larger issues of desertification. Elsewhere in these proceedings the results of the windfence designed by IDRAS are reported (Ling et al. herein). The present paper complements that of Ling et al.

Previously, attempts at sand control by dry-brush fences were undertaken at Mogao. These were ineffectual. In 1990, the synthetic fabric windbreak fence, referred to above, 3.4 km long, was built on the plateau above the grottoes as a measure to control the problem. This fence has reduced sand accumulating at the base of the cliff by 60%. The fence was designed using data on wind speed, wind direction, and wind duration collected by an automatic weather station on the cliff top. The design takes into account diurnal and seasonal changes in wind and minimizes accumulation of sand along the fence. The fencing material has a life expectancy of at least fifteen years. As a permanent solution to sand control at Mogao, a vegetation windbreak was planted. Because of the extreme aridity of the region, it was necessary to select plant species adapted to the harsh environment. The following reports the results of the trial windbreak and its extension.

A trial vegetation windbreak fence was planted at Mogao in May 1992. An experimental area 200 m long and 10 m wide was selected to supplement the performance of the fabric fence. A drip irrigation system with twelve hundred emitters was installed. Four species of indigenous desert-adapted plants, totaling about six hundred young trees, were planted. These plants can tolerate extreme weather conditions and saline sand. After one year, the results looked promising. The survival of the four species ranged from 82% to 100%. Among them, *Haloxylon ammodendron* had the highest survival and grew fastest. The experimental site was expanded to 8,000 m² in the spring of 1993.

The Mogao grottoes, one of China's most prestigious sites, has been affected by sand erosion since the earliest times. Excavated into the cliff face on the west bank of the Daquan River, the grottoes consist of some five hundred caves divided into southern and northern regions. In the southern region, the caves are decorated with wall paintings and sculptures; most of the caves in the north region are not decorated. At the top of the cliff is a plateau. Part of the Gobi Desert, the plateau is covered with sand, pebbles, and a small amount of vegetation. The plateau ends about 1 km to the west of the cliff, where the huge Mingsha sand dunes rise abruptly. These are stable, yet feed sand migration to the grottoes, and are themselves replenished by sand farther to the west.

The persistent wind is from the south with low speed. Minor wind directions are from the west and east but with much higher speed than that of the south wind. The average wind speed is 3.5 m s⁻¹. The highest wind speed can reach 16 m s⁻¹. Prevailing winds drive sand toward the cliff where an approximately 35–45° slope has been eroded between the plateau and the vertical face of the escarpment.

There is no record of how the sand problem at the Mogao grottoes was dealt with in ancient times. In the 1950s and 1960s, site personnel tried to stop sand migration by erecting dry-brush fences at the edge of the cliff and at the foot of the Mingsha dunes. None of these methods was effective. As described by Ling et al. (herein; Ling et al. 1993), a synthetic fabric windbreak fence was designed and constructed as part of the collaboration with the Getty Conservation Institute. Prior to the installation of the synthetic fabric fence, about 3,000 m³ of sand were swept up and removed annually from the grotto site. Frequently, walkways and entrances to caves were blocked by accumulated sand; it gets into caves via entrances, and fine dust is deposited on the surfaces of sculptures and wall paintings, obscuring them. In addition, sand erosion of the cliff slope has cut through the rock roofs of the upper-level caves, resulting in collapse in some instances.

An A-shaped synthetic fabric windbreak fence 3.4 km long was built on the plateau above the grottoes in 1991 to control the sand problem. The fence reduced sand accumulation at the base of the cliff by 62% (Ling et al. 1993). However, the fence may be subject to vandalism as well as eventual deterioration, and sand accumulation has occurred in some areas of the fence, necessitating manual removal. As a permanent solution

to the problem, a vegetation windbreak was proposed—one that would supplement the fabric fence and eventually supplant it.

The objective was to establish a permanent zone of indigenous, desert-adapted plants on the plateau to control sand movement.

A drip irrigation system was installed to provide adequate water during the period when the plants were establishing themselves. Other factors that needed to be taken into consideration were climate, choice of appropriate plants, water quantity and quality, and soil type.

Location

The test site is located about 1 km south of the existing synthetic fabric fence and about 100 m from the nearest sand dune (Fig. 1). To protect the young plants while they were establishing themselves, a supplementary synthetic fabric windbreak fence was built. This fence is 1 m tall, 200 m long, and was situated between the experimental area and the sand dunes, parallel to the tree lines.

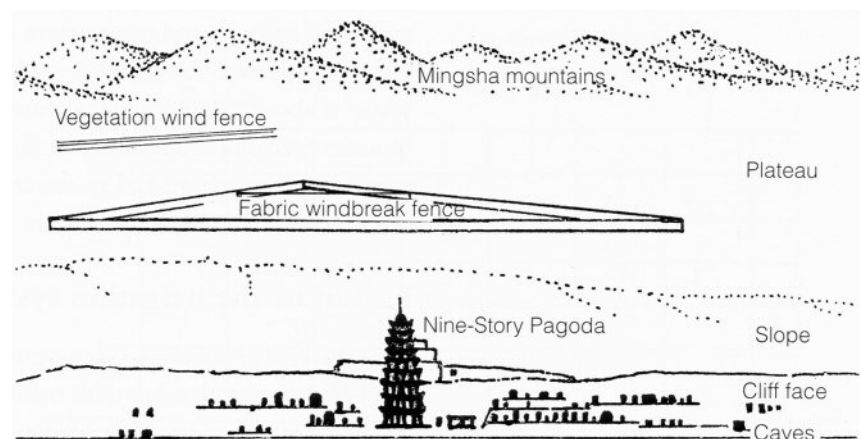
Soil

The area between the grottoes and the Mingsha dunes is typical Gobi Desert, consisting of sand, pebbles, some silt, soluble salts, and no organic matter. This type of soil has very high permeability and low moisture-retaining capability. Furthermore, evaporation is much higher than precipitation in this region. Thus, topsoil was brought in and placed in the holes for the seedlings.

Vegetation

Haloxylon ammodendron, *Tamarix chinensis*, *Calligonum arborescens*, and *Hedysarum scoparium* were selected for the experiment. These plants are native to the region; tolerate dry, cold, and hot weather; and survive in saline soils. They grow 6–9 m high if enough water is provided; and they mature, bloom, and seed within four to five years. Seedlings were obtained by the Dunhuang Academy from a nursery in Lanzhou.

Figure 1
Schematic drawing showing the location of the vegetation windbreak fence.



Water

Annual precipitation in the Dunhuang area is 16–24 mm. Water for irrigation and daily living at the Mogao grottoes is obtained from the Daquan River, which flows through the site. The ultimate source is mostly melt-water from snow in the distant Qilian mountains. The river contains a high concentration of salts. It has long been used to periodically irrigate the trees growing in front of the grottoes, without harmful effects to them.

Drip Irrigation

Drip irrigation systems are more effective and less wasteful of water than traditional surface furrows. A network of closed conduits supplies small amounts of filtered water to the plants according to a regular schedule. Weed growth and water consumption by weeds are limited, because only a small surface area of the soil is irrigated.

The major disadvantage of drip irrigation systems is clogging of emitters and drip lines. Clogging can be physical, chemical, or biological. Physical clogging is caused by particles of sand, silt, clay, and waterborne debris too large to pass through the small openings of the emitters; particles may also be deposited in the lines, reducing water flow. Chemical clogging is caused by soluble salts that precipitate on emitters as water evaporates from the emitter surface between irrigation cycles. Biological clogging is caused by microorganism growth inside the system. Certain species of bacteria and algae flourish inside drip systems and produce deposits, often of iron oxides, that clog pipes and emitters.

To prevent clogging of the system, some preventive approaches were adopted. An in-line filter was installed to prevent clogging caused by particles; a chemical injector was added to the system for application of acid and/or chlorine at the end of each watering period to deal with chemical and biological clogging. The injector can also be used to fertilize the plants. Chlorination is an effective measure against biological clogging. Sodium hypochlorite solution is the easiest form of chlorine to handle and is most often used in drip irrigation systems. However, excessive amounts of chlorine result in injury to young trees and other plants. Tyson and Harrison (1987) have recommended 5 ppm as an effective concentration. However, sodium hypochlorite increases the pH of water, and precipitation of calcium and magnesium carbonate tends to occur. Bucks, Nakayama, and Gilbert (1979) pointed out that when the pH of irrigation water is above 7.5 and high calcium or magnesium levels are present, carbonates precipitate out either in filters, tubing, or emitters. Therefore, it was decided to use acid, if necessary, to prevent the formation of deposits. Sulfuric and hydrochloric acids are the most widely used.

Layout of the irrigation system

Two water-storage containers were built to supply the system. An 18,000 l semi-underground water tank equipped with a 7-Hp pump located at the riverbank supplies water to a 9,000 l tank equipped with a 3-Hp pump located on-site. Water diverted from the Daquan River flows to a small

settlement pond, then is pumped to the larger water tank. The elevation difference between the two tanks is 50 m, and the horizontal distance between them is about 1,150 m. Connecting the two tanks is steel pipe 5 cm in diameter.

Figure 2 schematically illustrates the layout of the system. The submain pipes are about 15 m long and 100 m apart. A control valve, a Y-shaped in-line filter, and chemical injector are installed at the head of each submain pipe. Each submain pipe is connected to twelve lateral pipes spaced 2 m apart. The lateral pipes are 50 m long and equipped with two emitters every 2 m, spaced 0.6 m apart. Shrubs are planted between the two emitters.

Initially, the experimental area was about 10 m wide and 200 m long. This area was divided into five zones. One species of shrub was planted in each zone. In the fifth zone, the four species were mixed, as a possible means of reducing plant disease. About six hundred, year-old seedlings were planted in six rows and one hundred columns. The spacing was 2 m between rows and columns. To increase wind resistance, the offset between columns was 1 m (Fig. 3).

System design

When designing a drip irrigation system, factors such as water delivery distance, diameter of pipes, type of emitter, and weather conditions need to be taken into consideration. After design criteria are decided, the procedure is as follows:¹

1. Estimate water consumption per plant per day:

Liters per plant per day

= constant \times plant area \times plant factor \times P.E.T. (potential evapotranspiration) / drip irrigation efficiency

= $10.2 \times 2 \times 0.45 \times 1.143 / 0.75 = 14$ l

Then the total water consumption = $1 \text{ plant}^{-1} \text{ day}^{-1} \times$ number of trees = $14 \times 600 = 8,400 \text{ l day}^{-1}$.

Figure 2
Layout of the system.

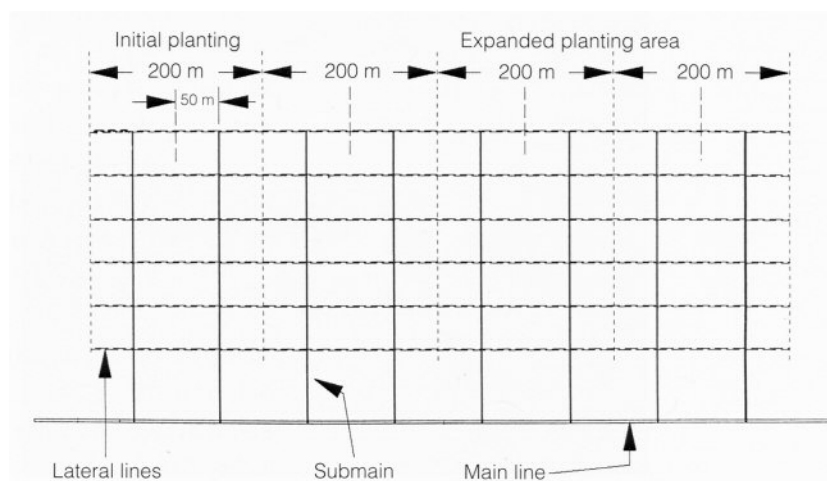
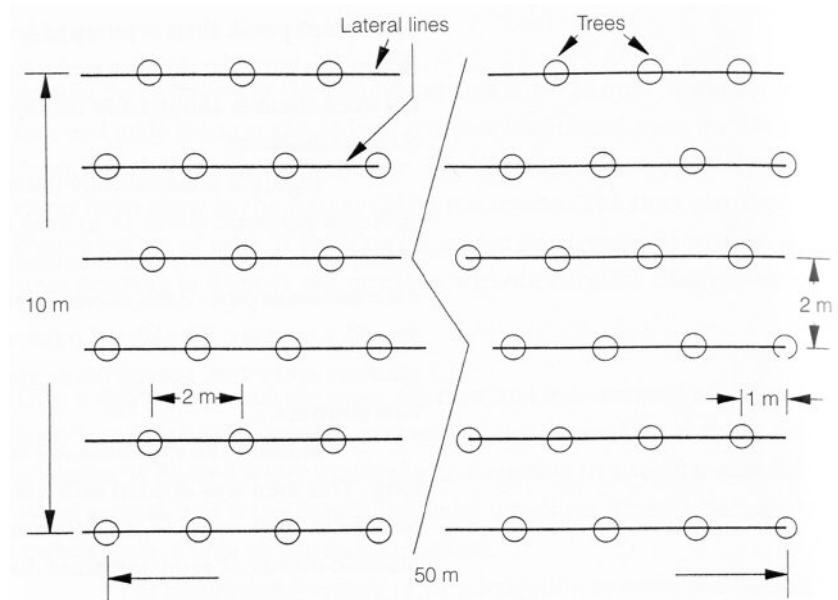


Figure 3
Offset pattern of planting.



2. Determine number of emitters needed:

Number of emitters per plant

$$= \text{area per plant} \times \% \text{ to be wetted} / \text{area wetted per emitter}$$

$$= 2 \times 0.6 / 0.65 = 1.85 \approx 2 \text{ emitters}$$

Therefore, this design requires 1,200 emitters.

3. Select emitter type:

Pressure compensation, single outlet, flow rate 7.6 l hr^{-1} , flow pressure 1.41 kg cm^{-2} , 140 mesh filter.

4. Set emitter running time:

Hours per day

$$= \text{water consumption per tree per day} / \text{emitter} / \text{flow rate no.}$$

$$= 14 / 2 / 7.6 = 0.92 \approx 1 \text{ hour}$$

5. Select pipe size and calculate pressure loss:

Lateral: 1.5 cm drip tubing

Pressure loss for 60 m in length and 378 l hr^{-1} is
 0.13 kg cm^{-2}

Submain: 2.54 cm tubing

Pressure loss for 15 m in length and $4,536 \text{ l hr}^{-1}$ is
 0.13 kg cm^{-2}

Main: 5.08 cm steel pipe

Pressure loss for 1,000 m in length and 9072 l hr^{-1} is
 2.67 kg cm^{-2}

6. Calculate other pressure losses:

Elevation loss: $0.101 \times 50 \text{ m} = 5.05 \text{ kg cm}^{-2}$

Filter, fitting, and valve loss: $\approx 1.41 \text{ kg cm}^{-2}$

Safety factor: 1.5

7. Calculate required pump capacity:

The pressure required to deliver water from source to supply tank is the actual pressure loss multiplied by the safety factor:

$$(5.5 + 2.67) \times 1.5 = 11.58 \text{ kg cm}^{-2} = 115.8 \text{ m.}$$

The pressure required to deliver water from the storage tank to the emitters is $(1.41 + 0.13 + 0.13 + 1.41) \times 1.5 = 4.62 \text{ kg cm}^{-2} = 46.2 \text{ m.}$

Pump no. 1

$$H_p = \frac{1 \text{ s}^{-1} \times \text{m of head}}{7.61 \times \text{pump efficiency}} = \frac{2.33 \times 115.8}{76.1 \times 0.6} = 5.9 \approx 6$$

Pump no. 2

$$H_p = \frac{1 \text{ s}^{-1} \times \text{m of head}}{7.61 \times \text{pump efficiency}} = \frac{2.33 \times 46.2}{76.1 \times 0.6} = 2.35 \approx 3$$

Monitoring Systems and Maintenance

A portable irrometer was used to monitor the moisture content of soil in the root zone at depths of 15 cm and 30 cm. Based on the results, the watering frequency was set at one hour every seven to ten days.

During the watering period, the system and plants are examined. Special attention is paid to evidence of clogging and leakage of the filter, the emitters, and other fittings. Lateral lines and emitters are always covered by sand to extend the life of the PVC tubing. In September 1993, fifteen months after the system was installed, no deposits in the tubes and no deterioration of the PVC tubes were noted. Although it seemed likely, when designing the present system, that the high levels of calcium, magnesium, bicarbonate, and sulfate in the Daquan River water would deposit salts (carbonates and gypsum) on the emitters, such has not been the experience to date. Thus, neither acid nor bleach has been used so far.

As of 1993, the four species of shrubs were growing well (Fig. 4), and the survival rates were *Haloxylon ammodendron* 100%, *Tamarix chinensis* 99.2%, *Calligonum arborescens* 82%, and *Hedysarum scoparium* 94.2%.

Figure 4
Plateau above the Mogao grottoes, showing the growth of vegetation in 1993.



Conclusions

The experimental drip irrigation system described here was implemented in May 1992. By September 1993, only a few plants had died, and these were replaced. The system has been working properly, and no clogging has been reported. These preliminary results are encouraging.

To better evaluate the effectiveness of the vegetation windbreak fence, the experimental area was subsequently enlarged to 800 m in length and divided into four lots. Each lot is 200 m long by 10 m wide. The capacity of the pumping system and the duration of watering for each lot remain the same.

To date, the effectiveness of the vegetation windbreak fence has not been assessed, though when on site, one can clearly observe piles of sand trapped at the base of the shrubs.

Note

- 1 Formulas for estimated water consumption, number of emitters needed, emitter running time, and pressure loss are derived from Shepersky 1990. Calculation of pump capacity is from Wood 1988.

References

- Bucks, D. A., F. S. Nakayama, and R. G. Gilbert
 1979 Trickle irrigation water quality and preventive maintenance. *Agriculture Water Management* 2:149–62.
- Ling, Y. Q., J. J. Qu, J. S. Fan, Y. H. Li, N. Agnew, and P.-M. Lin
 1993 Research into windblown sand damage on the cliff top of the Mogao grottoes. *Dunhuang Studies Special Publication* 1:134–35 (in Chinese).
- Shepersky, K., ed.
 1990 *The Rain Bird Landscape Irrigation Design Manual*. Glendora, Calif.: Rain Bird Sprinkler Manufacturing Corp., Inc. (Published in 1983 as Fry, A. W. "Bill," *Rain Bird International Drip Irrigation Systems Design Manual*. Glendora, Calif.: Rain Bird International, Inc.)
- Tyson, A. W., and K. A. Harrison
 1987 *Chlorination of Drip Irrigation Systems to Prevent Emitter Clogging*. Atlanta: Cooperative Extension Service, the University of Georgia, College of Agriculture.
- Wood, F.
 1988 Making deserts bloom worldwide: Panacea or Pandora's box? In *1988 Technical Conference Proceedings*, 48–58. Arlington, Va.: The Irrigation Association.

Conservation of the Engraved Rock Wall in the Temiya Cave, Japan

Akito Uchida

THE TEMIYA CAVE is a prehistoric site at Temiya, Otaru City, Hokkaido, Japan. The cave measures approximately 5×3 m and is situated about 3 m above ground level under an overhang of a cliff. As a result of excavation by road construction and collapse of the cliff face, the cave today is little more than a recess (Fig. 1).

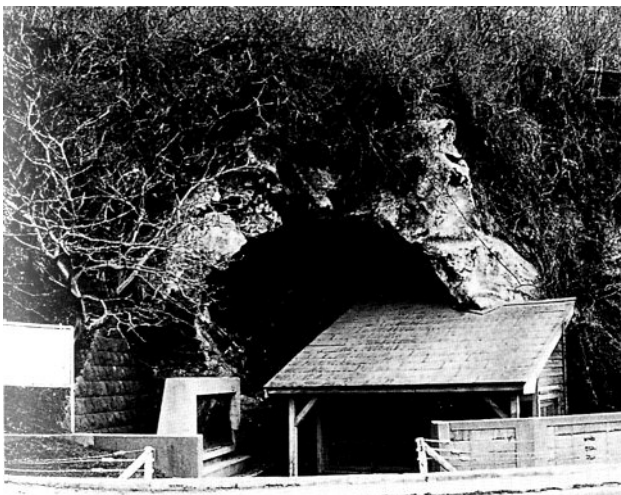
The Temiya cave is important from an anthropological and archaeological perspective because it contains ancient, engraved characters. In 1866, while prospecting in the cave for stone for building materials, a mason discovered the markings on an inner wall (Fig. 2). In 1920, the cave was designated a national historic site. Excavation research at the front of the cave in 1990 certified the characters as having been engraved about sixteen hundred years ago (Fig. 3).

Generally known as “ancient letters,” the characters are also described variously as inscriptions, symbols, and primitive art. However they are interpreted, these engravings are clearly recognized as valuable in terms of cultural heritage (Fig. 4).

Exfoliation and scaling of the cliff rock, a tuff, had become so extensive that it would have been increasingly difficult to identify the

Figure 1
The Temiya cave and its old shelter.

Figure 2
Ancient, engraved characters.



characters if no conservation measures had been taken. The following describes the measures that have been and are currently being implemented for protection of the site.

Geological and Condition Survey

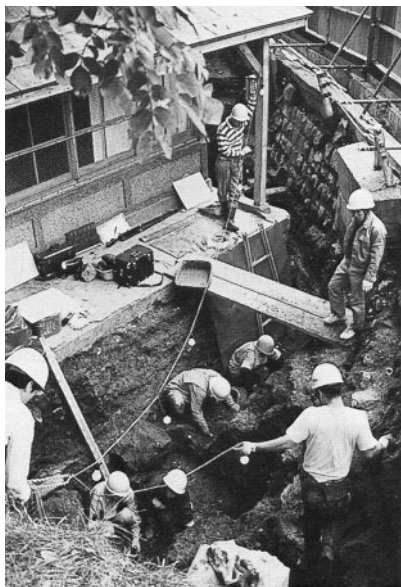
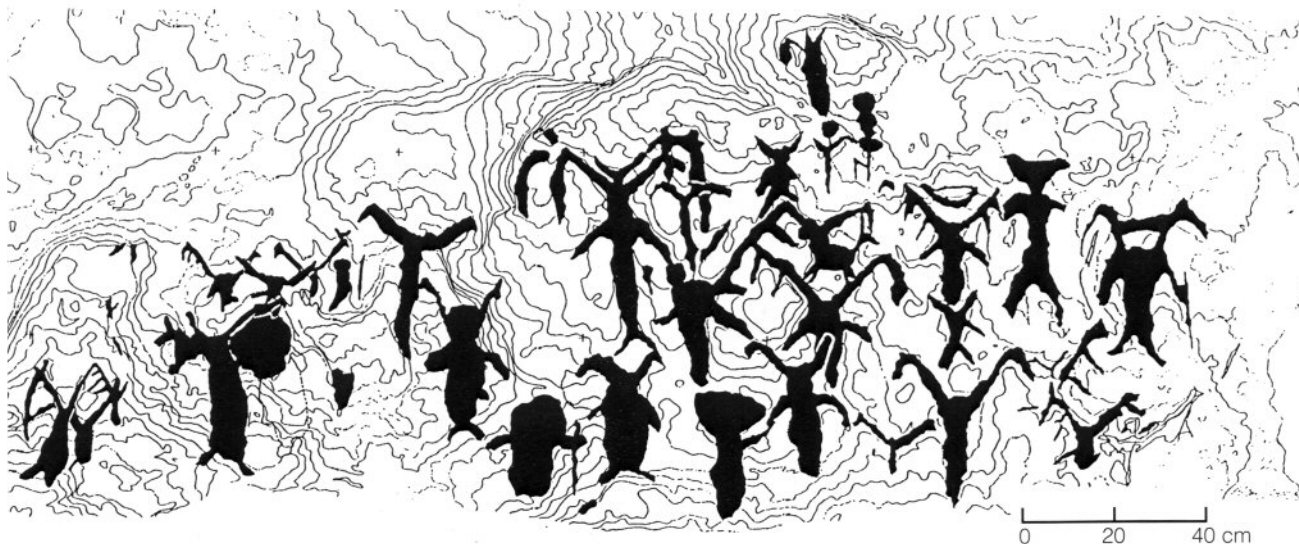


Figure 3
Excavation research.

Figure 4
Photogrammetric plot of the inscribed characters, 1993.



A survey of the geology and condition of the rock was conducted at the Temiya cave in 1986 to obtain information about the geological features in and around the cave and cracks in the character-inscribed surface.¹

Core samples 9 m long were taken by drilling into the cliff rock at two locations on either side of the existing protective shelter over the cave. Microscopic examination and dye-penetration observations were also carried out to determine the extent of weathering of the rock from the drill-core samples.

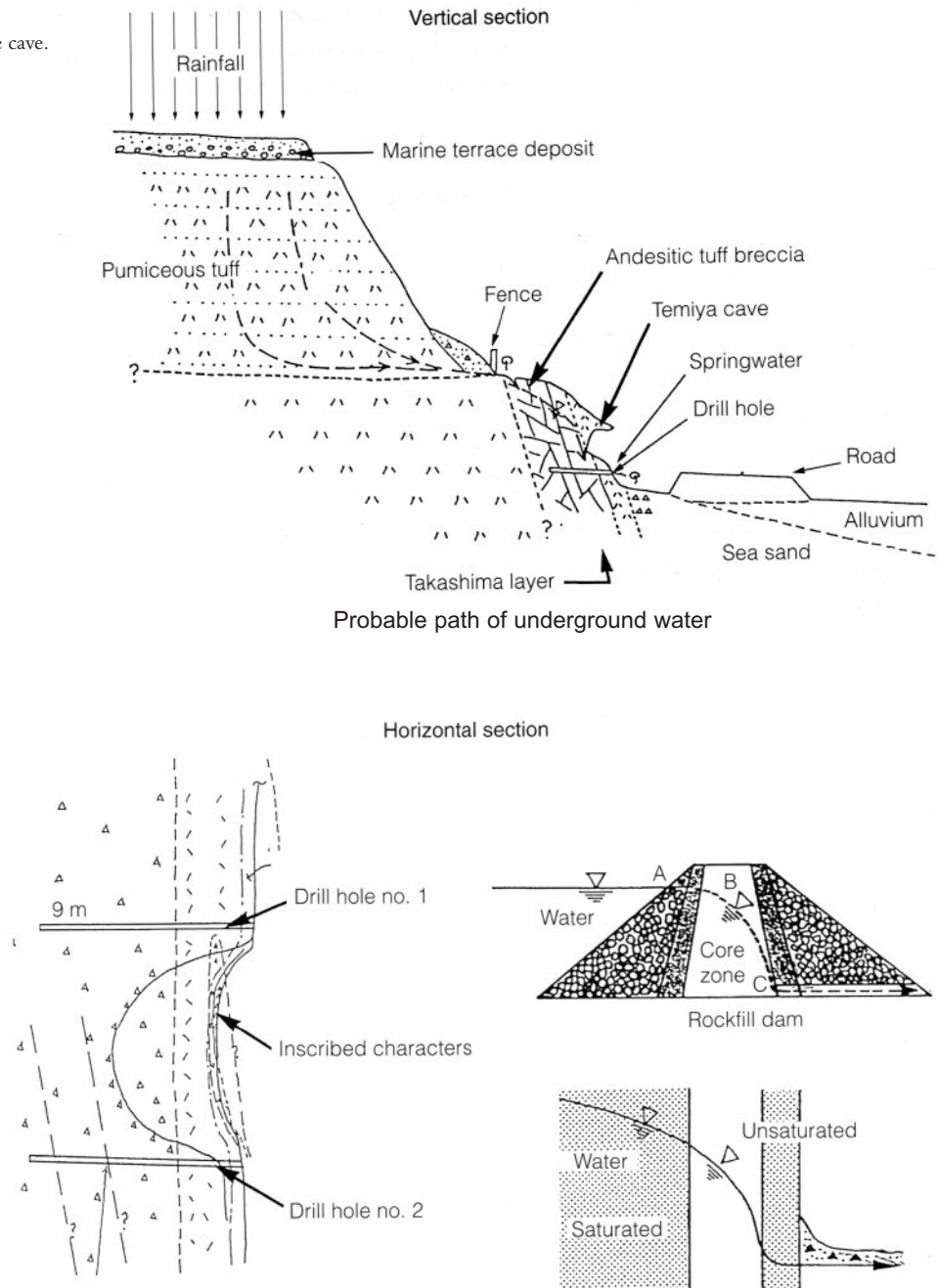
To investigate cracks and porosity in the wall surfaces inscribed with the ancient characters, infrared thermography, subsurface radar, and some measurements were made.

Geological structure

The geological material in and around the Temiya cave is classified as the Takashima stratum of the Pliocene. The drilling survey showed the presence of pumiceous tuff to a depth of 2.2–2.65 m and andesitic tuff breccia to a depth of 9 m from that point. The same geological features were found at both of the locations tested.

The pumiceous and andesitic tuffs corresponding to the Takashima stratum form alternating layers, and their distribution is considered to be nearly parallel to the slope surface. The surface on which the ancient characters are inscribed consists of andesitic tuff breccia, which is considered to be different from the geological feature found by drilling to a depth greater than 2.5 m. The andesitic tuff breccia is presumed to be distributed in a lens shape, judging from its relationship to surrounding geological features (Fig. 5).

Figure 5
Geological structure in and around the cave.



Cracks in the inscribed rock surface

Open cracks found at the top of the inscribed rock surface seem to occur at the boundaries of portions composed of different types of rock and the andesitic tuff breccia of the character-inscribed surface. The rear side of the crack was thought to be pumiceous tuff, based on its surrounding condition. The result of sonic measurements showed that the open crack is deepest, approximately 90 cm, in the center of the inscribed area, and approximately 25 cm on both sides of the area. The subsurface radar results showed that the left portion of the inscribed area in the center of the wall surface is as thin as 10–15 cm to the reflection surface.

Infrared thermography showed that the temperature of the lower portion of the character-inscribed area is relatively low. This is considered to be due to the fact that moisture seeps from the back of the cave wall, behind the cracks, at the boundary of the pumiceous tuff.

Underground water

The andesitic tuff breccia contains a large amount of underground water in its cracks. The source of this underground water is the rain and snow that falls on the stepped slope of the hill behind the cliff.

It is thought that the moist environment surrounding the general area of the Temiya cave results from the relatively abundant supply of underground water behind the cliff, while the presence of a second weathering zone has formed a wall-surface condition with local moisture near the cave only. This provides conditions conducive to the freezing of water and favorable to biological growth. It is possible that the same conditions that promote this growth also cause biochemical deterioration (Table 1).

Survey of Wall Movement

A survey to measure the annual movement of the inscribed rock face was begun in March 1990. The purposes of the survey were

- to observe movement of open cracks over a period of years by regularly recording displacement;
- to observe the effects on the inscribed rock of vibration by construction work on a new shelter and the effect of conservation work on the cave; and
- to collect basic data for the conservation and repair of cultural sites such as this one in the future.

Table 1 Classification of weathering zones

Depth	0 m	0.5 m	2.5 m	9.0 m
Weathering zone	1	2	3	
Rock property	Pumiceous tuff		Andesitic tuff	
Cracks	Many, open	Very few	Many, degraded	
Leaching	Little	Much	—	
Strength	Low	Low	Low	
Ultrasonic propagation velocity	Low	Somewhat high	High	
Underground water	Unsaturated	Nearly saturated	Present (springwater)	
Fluidity of underground water	—	Low	High	
Porosity of rocks	High	High	Medium	
Water permeability	High	Low	High	
Weathering	Great	Medium	Medium	

Displacement of forward and backward movement of the inscribed rock surface and also of the width of open cracks in the wall's surface was measured. Construction of a new shelter covering an older one was begun in September 1990. Temperature and relative humidity levels were measured inside and outside the new shelter, factors that were believed to be affecting displacement of the inscribed rock and open cracks.

Monitoring instruments could not be installed directly on the inscribed characters because of their cultural value. Therefore, six displacement meters (transducers) with highly sensitive dial gauges were installed at different positions in the vicinity of the inscribed characters. Each of the meters was attached to a specially made magnetic stand with steel legs. The bottom of each leg was fixed to a concrete base (Fig. 6). In addition, nine displacement meters were installed across the open cracks at different points to measure changes in crack width (Fig. 7).

The individual displacement meters were connected to a central monitor (Fig. 8) connected to a personal computer that automatically records the data sent from each of the displacement meters. Measurements are taken four times a day, and the average value constitutes the displacement value for the day.

Monitoring Results

Changes in temperature and relative humidity

Temperature changes in and outside the old shelter throughout the year described an S curve. The outside temperature changed from -4°C to 25°C , and the temperature on the rock surface with the inscribed characters in the old shelter changed from -2°C to 23°C . This showed that the surface had long been affected by repeated freezing and thawing.

Soon after construction began on the new shelter, and particularly after the outer wall and the roof were completed, the inside temperature

Figure 6
Displacement meters (transducers) installed inside the cave.

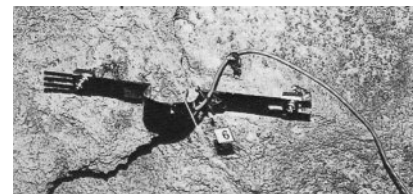
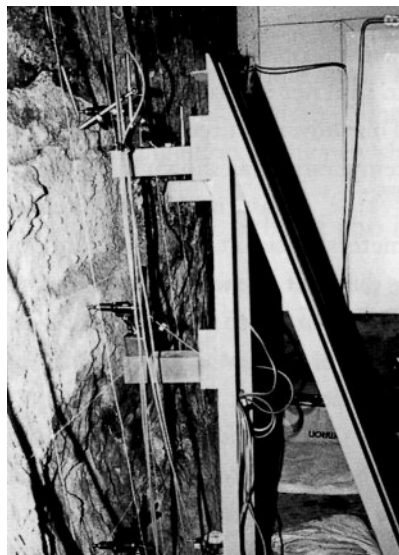
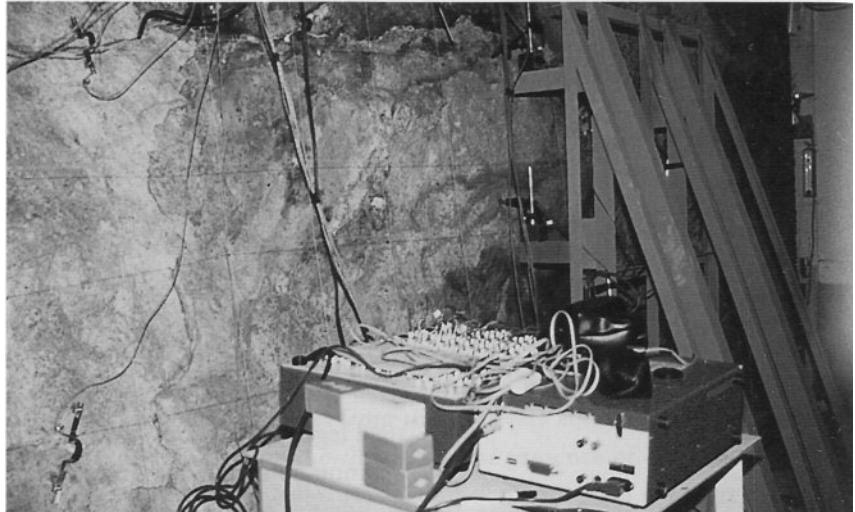


Figure 7
Displacement meter (transducer) installed across an open crack.

Figure 8
Displacement monitor shown inside the cave.



did not fall to the same extent as before, and the inscribed rock surface has not frozen since.

In the old shelter (before the new shelter was constructed over the old one), the average relative humidity at the inscribed rock surface was about 80%. Now it is over 90%, as the area is more completely enclosed. The temperature and relative humidity are expected to be properly stabilized with air conditioners after the inscribed rock is covered by a capsule and the interior construction is completed (the new shelter was completed in March 1995).

It is not possible to determine at this time whether the respiration of visitors affects the microclimate on an annual basis, as these measurements have not been made over a long enough period. But such a determination will become possible as the monitoring continues. Measurements will continue for several more years after the environment around the inscribed rock is stabilized in the new shelter.

Contraction and expansion

The inscribed rock surface moves toward the rear of the cave from spring to summer and returns to its forward position from autumn to winter. This movement recurs regularly every year in proportion to the change in temperature, as shown in Figure 9.

Measuring the amplitude of this movement with displacement meters placed at three different points shows that the extent of movement is different at each point. The amplitude is found to be greatest at the upper part of the surface that is exfoliating parallel to the inscribed surface—namely, at the mouth of the crack; and it becomes smaller as it goes deeper.

The effect on the condition and environment of the inscribed rock surface made by the completion of the roof and the outer wall of the new shelter is already remarkable. Since these structures have been completed, the amplitude of backward movement has lessened considerably.

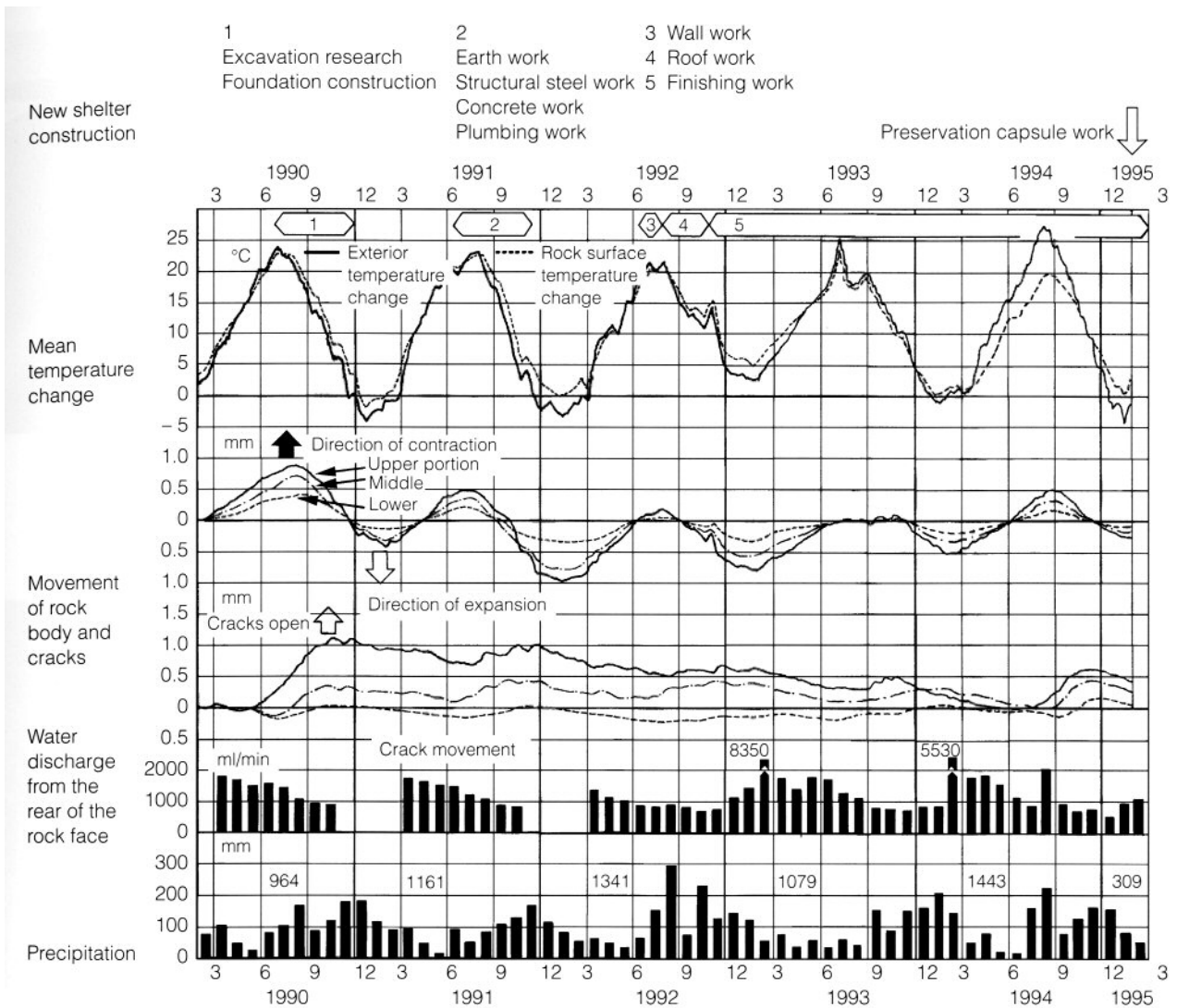


Figure 9
Observation of annual cyclical change. Numbers in bands at top of table indicate stages of new shelter construction and conservation research over a period of five years: 1 = excavation research and foundation construction; 2 = earth work, structural steel work, and concrete and plumbing work; 3 = wall work; 4 = roof work; 5 = finishing work. The arrow at the upper right indicates work on the preservation capsule, which is not yet complete.

Change in crack width

Since the measurement survey began, the width of the open cracks around the characters has become larger, but the degree of change has stayed almost the same. The width of the cracks is expected to become smaller with the completion of the new shelter.

Drainage from behind the inscribed rock

Water is being pumped out from behind the inscribed rock, using the holes made during the core-sample drilling. Drainage volume is measured in milliliters per minute as it gushes out of the pumping holes each month (Fig. 9). Previously, this measurement had not been taken in winter because the water was frozen. The construction of the new shelter, however, has retained warmth and has made it possible to measure pumped water throughout the year. The new shelter has thus had a profound effect on the ability to remove the water that has long been destroying the rock.

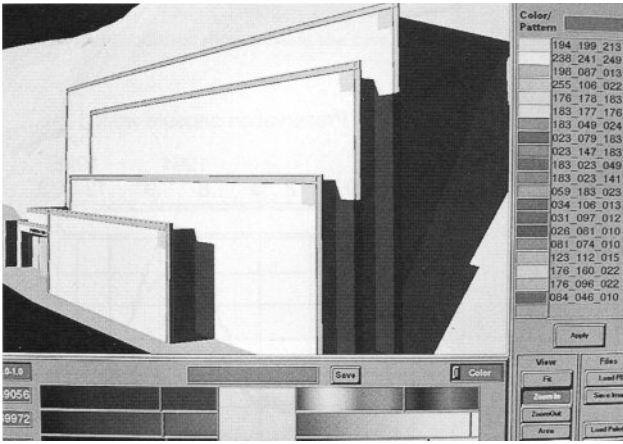


Figure 10
Computer simulation of cave exterior.

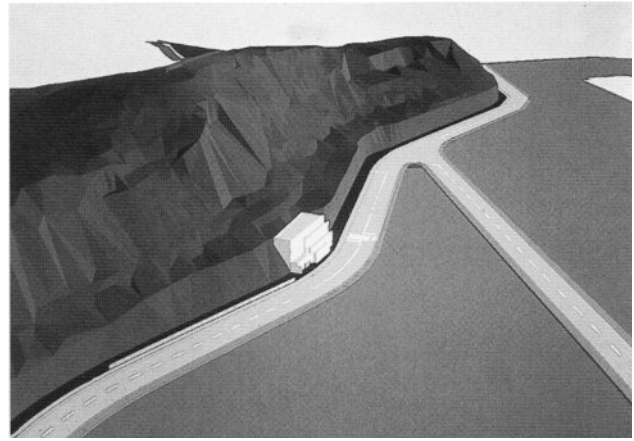


Figure 11
Computer simulation of shelter location and environment.



Figure 12
Computer simulation of shelter interior.

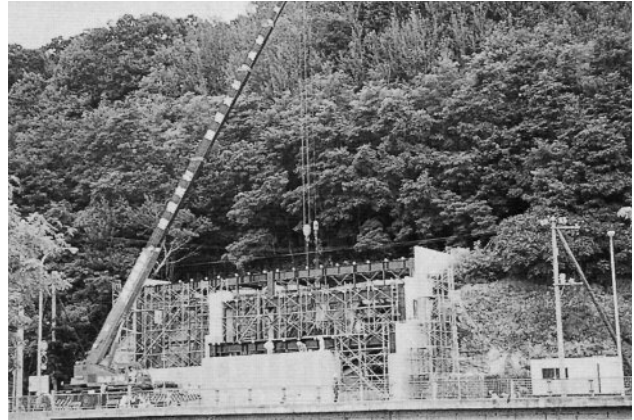


Figure 13
The new shelter under construction.

Computer Graphic Simulation of Surface Conditions

Conditions of the inscribed rock surface were simulated using computer graphics software. Topographical data and information about the conditions of the road running close to the side were based on existing topographical maps on a reduced scale of 1:2500, with data on the new shelter provided by blueprints (Fig. 10). The colors of the exterior of the shelter can be easily simulated by balancing red, blue, and green color values in many different ways on the computer. Different appearances as seen from different perspectives are also possible. Decisions can be made on how to match the shelter with its surrounding environment in regard to color, shape, and a range of other factors (Fig. 11). Many different plans are possible for a shelter's interior design—including colors, displays of exhibitions, lights, preservation capsules, and so on (Fig. 12).

Earthquakes are frequent in Japan, especially Hokkaido, and many people visit the Temiya cave. For this reason, the new shelter was constructed with a steel-reinforced concrete structure (Fig. 13).

Air conditioning installation is underway. To find suitable levels of temperature and humidity, it will be necessary to observe the development of conditions at the inscribed rock face for at least one year.

Note

- 1 The geological survey was undertaken through an arrangement with Takenaka Construction Company.

Geological Environment of the Mogao Grottoes at Dunhuang

Nobuaki Kuchitsu and Duan Xiuye

DUNHUANG IS LOCATED on the eastern edge of the Takla Makan desert. The average temperature is reported to be 9.4 °C and the average annual rainfall, 32.9 mm.

The Sanwei and Mingsha mountains are in the southern part of Dunhuang Prefecture, where Pre-Sinian (Precambrian) complex rocks are distributed (Fig. 1). On the northern side of these mountains, there are two main fan deposits of the Daquan River, locally called the “old fan” and “new fan” deposits, that cover the basement rock with irregular sediments. The fan deposits and basement rock are both partially overlaid by recent eolian sand, which is one of the threats to the Mogao grottoes.

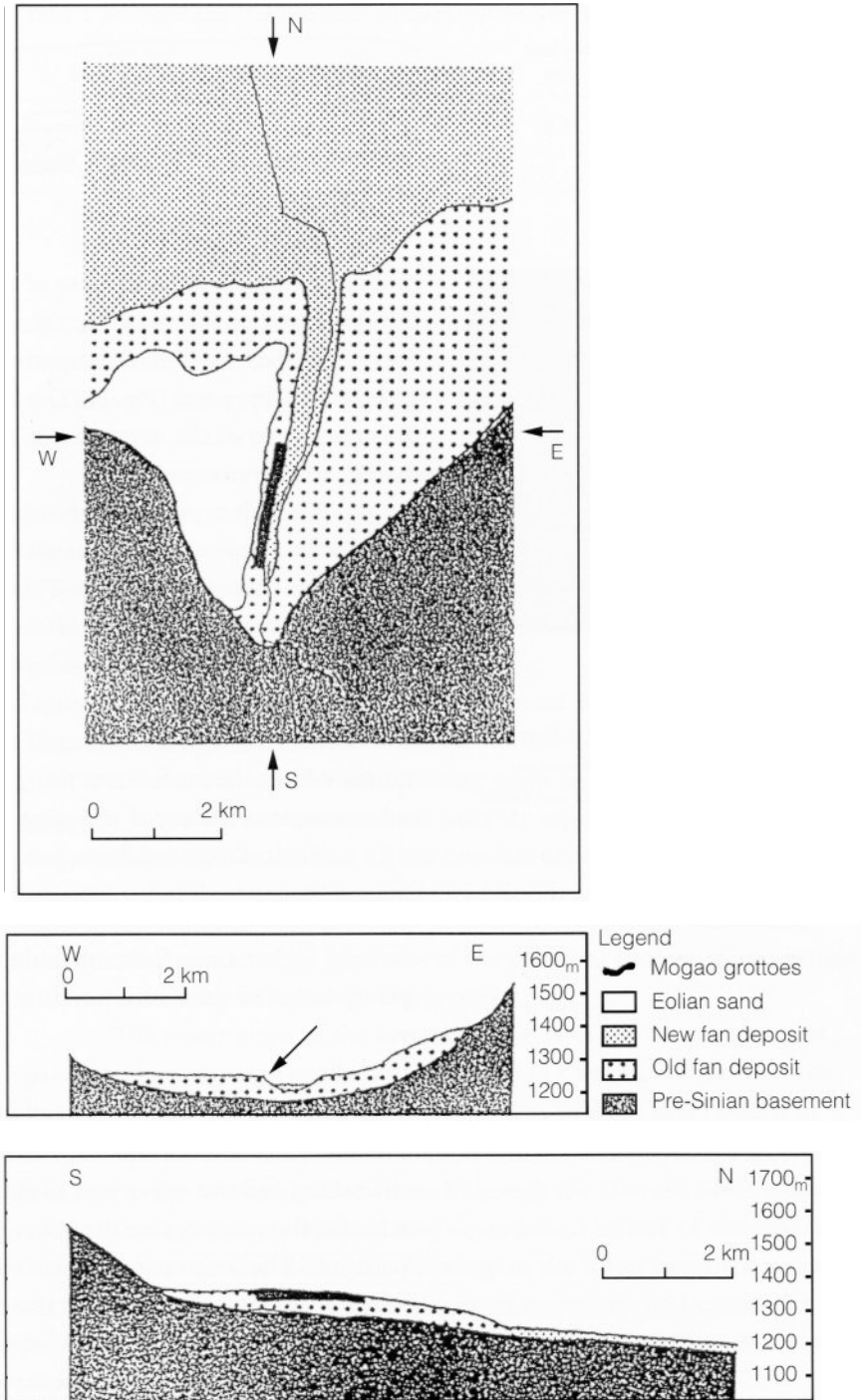
The basement Pre-Sinian rocks are so irregular that they are not suitable for the excavation of grottoes, and the new fan deposit is structurally too weak for digging. Thus, the old fan deposit is the only stratum suitable for the formation of caves in the vicinity of Dunhuang. The Mogao grottoes were excavated into the cliff of the old fan deposit along the Daquan River where the riverbed is deepest (Fig. 1), clearly the most favorable area for the construction of rock temples in the vicinity of Dunhuang.

Salt Crystallization

Salt crystallization is often observed in Dunhuang Prefecture as one of the typical geological phenomena in the desert area. It results from the leaching by water of soluble salts from rock and soil. When the moisture evaporates, crystalline deposits of salts remain. In general, the salt observed at the ground surface is composed mainly of halite (mineral NaCl). When salt crystallizes on the surface or subsurface of mural paintings in the grottoes, it causes flaking of the paint layer. Therefore, it is important to study this process in order to protect the mural paintings from further deterioration.

The approximately five hundred grottoes of Mogao are roughly divided into three groups, based on their location: the higher-, middle-, and lower-level groups. Paintings in the middle-level caves do not show any salt crystallization and are generally well preserved. In contrast, the upper part

Figure 1
Geological map and cross sections in the vicinity of the Mogao grottoes, Dunhuang.



of the paintings in the higher-level caves and the lower part of the paintings in the lower-level caves are often damaged by salt crystallization.

Two of the grottoes have been studied in a collaboration between the Dunhuang Academy and the Tokyo National Research Institute of Cultural Property. These are Caves 194 and 53 (Fig. 2).

Cave 194

Cave 194 belongs to the higher-level group, approximately 29.3 m above the average water table of the Daquan River. In this cave, virtually no

Figure 2

Site map of Caves 194 and 53 (after Sun Rujian).

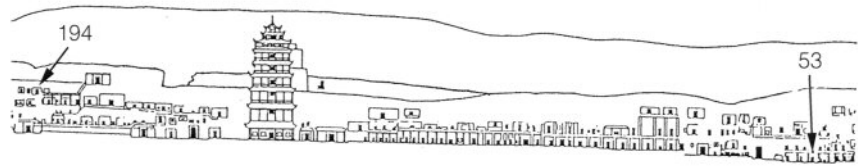


Figure 3

Deterioration of mural paintings in Cave 194. Salt crystals of approximately 2–5 mm in diameter push up the surface layer and cause the paint to flake.

ceiling paintings remain because of flaking. In contrast, the paintings of the lower part of this grotto are generally well preserved. Observations of the walls indicate salt crystals approximately 2–5 mm in diameter, resulting in flaking of the paint (Fig. 3). The flaking is generally more extensive in the upper parts of the cave because the salt crystals tend to be larger there than in the lower areas.

The salt crystals have been identified by X-ray diffraction as halite, which is also observed in the cementing of the pores of the old fan deposit where Cave 194 was excavated. This cave is located below a slight depression in the plateau above the cliff face, where the influence of rainwater, carrying large amounts of soluble halite, appears to be extreme. Thus, the deterioration of the wall paintings in Cave 194 is the result of infiltration of rainwater through the ceiling of the grotto, followed by evaporation of moisture from the surface, resulting in the recrystallization of the salt and consequent flaking of the paint.

The ceilings and the upper parts of the walls of the higher-level caves at Mogao tend to be damaged similarly to those in Cave 194, presumably through the same process. Therefore, it may be necessary to protect the higher caves from exposure to rainwater, although the average precipitation in the area is no more than approximately 30 mm yr⁻¹.

Cave 53

Cave 53 belongs to the lower-level group, approximately 1.8 m below the average water level of the Daquan River. In this grotto, the paintings on the ceiling and the upper part of the walls are generally well preserved, whereas the paintings on the lower portion are severely damaged or have fallen off. The lower part of this cave had been partially covered with sand, which may be one of the main reasons for the deterioration of the paintings. In addition, salt crystals of approximately 2 mm—some as large as 20 mm—diameter have been observed on the lower part of the walls. Salt crystals in this cave were also identified by X-ray diffraction. Halite was not found, whereas gypsum ($\text{CaSO}_4 \cdot 2\text{H}_2\text{O}$) was identified as the dominant component of the salts in this cave. Although gypsum is a common mineral in desert areas, it is seldom observed in the fan deposits around the Mogao grottoes.

Limestone, which consists mainly of calcium carbonate, is commonly found in the fan deposits and in the paintings' ground layer, or preliminary coating. The main mineral component of the paint ground is not gypsum, however, but calcite (CaCO_3). Where, then, did the sulfate (SO_4^{2-}) ion of the gypsum originate? Certain data suggest an answer to

Table 1 Analytical data of the water of the Daquan River (after Duan [1988] and Kitano [1984])

Samples	Cl	NO ₃	SO ₄ ²⁻
Daquan River water	463.19	3.46	824.20
Average river water	7.9	1	11.2

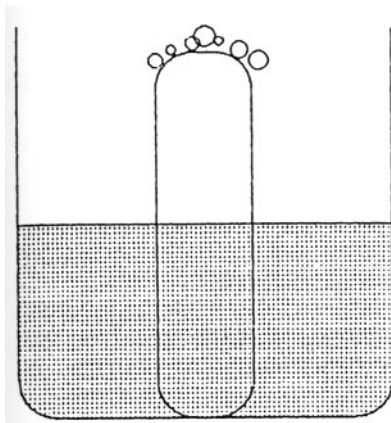


Figure 4 Research on the interaction between river water and the ground layer of paint. A sample of the ground layer of Cave 53 was added to a water sample from the Daquan River. Results show that gypsum crystals form in three days.

this question: Duan (1988) pointed out that the water of the Daquan River has extremely high concentrations of the sulfate ion (Table 1). Therefore, it is thought that gypsum crystallizes when the river water enters the cave and reacts with the paint ground.

An experiment has been carried out to test this theory: A sample of the paint ground of Cave 53 was treated with water from the Daquan River (Fig. 4). Pure gypsum crystals formed on the surface of the ground layer in less than three days. This result indicates that gypsum can be formed rather swiftly in the reaction between the river water and the paint ground.

In 1979, an unusually heavy rain caused flooding of the Daquan River, and the floodwaters entered Cave 53. It is quite likely, therefore, that river water came in contact with primary paint layer in the past to form gypsum. It has not been ascertained whether capillary rise of moisture from soil and rock at the base of the cave has exacerbated the problem, but it is likely that the grotto has experienced floods at least several times during the approximately one thousand years of its existence. Floodwater, therefore, has undoubtedly been one of the principal sources of moisture—with its attendant problems—in this grotto.

The lower areas of the lower-level caves of the Mogao grottoes generally show damage similar to that found in Cave 53. White materials have been observed in some other caves of this stratum that flooded in 1979. It is probable that the white efflorescence is also gypsum that crystallized due to the action of floodwater. Although the Daquan River is ordinarily a nearly dry river, flooding may nevertheless be one of the essential causes of the deterioration of the paintings in the lower caves. Therefore, it is necessary to consider not only the usual environmental conditions but also less frequent natural occurrences, such as flooding, as part of an overall conservation strategy.

Conclusions

Even at the Mogao grottoes, where the average precipitation is no more than approximately 30 mm, rainwater infiltration plays an important part in the deterioration of mural paintings, especially in the higher caves. Floods, which seldom occur in desert areas such as Dunhuang, can also contribute to the deterioration of the mural paintings, especially in the lower caves. Therefore, both typical environmental conditions, such as rainfall, and infrequent natural disasters, such as flooding, must be taken into account in the preservation of this historic site.

Acknowledgments

The authors would like to express their sincere gratitude to all the people who assisted in this collaborative project between China and Japan.

References

- Duan Xiuye**
1988 Study on the productive materials of Mogao grottoes. *Dunhuang Yanjiu* 16:41–59.
- Kitano, Y.**
1969 *Science of Water*. Tokyo: Nippon Hoso Shuppan Kyokai.

Geotechnical Stability Problems of the Dafosi Grotto

Gerd Gudehus and Thomas Neidhart

THE DAFOSI (Great Buddha Temple) Grotto, about 200 km northwest of Xian, was completed approximately fourteen hundred years ago. It was excavated in a sandstone cliff by the extension of a natural cavern to about 35 m in breadth, 15 m in depth and 21 m in height. Inside the grotto, three sandstone statues were carved in high relief from the rock of the walls: a sitting Buddha 17.5 m high and two bodhisattvas, each 12 m high. The statues were covered with clay plaster, then painted. The walls and ceiling of the grotto are decorated with hundreds of figures and ornaments carved into the stone. Openings in the partially remaining cliff wall and in the front temple (which was added much later) permit access of light and visitors. Over seventy years ago, a description of the Dafosi grotto was published by Pelliot (1924).

The grotto is currently in dire need of preservation. Parts of the jointed rock ceiling have collapsed, and other parts appear ready to do so. The necks of two statues are cracked and could topple at any time. Immediate support is needed at some points in the ceiling. Sufficient permanent stabilization—carried out with due respect to the monument—should follow. The lower half of the cave temple is seriously weathered from the infiltration of water and salt. Some areas of the ceiling—as well as some of the statues and walls—must be immediately supported, and further deterioration needs to be reduced by stabilization measures.

The geotechnical problems of this grotto and ones like it are rather uncommon, so commonly used tunneling and mining practices are not necessarily applicable.

Geometry

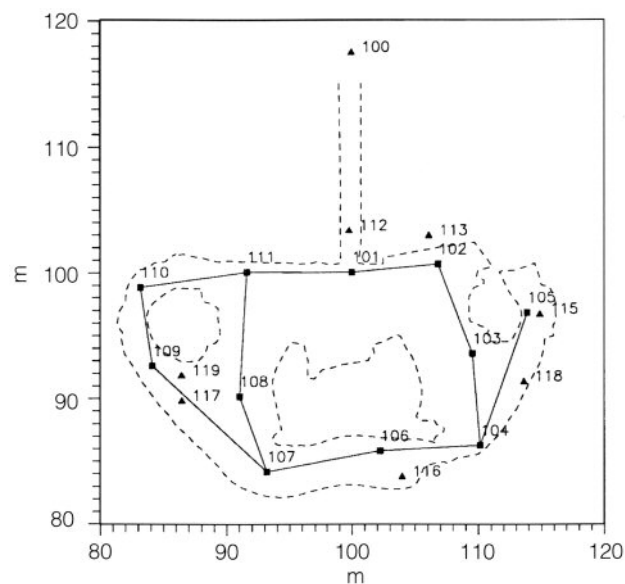
Neither ordinary photographs nor drawings can yield a representation of the complicated spatial geometry of the Dafosi grotto that is sufficiently precise for the geotechnical analysis needed for conservation purposes. While detailed photogrammetric images of the statues have been made, this technique is not suitable for the grotto as a whole. A project supported by the Geodetic Institute of the University of Karlsruhe, with the significant involvement of Manfred Vogel, was undertaken to generate

sophisticated computer graphic illustrations to aid in conservation of the site. As a result, the coordinates of about 6,300 points of the grotto have been determined with an electro-optical total station (Leica and Wild T2002, and DI3000s Rangefinder). The computer graphic illustrations were processed from these data by Neidhart. The software packet AutoCAD Release 12 was used for image processing and computer-aided design (CAD).

To determine spatial geometry, eleven observation points were distributed on the floor, so that almost all parts of the grotto could be surveyed (Fig.1). These, together with five marked reference points at the same level and three at the openings of the temple, formed a sufficient base of reference. The surfaces of the grotto and statues were scanned according to a grid of roughly 0.5 m mesh width; clearly visible marks, such as sharp edges or a change in surface texture, were used. Because of the shape of the grotto and the fact that the statues hide some of the side walls, it was not possible to methodically conduct an exhaustive survey. As a result, some patches of the surfaces of the grotto and the statues were repeatedly surveyed from several points of view. Only small areas (at the shoulders of the statues) remained hidden from every point of view. The data for every point measured consisted of its Cartesian coordinates and a number through which four typical surface types (rock, ornaments, masonry, and weathered fill) were coded. These numbers enabled the scientists to differentiate and color a CAD model.

Vertical coordinates were interpreted from the reference points, a process that yielded forty-one sets of elevation data (0.5 m, 1.0 m, 1.5 m, and so on) with a range of 0.25 m. The coordinates of the whole ceiling, with a wider range, were stored in the forty-first set. Figure 2 shows horizontal cross sections in four elevations that were prepared with these data sets. Figure 3 demonstrates how the same can be done for any vertical section. Other sections of this kind can easily be made so a rough impression of shape, size, and relative orientation can be obtained.

Figure 1
Survey reference points. Points 112 and 113
are in the openings on the first floor of the
front temple.



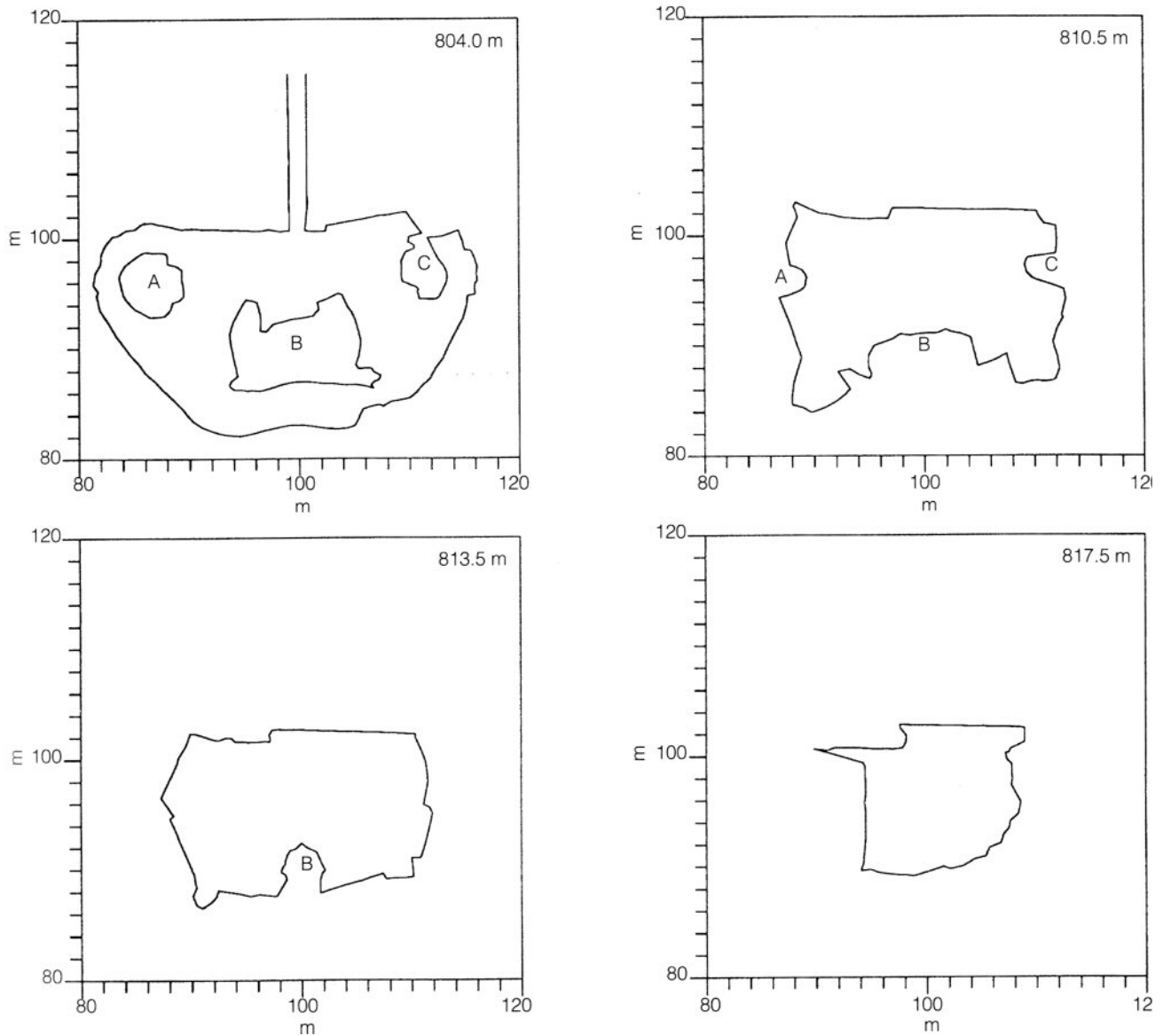
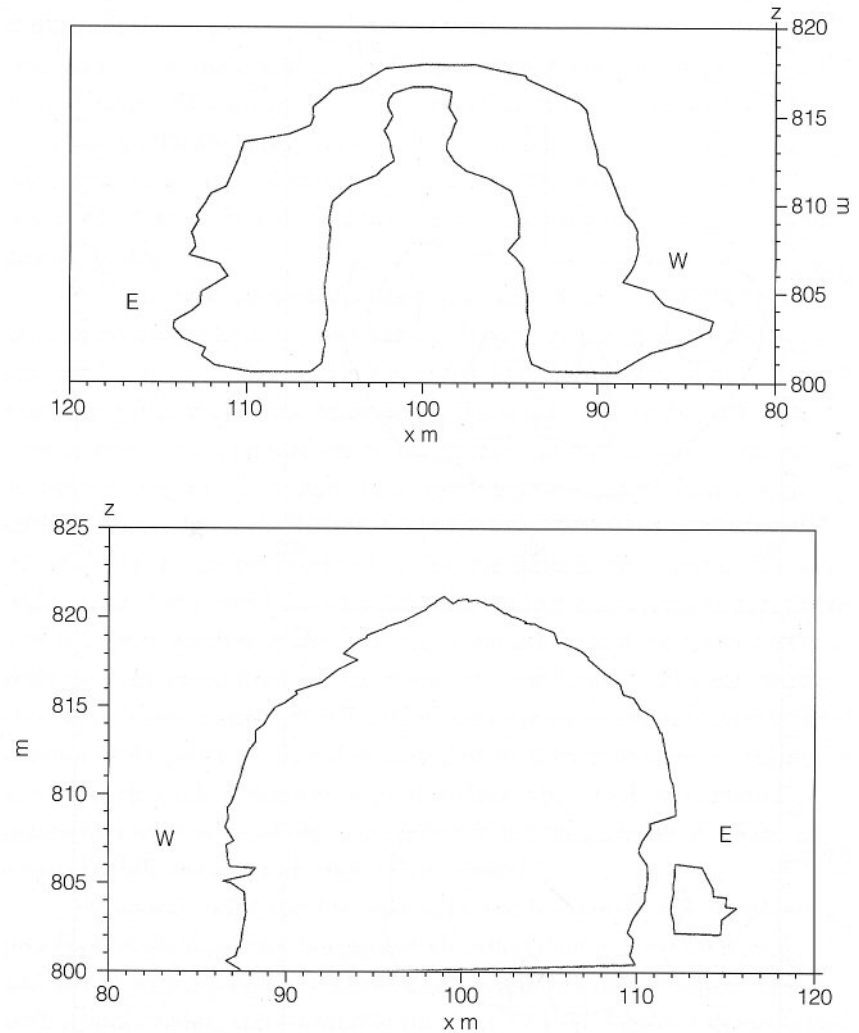


Figure 2
Horizontal cross sections at four elevations above the grotto floor with letters indicating the statues, as follows: A = Bodhisattva Avalokiteshvara, B = the Great Buddha, C = Bodhisattva Mahastamaprapta.

It is much more difficult to generate a complete spatial impression of the grotto with computer graphics. The problem lies in the concavity of the surfaces, the possible loss of specific detail, and the omission of hidden parts that might be necessary to fully model the chosen point of view. As standard procedure, the points in every data set were rearranged to unify the sense of rotation (in a right-handed Cartesian coordinate system), which is necessary for the CAD software to generate surfaces with normal vectors extending from the surfaces into the grotto. Finally, every data set was split according to the change of materials, corners, and edges, to prevent the CAD software from producing any smoothing of these significant parts of the grotto. The points of each subset were interpreted by the CAD program as three-dimensional polygons connected with rectangular surface patches.

Figure 4 gives a rather complete impression of the grotto except for the remaining cliff wall and the front temple, which are omitted. The

Figure 3
Two vertical cross sections.



sitting Buddha fills the grotto almost to the ceiling. The two bodhisattvas are leaning toward the walls and are clearly subordinate. A kind of circuit surrounds the statues near their bases. The grotto surface is roughly shaped as one-quarter of an ellipsoid. Convexities of this surface carry decorative parts, such as the Buddha's halo. Concave parts are largely the result of losses from rupture in the upper half of the grotto and erosion in the lower half.

Figure 5 shows another image of this kind. The observer's point of view can be chosen arbitrarily, and various parts of the CAD model can be removed to achieve a better perspective. The images have been enhanced with shadows and colors to strengthen the spatial impression. It is evident that photographs and videos are needed to obtain more detailed pictures, but these can be far better understood with the aid of the CAD images. These graphics form a substantial part of the authors' geotechnical reports; they are also useful in the authors' own work and in collaborating with other scientists.

Upper Half of the Grotto

Toward the ceiling of the grotto, the rock is almost pure sandstone, rather dry, and as permeable as fine sand. It has an old system of fissures, typical

Figure 4

Unshaded CAD model. Point of view from the northeast. Letters mark vulnerable parts of the grotto surface and statues: A = head of the Great Buddha, B = eastern bodhisattva, C = ceiling to the left and in front of the Buddha, D = area of dangerous “coffin lids,” E = foot of the eastern bodhisattva, F = circuit behind the statues, G = base of the Buddha.

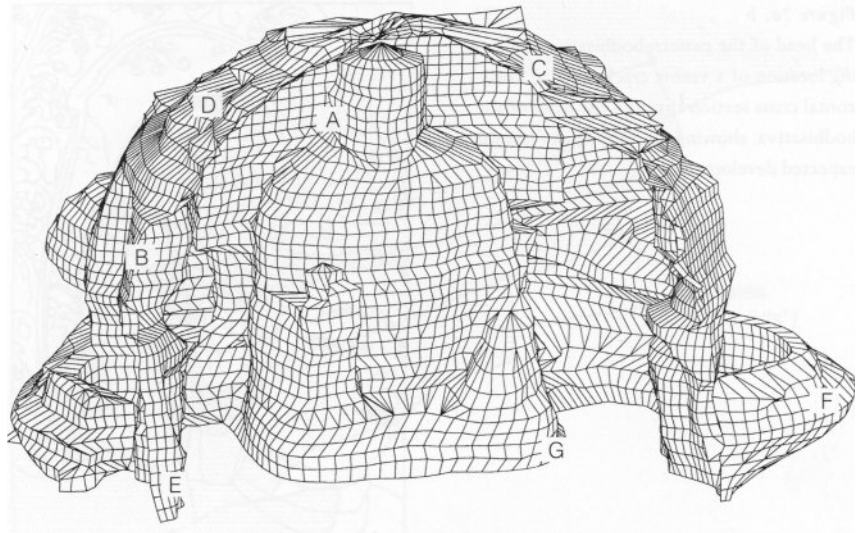


Figure 5

Unshaded CAD model. Point of view from the north.

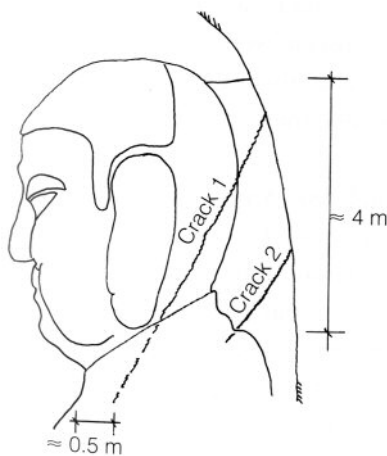
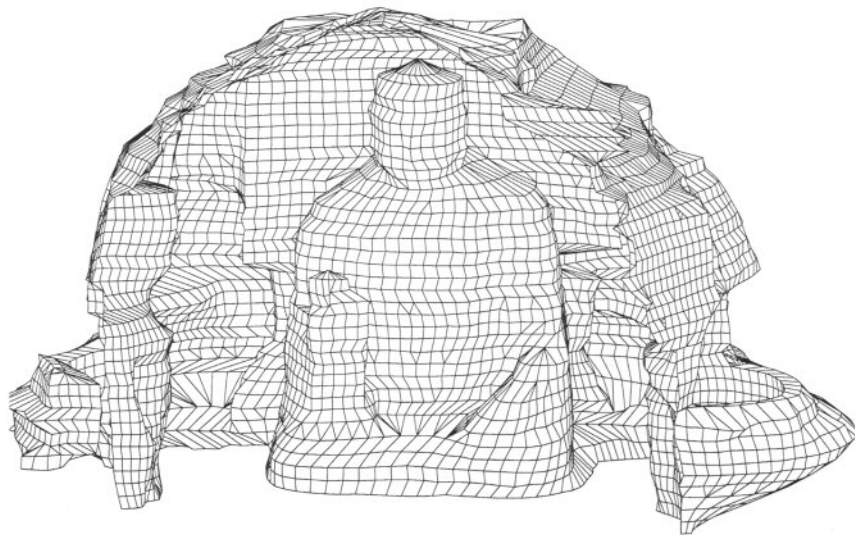


Figure 6

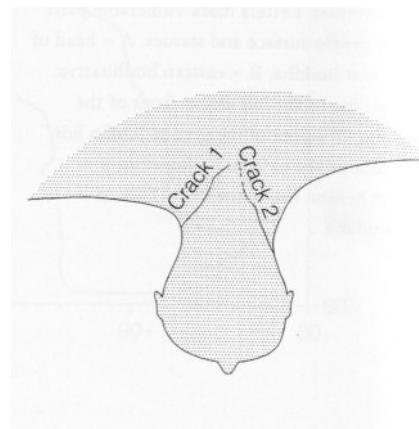
Cracks at the Buddha's head with an inclination of approximately 60°.

of cliffs, which can be seen from the outside. These cracks have extended and opened as the stress release along the grotto surface has produced stress concentrations close to the cracks. Also, the cracks tend to expand with time as a result of reduction of strength caused by weathering, temperature changes, and occasional dynamic impacts. The rubble on the floor indicates that, over time, substantial parts of the former ceiling collapsed long ago, but it is not possible to determine from below which parts are likely to fall next. A scaffold has therefore been erected; from it, close inspection of the whole grotto surface and the statues was conducted by Zou Yazhou of the University of Hydraulic and Electric Engineering in Wuhan. The inspection revealed a far more dangerous situation than had been expected. Vulnerable portions are labeled in Figure 4.

The Buddha's head (Fig. 4, area A) has two visible parallel cracks that extend from the back almost to the chest (Fig. 6). They can barely be seen from the floor, and an even closer view does not fully reveal them because of the clay-plaster cover. Measurement of the attenuation of weak

Figure 7a, b

The head of the eastern bodhisattva (a) showing location of a visible crack; and (b) horizontal cross section through the head of the bodhisattva, showing existing cracks and their expected development.

*Figure 8*

View of the Dafosi grotto, showing rock outcrops (upper right) in ceiling area to the left of the Buddha.

shock waves reveals that the two cracks pass through the stone horizontally. It can also be seen that part of the cracks appear to be fresh and thus are developing. Indeed, the head will eventually break off when the cracks are sufficiently deep. The eastern bodhisattva, on the right side of the Great Buddha, has a similar weakness: the head is partly separated from wall and body by two cracks (Fig. 4, area B; Fig. 7a). Only one crack is visible from the floor, and only a very close inspection revealed the danger presented by the second one (Fig. 7b). As the head is inclined toward the Buddha, it is likely to fall in this direction.

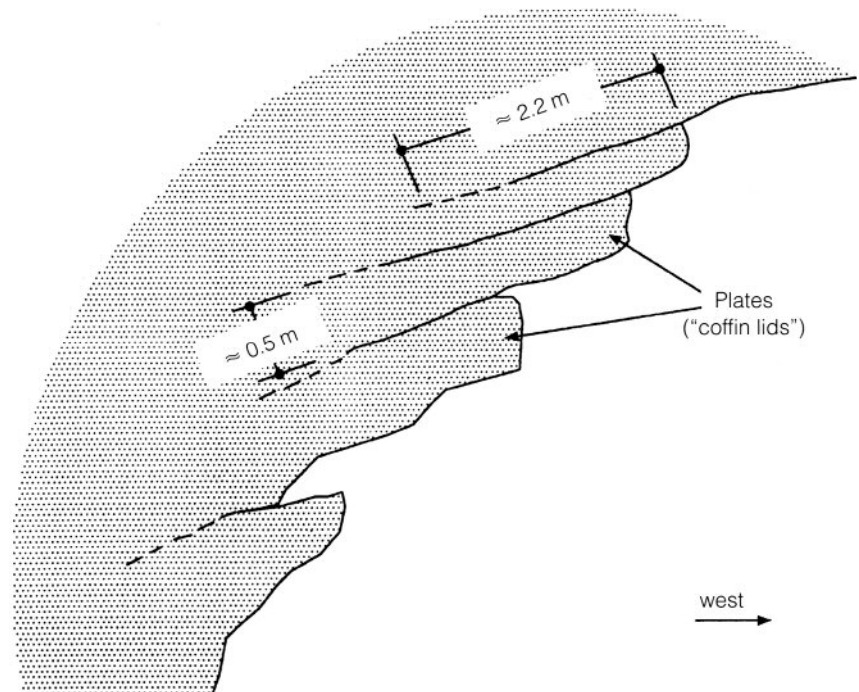
The ceiling to the left and in front of the Great Buddha (Fig. 4, area C; Fig. 8) contains a few very loose protruding blocks with masses of up to about 50 kg. One of these blocks fell in 1992; this dangerous event led to the decision to erect the scaffold and conduct a close inspection. Other very loose small blocks, previously unseen, were then identified from the vantage point of the scaffold. Because their documentary value appeared low relative to the cost of stabilizing them, they were removed immediately.

Close inspection itself posed a high risk. A very dangerous area was discovered to the right of the Buddha's head (Fig. 4, area D). In that spot, orthogonal patterns of joints almost permit the separation and falling of a series of slabs or plates weighing about 2 t each (Fig. 9). Gentle tapping applied experimentally to these plates caused them to vibrate with a low frequency—an indication that the plates are attached on only one side. The term “coffin lids,” used by miners for such slabs, indicates the danger they pose.

The authors, together with Ge Xiurun of the Academia Sinica in Wuhan, conducted a detailed stability analysis and designed proposals for stabilization. The two bodhisattva heads will be temporarily secured by

Figure 9

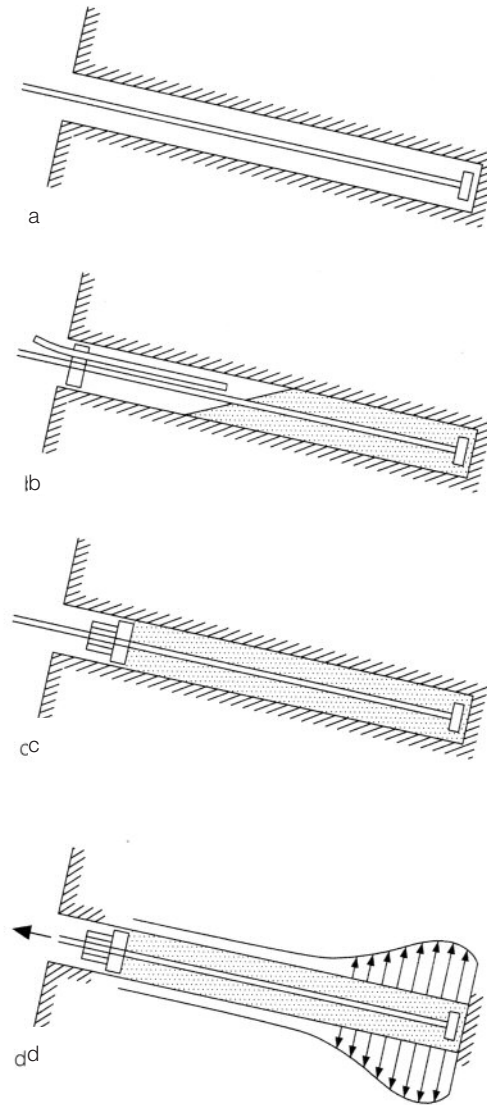
Vertical cross section through the ceiling and head of the eastern bodhisattva, showing the dimensions and shape of the "coffin lids."



steel brackets traversing the cracks. The use of small-diameter drill holes with interior application of glue is an acceptable intervention, considering the otherwise high risk of loss. Subsequent long-term stabilization will require bolts placed nearly vertically with reference to the cracks; it is possible that filling the cracks with mortar would worsen the situation. Respect for the statues precludes bolting their heads from the front; instead, holes must be drilled from behind or from the sides. There is a narrow cavity behind the Buddha's shoulders that should permit drilling. Holes drilled from the side at appropriate angles can reach the cracks behind the bodhisattva.

For this type of repair, stainless steel or fiberglass bolts will be placed into the drill holes (Fig. 10a). Filling the holes with compacted sand (Fig. 10b) and prestressing the bolts with screw nuts (Fig. 10c) will achieve the necessary static contact (Fig. 10d). This type of rock anchor, which was developed at the Institute of Mining of the Russian Academy of Science in Novosibirsk (Stashevski and Kolymbas 1993), is strong and durable. It is also chemically neutral and therefore reversible from a conservation standpoint. The anchor system was further developed at the Institute of Soil and Rock Mechanics in Karlsruhe and tested on sandstone blocks, including overhead installations. Field tests have also been performed on this anchor system in soil—for example, in the stabilization of retaining structures. The installation of anchor systems combining bolts and sands has been extensively and successfully achieved under various conditions (Gudehus 1994). In Bulgaria, such sand anchors have been used to fix rock blocks in steep slopes in cases where they threaten to destroy historic buildings (Stashevski and Kolymbas 1993).

Figure 10a–d
Schematic drawing, showing installation of a sand anchor in rock.



Before applying rock anchors at the Dafosi grotto, the coffin lids require temporary props; otherwise they cannot be touched. Of course, the floor below them must be closed off. Drill holes with bolts and sand, such as those used for the heads of the statues, have been prepared and will be prestressed so as to carry the entire weight of the rock plates.

Ge Xiurun is analyzing the stability of the upper half of the grotto using a finite element method to calculate the stresses caused by the excavation of the grotto and to estimate stresses that may be caused by future earthquakes. These calculations will aid in identifying zones of impending rupture. A further, more detailed but protracted calculation was made for some cracked areas of the ceiling. These calculations are more difficult to carry out than are similar ones currently used in rock mechanics for the analysis of storage dams and rock cavities.

Consideration has been given to the placement of monitors to signal an impending rockfall. These monitors are desirable because an accurate mechanical analysis of stability is beyond the scope of present geomechanical calculations. An indicator of insufficient stability is an

increasingly abnormal wave transmission and emission behavior. Even though this relationship is qualitatively known in mining and earthquake engineering, a consistent mathematical predictor is not yet available. Therefore, at the present time, intuition based on experience is the best guide.

Lower Half of the Grotto

Toward the bottom of the grotto, nearly horizontal layers of clay are embedded in sandstone. Seepage of moisture from the loess cap of the sandstone formation migrates above the clay toward the cliff wall in the grotto. Capillary rise of moisture is nourished by this horizontal flow and strengthened by evaporation along the wall of the grotto. The lower half of the sandstone is wet, and water content decreases toward the ceiling. Dissolved salts, which migrate in the capillary water, crystallize at the surface to develop a white efflorescence. Part of the salt crystallizes below the stone surface; the resultant expansion has produced spalling of parts of the rock surface. In principle, this mechanism of weathering is well understood in geology and in the deterioration of monuments. Nevertheless, it is very difficult to analyze the process precisely and prevent further deterioration by technical means.

Such defects, caused by salt crystallization in the stone, can be seen in other areas of the grotto shown in Figure 4. Part of the foot of the eastern bodhisattva (area E) has been lost, and the entire statue could break down in the near future. The circuit behind the statues (area F) is expected to enlarge, causing the rock above to lose support. The base of the Great Buddha (area G) has become so soft that parts of it have already crumbled away. It is now inadequately supported by a buildup of sediments from the river and by rock material from the grotto.

Even without an analysis of mechanical stability, it is clear that this weathering will completely destroy the lower part of the grotto and the statues over the course of time. Some parts—as, for example, the right side of the Great Buddha's halo—are already approaching collapse and require immediate support. Disintegration of the rock face must be stopped or at least reduced.

One remedy to these problems, theoretically, would be to interrupt or reverse the flow of water and dissolved salts into the grotto. This step is not practicable, however, because surface layers would spall off after some time; drainage holes would divert only part of the seepage water; and vacuum or electroosmosis methods are not reliable for sandstone.

It will therefore be necessary to tolerate an ongoing influx of water and salts into the grotto. But further damage can be reduced with sacrificial plaster layers, sometimes used for the conservation of buildings. In this scheme, transported salts accumulate on and inside the layer and do, indeed, eventually destroy it—but the layer can be easily replaced later. Tests have been made in Karlsruhe, in cooperation with visiting Chinese scientists, to demonstrate the use of sacrificial plaster layers in combating salt transport.

Various means of supporting endangered features of the grotto were studied. Strengthening the interior by injection or reinforcement was

rejected as too dangerous; and the long-term behavior of these methods with very soft rock is unpredictable. The surface installation of metal and synthetic supports was also rejected as incompatible with the appearance of the monument.

A decision was made to employ masonry to support parts of the Buddha's halo and thereby also cover the scars of erosion. A brick wall for support had already been erected to the left of the eastern bodhisattva, but it was considered inadequate because of the incompatible surface and the deviation in shape from the original wall. The new supporting masonry will be made of sandstone blocks joined with a small amount of compatible mortar, so the facade will resemble the former grotto surface. Areas of the grotto affected by substantial amounts of water containing dissolved salts will receive a surface coat of sacrificial plaster.

The bottom fill will be removed to return the grotto to its former level. This will be done in small, careful steps, to secure historically important inclusions, as well as to maintain stability. The excavation is being performed under the direction of archaeologists. Only narrow pits have been excavated, so the remaining parts can still provide sufficient support. The supporting masonry will be placed on firm ground and built up to the intact rock surface. At some points, it will be necessary to connect the masonry to the rock behind it by the use of bolts with sand, as described.

Acknowledgments

The conservation of the Dafosi grotto is the aim of a collaborative project undertaken by the Ministry of Cultural Goods in Xian and the Bayerisches Landesdenkmalamt in Munich. The support of the project by the German Ministry for Science and Technologies is gratefully acknowledged, along with that of the Geodetic Institute of the University of Karlsruhe, and the work of Manfred Vogel. Geotechnical work was substantially supported by the following Chinese colleagues: Ge Xiurun of the Academia Sinica in Wuhan; We Wei of Xian Technical College, now working with a German company; and Zou Yazhou of the University of Hydraulic and Electric Engineering in Wuhan, working at the time of this writing with the authors in Karlsruhe.

References

- Gudehus, G.
1994 Stabilization technologies with dry mineral granulates (in German). In *Sonderheft aus der Publikationsreihe der BMFT-Verbundforschung zur Denkmalpflege*. Berlin: Ernst and Sohn.
- Pelliot, P.
1924 *Les grottes de Touen-Houang: Peintures et sculptures bouddhiques des époques des Wei, des Tang et des Song*. Vol. 6, 372–75. Paris: Collège de France.
- Stashevski, S., and D. Kolymbas
1993 Prestressed sand-anchors (in German). *Geotechnik* (DGGEG) 4:202–3.